DOKUZ EYLÜL UNIVERSITY
GRADUATE SCHOOL OF NATURAL AND APPLIED SCIENCES

BALLISTIC PERFORMANCE OF HYBRID COMPOSITE STRUCTURES

by
Baha TEPEDÜZÜ

December, 2017
İZMİR

BALLISTIC PERFORMANCE OF HYBRID COMPOSITE STRUCTURES

A Thesis Submitted to the
Graduate School of Natural and Applied Sciences of Dokuz Eylül University
In Partial Fulfillment of the Requirements for the Degree of Master of Science
in Mechanical Engineering, Mechanics Program

by
Baha TEPEDÜZÜ

December, 2017
İZMİR

M.Sc. THESIS EXAMINATION RESULT FORM

We have read the thesis entitled **"BALLISTIC PERFORMANCE OF HYBRID COMPOSITE STRUCTURES"** completed by **BAHA TEPEDÜZÜ** under supervision of **PROF.DR. RAMAZAN KARAKUZU** and we certify that in our opinion it is fully adequate, in scope and in quality, as a thesis for the degree of Master of Science.

Prof. Dr. RAMAZAN KARAKUZU

Supervisor

Doç. Dr. Mehmet Cevik

(Jury Member)

Doç. Dr. Yusuf ARMAN

(Jury Member)

Prof. Dr. Kadriye ERTEKİN

Director

Graduate School of Natural and Applied Sciences

ACKNOWLEDGEMENTS

I wish to express my sincerest gratitude to my academic supervisor Prof. Dr. Ramazan KARAKUZU for the encouragement. He has instructed me with great guidance. I thank him for his endless patience and I will forever be indebted to him for providing me an opportunity in doing this study.

I would like to thank Ahmet Burak AYDOĞDU for helping me improve my numerical model.

I would like to thank my family, my mother Sultan, my father Süleyman, my brothers Baki and Barış for their endless support in my life and all this thesis period.

Baha TEPEDÜZÜ

BALLISTIC PERFORMANCE OF HYBRID COMPOSITE STRUCTURES

ABSTRACT

The aim of this study is to numerically investigate the ballistic behavior of composites with different thicknesses and different reinforcements. The guns were shot at four different velocities on composite models using armor-piercing 7.62 M61 AP projectiles.

The alumina ceramics forming the front surface of the composite structure were used in three different thicknesses, 6 mm, 8 mm, 10 mm. The fabric-reinforced epoxy composite, which forms the back surface of the composite structure, is modeled to have six different compositions in total, using three different reinforcing elements, with a total thickness of 10 mm. Aramid, S2 glass and hybrid carbon-aramid fabrics were used as reinforcement. In addition, the aramid/S2 glass/epoxy model has been produced at three different thickness ratios, with aramid and S2 glass fibers having a total thickness of 10mm. In the study, Ansys was used as preprocessor and Ls-Dyna as solver. Multilayer MAT 59 and MAT 22 for composite materials; MAT 110 material cards were used for alumina ceramic material.

For the composite structure: 72 different numerical analyzes were performed for four different velocities, three different ceramic thicknesses and six different composite compositions. As a result, the numerical analysis revealed that the alumina/S2 glass/ epoxy composites had a higher ballistic performance than the others in the data, based on the input-output velocity of the projectiles when the areal density of armors is not considered. Also, when the all ceramic thicknesses and areal density of armors are considered, it is found that the aramid/epoxy backing plate had a higher ballistic performance than the others.

Keywords: Ballistic performance, alumina, M61 7.62 AP, hybrid composite, Aramid/epoxy, carbon-aramid/epoxy, S2 glass/epoxy

HİBRİT KOMPOZİT YAPILARIN BALİSTİK PERFORMANSI

ÖZ

Bu çalışmanın amacı farklı kalınlıkta olan ve farklı takviye elemanlarıyla oluşturulan kompozit yapıların balistik davranışlarını numerik olarak incelemektir. Zırh delici 7.62 M61 AP mermi tipi kullanılarak oluşturulan kompozit modeller üzerine dört farklı hızda atış yapılmıştır.

Kompozit yapının ön yüzeyini oluşturan alümina seramik 6 mm, 8 mm, 10 mm olmak üzere üç farklı değişken kalınlıkta kullanılmıştır. Kompozit yapının arka yüzeyini oluşturan kumaş takviyeli epoxy kompozit, toplam kalınlıkları 10mm olacak şekilde üç farklı takviye elemanı kullanılarak toplamda altı farklı kompozisyona sahip olacak şekilde modellenmiştir. Takviye elemanı olarak aramid, S2 glass ve hibrit karbon-aramid kumaşlar kullanılmıştır. Ayrıca aramid ve S2 glass elyaflarından toplam kalınlıkları 10mm olacak şekilde hibrit aramid/S2 glass/epoxy modeli üç farklı kalınlık oranlarında oluşturulmuştur. Çalışmada Ansys ön işlemci, Ls-Dyna ise çözücü olarak kullanılmıştır. Kompozit malzemeler için çok katmanlı MAT 59 ve MAT 22; alüminyum oksit seramik malzeme için MAT 110 materyal kartları kullanılmıştır.

Kompozit yapı için: dört farklı hız, üç farklı seramik kalınlığı ve altı farklı kompozit kompozisyonu için 72 farklı numerik analiz yapılmıştır. Sonuç olarak numerik analizin sonunda modellere atılan mermilerin giriş-çıkış hızına bağlı olarak çıkan verilerde, zırhların alansal yoğunluğu dikkate alınmadığında, alüminyum oksit/S2 glass/epoksi kompozit yapı diğerlerine nazaran balistik performansı daha yüksek bulunmuştur. Diğer taraftan bütün alansal yoğunluk ve seramik kalınlıkları dikkate alındığında Aramid/epoksi destek plakasının diğerlerine nazaran balistik performansı daha iyi olduğu bulundu.

Anahtar kelimeler: Balistik performans, alüminyum oksit, M61 7.62 AP, hibrit kompozit, Aramid/epoksi, Karbon-aramid/epoksi, S2 glass/epoksi

CONTENTS

Page

M.SC. THESIS EXAMINATION RESULT FORM ii
ACKNOWLEDGEMENTS iii
ABSTRACT iv
ÖZ v
LIST OF FIGURES ix
LIST OF TABLES xiv

CHAPTER ONE INTRODUCTION 1

CHAPTER TWO HISTORY OF ARMOR 9

CHAPTER THREE CLASSIFICATION OF MATERIALS AND METHOD 14

3.1 Ceramics 14
3.1.1 Classification of Ceramics 16
3.1.1.1 Advanced ceramics 17
3.1.1.1.1 Structural ceramics 17
3.2 Composites 19
3.2.1 Classification Based on Matrix Materials 21
3.2.2.1 Polymer Matrix Composites 21
3.2.2.1.1 Thermosets 21
3.2.2.1.2 Thermoplastics 22
3.2.2 Classification Based on Reinforcements 22
3.2.2.1 Fiber reinforced composites 22
3.2.2.1.1 Glass Fibers 23
3.2.2.1.2 Carbon Fibers 24
3.2.2.1.3 Aramid Fibers 24
3.2.2.2 Hybrid composites 25

CHAPTER FOUR NUMERICAL SIMULATION OF BALLISTIC IMPACT 26

4.1 Ballistic Impact Setup 26
4.2 Finite Element Simulation 27
4.2.1 Explicit Dynamic 28
4.2.1.1 Lagrangian Approach 28
4.2.2 Material Models 28
4.2.2.1 Ceramic 29
4.2.2.2 Composite 31
4.2.2.2.1 Mat22 31
4.2.2.2.2 Mat59 33
4.2.2.3 Projectile 35
4.2.3 Mechanical Properties and Model Parameters of Structures 37
4.2.3.1 Ceramic 37
4.2.3.2 Composite 37
4.2.3.3 Projectile 38
4.2.4 Geometry of Structures 39
4.2.4.1 Ceramic Front Layer 40
4.2.4.2 Backing Plate Composites 41
4.2.4.3 Projectile 41
4.2.5 Element Types and Meshes 42
4.2.6 Combination of Target Placing 44
4.2.7 Boundary Conditions 46
4.2.8 Initial Conditions 47
4.2.9 Contacts 48
4.2.10 Hourglass 48
4.2.11 Time Step 48

CHAPTER FIVE NUMERICAL RESULTS 49

5.1 Verification of Model 49

5.1.1 Reference 1: Finite Element Simulation of Ceramic/Composite Armor under Ballistic Impact (S. Feli, M.R. Asgari, 2011) 49
5.1.1.1 Preparation 49
5.1.1.2 Results and Comparison 51
5.1.2 Reference 2: Finite Element Simulation of Ballistic Impact on Composite Plates (Berk, 2014) 53
5.1.2.1 Preparation 53
5.1.2.2 Results and Comparison 54
5.2 Numerical Results for Present Study 56
5.2.1 Numerical Results of Case 1: 6 mm Alumina Ceramic Front Faced Targets 56
5.2.2 Numerical Results of Case 2: 8 mm Alumina Ceramic Front Faced Targets 62
5.2.3 Numerical Results of Case 3: 10 mm Alumina Ceramic Front Faced Targets 68

CHAPTER SIX CONCLUSIONS AND RECOMMENDATIONS 77

REFERENCES 80

APPENDICES 87

LIST OF FIGURES

Page

Figure 2.1 Armor for man and horse, Bavaria, Germany about 1480 10
Figure 2.2 Development of armor in Europe through to centuries 11
Figure 2.3 British Challenger tank 12
Figure 3.1 The importance of materials according to years 14
Figure 3.2 Usage of ceramics in industries (a) Silicon nitride ceramic bearing balls, (b) alumina electrical insulators 15
Figure 3.3 Classification and definition of ceramics 16
Figure 3.4 Application fields of some advanced ceramics 18
Figure 3.5 Material distribution used to construct the Boeing 787 Dreamliner..... 20
Figure 3.6 Classification composite materials based on Matrix Materials 21
Figure 3.7 Classification of composite materials based on reinforcements..... 22
Figure 3.8 Glass fiber..... 23
Figure 3.9 Carbon fiber..... 24
Figure 3.10 Aramid fiber..... 24
Figure 3.11 Carbon-aramid hybrid..... 25
Figure 4.1 Test range configuration..... 26
Figure 4.2 Lagrangian meshes of normal and deformed material 28
Figure 4.3 Display of JH-2 Model card (Mat 110) in LS-Dyna preprocessor 29
Figure 4.4 Display of Composite Damage Model card (Mat22) in LS-Dyna preprocessor 31
Figure 4.5 Display of Composite Failure Solid Model card (Mat59) in LS-Dyna preprocessor 33
Figure 4.6 Display of Johnson Cook Model card (Mat15) in LS-Dyna preprocessor 35
Figure 4.7 Display of Simplified Johnson Cook Model card (Mat98) in LS-Dyna preprocessor 36
Figure 4.8 Isometric view of Ballistic Test Model Geometry 39
Figure 4.9 Isometric view of quarter Geometry model..... 40
Figure 4.10 Front view of quarter ceramic geometry 40

Figure 4.11 Front view of quarter composite geometry 41
Figure 4.12 Isometric view of quarter composite geometry 42
Figure 4.13 Front view of quarter geometry mesh 43
Figure 4.14 Zoomed in ceramic front view of quarter geometry mesh 43
Figure 4.15 Right view of quarter geometry mesh 44
Figure 4.16 Bottom view of quarter geometry mesh 44
Figure 4.17 View of the 3 different ceramic thickness, (Case 1) 6 mm, (Case 2) 8 mm, (Case 3) 10 mm 45
Figure 4.18 Isometric view of quarter geometry's symmetry planes 46
Figure 4.19 Isometric view of quarter geometry's fixed nodes 47
Figure 5.1 View of Feli and Asgari's quarter model, (a) front view, (b) bottom view 50
Figure 5.2 View of Feli and Asgari's quarter model after 1200m/s strike velocity, (a) t=0 ms, (b) t=0.04 ms, (c) t=0.078 ms 52
Figure 5.3 Velocity versus Time curve for 1250 m/s strike velocity of validation study 52
Figure 5.4 Front view of Berk's quarter model, (a) Aramid/epoxy, (b) Carbon-aramid/epoxy 53
Figure 5.5 Bottom view of Berk's quarter model, (a) Aramid/epoxy, (b) Carbon-aramid/epoxy 54
Figure 5.6 View of Berk's quarter model after impact (a) 852 m/s strike velocity for Aramid/epoxy, (b) 850 m/s strike velocity for Carbon-aramid/epoxy 55
Figure 5.7 Velocity versus Time curve for 852 m/s strike velocity for Aramid/epoxy and 850 m/s strike velocity for Carbon-aramid/epoxy of validation study 55
Figure 5.8 Strike velocity versus residual velocity of projectile on 16 mm thickness target model with all used backing plates 57
Figure 5.9 Views of 16 mm thickness target model with Aramid/epoxy backing plate after 800 m/s strike velocity, (a) t=0 ms, (b) t=0.025 ms, (c) t=0.05 ms, (d) t= 0.05 ms without projectile view 58

Figure 5.10 View of 16 mm thickness target model with Carbon-aramid/epoxy backing plate after 800 m/s strike velocity, (a) t=0 ms, (b) t=0.025 ms, (c) t=0.05 ms, (d) t= 0.05 ms without projectile view..... 58
Figure 5.11 View of 16 mm thickness target model with S2 glass/epoxy backing plate after 800 m/s strike velocity, (a) t=0 ms, (b) t=0.025 ms, (c) t=0.05 ms, (d) t= 0.05 ms without projectile view 59
Figure 5.12 View of 16 mm thickness target model with Hybrid 1 backing plate after 800 m/s strike velocity, (a) t=0 ms, (b) t=0.025 ms, (c) t=0.05 ms, (d) t= 0.05 ms without projectile view 59
Figure 5.13 View of 16 mm thickness target model with Hybrid 2 backing plate after 800 m/s strike velocity, (a) t=0 ms, (b) t=0.025 ms, (c) t=0.05 ms, (d) t= 0.05 ms without projectile view 60
Figure 5.14 View of 16 mm thickness target model with Hybrid 3 backing plate after 800 m/s strike velocity, (a) t=0 ms, (b) t=0.025 ms, (c) t=0.05 ms, (d) t= 0.05 ms without projectile view 60
Figure 5.15 Comparison of Velocity versus Time curve of 16 mm thickness target model with all used backing plates at 800 m/s strike velocity 61
Figure 5.16 Strike velocity versus residual velocity of projectile on 18 mm thickness target model with all used backing plates 63
Figure 5.17 View of 18 mm thickness target model with Aramid/epoxy backing plate after 800 m/s strike velocity, (a) t=0 ms, (b) t=0.03 ms, (c) t=0.06 ms, (d) t= 0.06 ms without projectile view 63
Figure 5.18 View of 18 mm thickness target model with Carbon-aramid/epoxy backing plate after 800 m/s strike velocity, (a) t=0 ms, (b) t=0.03 ms, (c) t=0.06 ms, (d) t= 0.06 ms without projectile view..... 64
Figure 5.19 View of 18 mm thickness target model with S2 glass/epoxy backing plate after 800 m/s strike velocity, (a) t=0 ms, (b) t=0.03 ms, (c) t=0.06 ms, (d) t= 0.06 ms without projectile view 64
Figure 5.20 View of 18 mm thickness target model with Hybrid 1 backing plate after 800 m/s strike velocity, (a) t=0 ms, (b) t=0.03 ms, (c) t=0.06 ms, (d) t= 0.06 ms without projectile view 65

Figure 5.21 View of 18 mm thickness target model with Hybrid 2 backing plate after 800 m/s strike velocity, (a) t=0 ms, (b) t=0.03 ms, (c) t=0.06 ms, (d) t= 0.06 ms without projectile view 65
Figure 5.22 View of 18 mm thickness target model with Hybrid 3 backing plate after 800 m/s strike velocity, (a) t=0 ms, (b) t=0.03 ms, (c) t=0.06 ms, (d) t= 0.06 ms without projectile view 66
Figure 5.23 Comparison of Velocity versus Time curve of 18 mm thickness target model with all used backing plates at 800 m/s strike velocity 66
Figure 5.24 Strike velocity versus residual velocity of projectile on 20 mm thickness target model with all used backing plates 69
Figure 5.25 View of 20 mm thickness target model with Aramid/epoxy backing plate after 800 m/s strike velocity, (a) t=0 ms, (b) t=0.05 ms, (c) t=0.1 ms, (d) t= 0.1 ms without projectile view 69
Figure 5.26 View of 20 mm thickness target model with Carbon-aramid/epoxy backing plate after 800 m/s strike velocity, (a) t=0 ms, (b) t=0.05 ms, (c) t=0.1 ms, (d) t= 0.1 ms without projectile view 70
Figure 5.27 View of 20 mm thickness target model with S2 glass/epoxy backing plate after 800 m/s strike velocity, (a) t=0 ms, (b) t=0.05 ms, (c) t=0.1 ms, (d) t= 0.1 ms without projectile view 70
Figure 5.28 View of 20 mm thickness target model with Hybrid 1 backing plate after 800 m/s strike velocity, (a) t=0 ms, (b) t=0.05 ms, (c) t=0.1 ms, (d) t= 0.1 ms without projectile view 71
Figure 5.29 View of 20 mm thickness target model with Hybrid 2 backing plate after 800 m/s strike velocity, (a) t=0 ms, (b) t=0.025 ms, (c) t=0.05 ms, (d) t= 0.05 ms without projectile view 71
Figure 5.30 View of 20 mm thickness target model with Hybrid 3 backing plate after 800 m/s strike velocity, (a) t=0 ms, (b) t=0.05 ms, (c) t=0.1 ms, (d) t= 0.1 ms without projectile view 72
Figure 5.31 Comparison of Velocity versus Time curve of 20 mm thickness target model with all used backing plates at 800 m/s strike velocity 72
Figure 5.32 Residual velocity of projectile versus thickness of ceramic curve with all used backing plates at 700 m/s strike velocity 74

Figure 5.33 Residual velocity of projectile versus thickness of ceramic curve with all used backing plates at 750 m/s strike velocity 75
Figure 5.34 Residual velocity of projectile versus thickness of ceramic curve with all used backing plates at 800 m/s strike velocity 75
Figure 5.35 Residual velocity of projectile versus thickness of ceramic curve with all used backing plates at 850 m/s strike velocity 76

LIST OF TABLES

Page

Table 4.1 Armor types and test ammunitions 27
Table 4.2 Mechanical parameters for 99.5% purity Alumina ceramic in JH-2 37
Table 4.3 Mechanical parameters for composite materials 38
Table 4.4 Mechanical parameters for 4340 Steel 39
Table 4.5 Layer numbers of composite materials in 10 mm thickness 41
Table 4.6 All combination of targets 45
Table 4.7 Initial velocity of projectile for each combinations 47
Table 5.1 Mechanical properties of Twaron (CT1000, 1680dtex/1000f) composite 50
Table 5.2 Mechanical parameters for tungsten alloy projectile in Johnson–Cook Model and the Mie–Gruneisen equation of state 51
Table 5.3 Comparison between residual velocities of reference versus residual velocity of present study 51
Table 5.4 Mechanical parameters for 4340 Steel 54
Table 5.5 Comparison between residual velocities of reference versus residual velocity of present study for Carbon-aramid/epoxy 54
Table 5.6 Comparison between residual velocities of reference versus residual velocity of present study for Aramid/epoxy 55
Table 5.7 Strike velocities and residual velocities of projectile on 16 mm thickness target model with all used backing plates 56
Table 5.8 Strike velocities and residual velocities of projectile on 18 mm thickness target model with all used backing plates 62
Table 5.9 Strike velocities and residual velocities of projectile on 20 mm thickness target model with all used backing plates 68

CHAPTER ONE
INTRODUCTION

The necessity of composite structures has been raised due to their high stiffness to weight and high strength to weight ratios. Therefore, composites are used in industries such as aerospace, automotive, military and many other fields in the past decades.

Ballistic protection is the one of the usage of composites in military field. Thanks to their light weight, composites are preferred for aircrafts, tanks and bullet proof body armors.

When the difficulty and expense of implementing the right composite material is considered, using computer programs is more logical for testing.

Sánchez-Gálvez & Díaz-Rubio (1998) investigated the ballistic performance of Alumina/Kevlar 29 in derivative thickness and areal density ratios with 3 different projectile types which were 7.62 AP 12.7 AP and 14.5 API. AUTODYN-2D and Chocron-Gálvez were used as the numerical solver and analytical model, respectively. Numerical, analytical and experimental results are compared and it was found similar results at three of them. It was specified that optimal design of ceramic/composite armor.

Benloulo & Sánchez-Gálvez (1998) developed a new analytical model of ceramic/composite structures on ballistic performance. Results were compared with both numerical study which was modelled in AutoDyn-2D and experimental study. In this study, analytical solution is almost in good agreement with the numerical and the experimental studies. However, when the initial velocity of projectile was close to ballistic limit of structure, analytical model was not working properly.

Zaera, Sánchez-Sáez, Pérez-Castellanos & Navarro (2000) studied the effect of the derivative thickness of adhesive layer between ceramic and metal layers on ballistic limit. Two different adhesive materials were used. These were polyurethane and

rubber-modified epoxy resin. Both experimental and numerical solutions were used. As a solver, AUTODYN-2D code was used. At the end of the work, it was shown that the adhesive that is applied between ceramic and metal layers should be reduced in thickness as much as possible to avoid side effects.

Roeder, Sun (2001) worked on ballistic impact on alumina/aluminum laminates in variable thickness, placement and temperature combination. In this study experimental and numerical methods were used. As a numerical solver, ABAQUS/Explicit code was used and results have been found good agreement with experimental data. It was observed that yield strength of the aluminum layers was effective on ballistic performance of the structure. Thicker layers also gave much better results than thinner layers which were in the same total thickness.

Gama, Bogetti, Fink, Yu, Claar, Eifert & Gillespie (2001) studied on new integrated armor design by using experimental and numerical method. Three different specimens were created except for the base line specimen to investigate the defining placement importance of aluminum foam. Eight-node solid model was chosen for modelling in LS-DYNA explicit solver. Aluminum foam was modelled by using, Type26_Mat_Honeycomb. Projectile and ceramic were modelled by Type3_Mat_Plastic_Kinematic and S2_glass/Vinyl-ester composite backing plate was modelled by Type59_Mat_Composite_Failure_Solid. It was found that after experiment and simulation of new aluminum foam which is known with lightweight-ballistic performance ratio, integrated armor design will take its place in the future usage.

Lee & Yoo (2001) worked on ballistic performance of ceramic/metal composite armor with using both numerically and experimentally. ANSYS-AUTODYN hydro-code solver was used for processor. Also, SPH element modelling was used instead of Lagrangian and Eulerian elements method. Thickness of layers was set by using Hetherington (1992) Optimization Equation method. Similar results were found with both numerical and experimental studies.

Fawaz, Zheng & Behdinan (2004) studied on normal and 30º oblique impact of ceramic/composite armor in finite element method by using Ls-Dyna explicit solver. Ceramic and 7.62 AP projectile was modelled in Mat_Plastic_Kinematic, composite was modelled in Mat_Composite_Failure_Solid. It was demonstrated that in oblique impact, the force applied by the projectile where effects on the ceramic face and the interface between ceramic and composite, was smaller than the normal impact one. Furthermore, erosion on the oblique impacted projectile was higher than normal impacted one.

Lopez-Puente, Arias, Zaera & Navarro (2005) studied ballistic limits of on the thickness effect of adhesive layer in ceramic/metal armor, both experimentally and numerically. As numerical solver AUTODYN-2D was used in Lagrangian element method and mechanical properties of epoxy resin and aluminum were used from Ansys library. Also mechanical properties of Alumina and 7.62 AP tungsten carbide core were used from Cortes et al. model (1992). After the study was done, it was observed that many thickness effect of adhesive layer.

Azevedo & Alves (2007) studied the bird strike on an airplane simulation. LS-DYNA-3D finite element solver was used for analytical model. Bird was modelled as a soft striker in Mat_Null and Eos_Linear_Polynomial and ALE (Arbitrary Lagrangian-Eulerian) element method have been used. The analytical results were in good agreement with the experimental results.

Übeyli, Yıldırım & Ögel (2008) worked on the laminated alumina/aluminum composite structure. Derivative thickness ratios and sequences of layers and also different adhesives which are epoxy and polyurethane were investigated on the ballistic performance. 7.62×51mm AP projectile was used in low velocity impact. As the result of this study, it was understood that alumina should be preferred as the front layer and optimum thickness ratio depends on the areal density ratio which is in the range of 1 to 3 of alumina and aluminum. In addition, there was no effect of adhesive which was used on the ballistic limit but the usage of polyurethane was very effective

against the epoxy in the prevention of debonding and spalling of the ceramic plates from the aluminum backing plate.

Shokrieh & Javadpour (2008) modelled the B_4C/Kevlar49 epoxy composite structure to investigate difference of oblique and normal ballistic impacts. Model is created with Ls-Dyna explicit solver. Thickness of structure was determined from Hetherington equation. This study was compared with Chocron–Gálvez analytical model to verify accuracy. At the end of the work, it was shown that the ballistic limit of composite structure increases when oblique impact is applied to composite structure.

Talib, Abbud & Mustapha (2011) studied on high velocity ballistic impact on composites which were woven Kevlar-29/epoxy and Al_2O_3 powder/epoxy both theoretically and experimentally. It was observed that changing the thickness and the placement of the composite have an effect on the ballistic limit and the absorbed energy which have a dependence on the loss of kinetic energy of the projectile. Theoretical and experimental results were in good agreement. The results of the study have demonstrated that the ballistic limit increases when thickness increases and also when using cross–ply laminated placing instead of unidirectional laminated placing on composite.

Feli, Yas & Asgari (2011) developed a new analytical model for ceramic/multilayered composites and flat-faced cylindrical projectiles. In this study Zaera–Sanchez-Gálvez analytical model which, with the help of the conoid fragmentation angle of ceramic, was used to improvement on the Chocron– Gálvez numerical and analytical model. Results were much better than Chocron– Gálvez analytical model when the initial velocity of projectile is close to ballistic limit of the structure.

Feli & Asgari (2011) modelled 2D-axisymmetric model of ceramic front faced composite armor. Simulation was modelled in LS-DYNA-2D with using Lagrangian elements method. Cylindrical tungsten projectile was modelled with Johnson-Cook

and EOS_MIE_GRUNEISEN, Twaron aramid composite layers were modelled with MAT_COMPOSITE_DAMAGE and alumina ceramic was modeled with the Johnson-Holmquist (JH-2). Study was compared with Chocron-Gálvez numerical and analytical model results were found good agreement. At the end of the study, it was shown that when the impact velocity of projectile increases on the ceramic face, the fracture behavior of ceramic tile changes. Moreover, impact velocity of projectile is close to ballistic limit of the structure and delamination between composite layers decreases.

Tasdemirci, Tunusoglu & Güden (2012) considered effects of various interlayers of Ceramic/S2-Glass-SC15 epoxy composite on the ballistic impact. LS-DYNA explicit solver was used as the numerical solver. In modelling, the Johnson-Cook was used for the 7.62 mm M61 type AP projectile, the Johnson-Holmquist (JH2) was used for the ceramic, MAT_COMPOSITE_DMG_MSC which is based on the Hashin's failure criteria was used for composite, the MAT_HONEYCOMB was used for Aluminum foam, MAT_CRUSHABLE_FOAM was used for the Teflon, MAT_PIECEWISE_LINEAR_PLASTICITY was used for Polyester mold and MAT_OGDEN_RUBBER was used for Rubber material. Good agreement with both numerical and experimental study was observed. As a result of this study, it was found that Teflon and aluminum foam interlayers gave better results for ballistic performance which are reduced stress and delayed stress distribution to composite instead of rubber interlayer and without interlayer.

Şevkat (2012) worked to define ballistic limits of composite beams which were consisted S2Glass/SC-79, IM7-Graphite/SC-79 and hybrid S2Glass/Graphite/SC-79, experimentally and numerically. For numerical analysis Ls-Dyna code was used. After simulation results are similar to experiment, Lambert-Jones parameters and ballistic limits of composite beams are determined.

Grujicic, Pandurangan & d'Entremont (2012) modeled a hybrid armor which contained ceramic and polymer matrix composites in ABAQUS/Explicit code to

investigated role of the adhesive on ballistic limit. Analytical model was compared with Zaera et al model (2000) and results were found similar.

Liaghat, Shanazari, Tahmasebi, Aboutorabi & Hadavinia (2013) developed a new analytical solution for laminated alumina ceramic as front plate and Al6061-T6 aluminum as backing plate for variable thicknesses based on Woodward (1990) analytical model. Projectile was modeled as 8.3gr 7.62 AP steel and was considered in 3 phases that were erosion, mushrooming and rigid for deformation behavior of ceramic cone's semi-angle. The study was good agreement with other same analytical models and experiments.

Mobasseri, Ansari, Zarei, Sedighi & Mobasseri (2013) studied thickness optimization on ballistic performance of ceramic/composite and ceramic/aluminum structures. Ls-DYNA explicit solver was used for numerical solution. Results were compared with to previous optimization studies by Wang, Ben Dor and Hetherington. Optimum thickness of ceramic/composite and ceramic/aluminum armors were specified with their best fit light weight/energy absorption ratio.

Hajheydari & Eftekhari (2014) modeled the ballistic impact of ceramic/composite armor with using a 9 mm caliber blunt projectile. LS-DYNA explicit solver was used for analytical solution. Projectile was modelled with Johnson-Cook and EOS_GRUNEISEN, alumina was modeled with the Johnson-Holmquist (JH-2), and composite was modeled with MAT_COMPOSITE_DAMAGE. Hetherington equation was used to adjust thickness. Numerical study was found in good agreement with Chocron-Gálvez analytical method.

Ni, Jin & Lu (2014) studied hybrid-cored ceramic/metal sandwich plates under oblique ballistic impact in finite elements code by using ANSYS/LS-DYNA solver. AISI 304 stainless steel projectile and cage were modeled by Johnson Cook with Mie_Gruneisen EOS model, AD 98 alumina ceramic was modeled by Johnson_Holmquist (JH-2) and epoxy resin was modeled in Euler element method by Elastic_Plastic_Hydro. Other materials were modeled in Lagrangian elements method.

After simulation, it was observed that ballistic resistance depends on the angle of the impact.

Randjbaran, Zahari, Jalil & AbdulMajid (2014) worked on laminated hybrid composites. In this study, used materials were Kevlar/epoxy, carbon/epoxy and glass/epoxy laminates which were same size, even so their placements were different in the structures. At the end of the work, placements of composites were suggested.

Tawadrous, Attia, Laissy (2015) modeled alumina, (99.7% purity) ceramic and concrete layer as a shield in ANSYS-AUTODYN code. Lagrangian and SPH element methods were combined for modelling ceramic and concrete in this study. Thickness and placement of ceramic plates were changed to see what would be the depth of penetration in the armor.

Liu, Chen, Chen, Cheng, Wang, Chen, Liu, Li & Wang (2015) investigated composition of laminated Ti6Al4V alloy and UHMWPE composite layers as the backing plate of ceramic armor on the ballistic performance. ABAQUS/Explicit code was used for numerical solver. Johnson–Holmquist (JH-2) material model, Johnson–Cook material model and Hashin-Damage material model were used for ceramic, steel projectile and UHMWPE, respectively. Also Ti6Al4V alloy was modeled with Johnson–Cook. At the end of the work, Ceramic/Ti6Al4V/UHMWPE/Ti6Al4V composite armor was shown as the best among the other compositions.

Carpenter, Anderson & Chocron (2015) simulated hyper velocity impact by using mesoscale models which were S2 glass/SC-15 epoxy resin composite. Models were created in Ls-Dyna code. Simulation showed that different delamination behaviors were found in plain weave and 3D weave composites. Since there was no experimental study on this subject before, this study may lead to subsequent experiments.

Kim, Woo, Cho, Kim & Kim (2015) carried out a high velocity impact in LSDYNA3D solver and studied on laminated Carbon/Epoxy composites which were laminated derivative stacking sequences and thicknesses. In modeling, composite was

preferred MAT59 (MAT_COMPOSITE_FAILURE_SOLID) material which provides eight failure modes and projectile was preferred MAT3 (MAT_PLASTIC_KINEMATIC). The numerical study was in good agreement with the experiment. At the end of the work, it was observed that the impact area type of composite was affected by the thickness of the structure and the initial velocity of the projectile.

Liu, Zhua, Yao, Wang & Bui (2016) modeled a scalelike ceramic/composite armor inspired by grass carp. LS-DYNA explicit was used for numerical solver. Steel projectile and aluminum were used in the MAT_SIMPLIFIED_JOHNSON_COOK model which is no need to use the EOS parameters, ceramic tiles were modeled with the Johnson-Holmquist (JH-2) and Kevlar was modeled with MAT_DRY_FIBER. Simulation results showed that bio-inspired scaled armors divert the projectile to a different way and help in decreasing the kinetic energy of projectile.

Huang & Chen (2016) investigated the functionally graded Al_2O_3–ZrO_2 ceramics with backing plate as 6061-T6 Aluminum composite on ballistic impact, based on NIJ IV standards. As a solver ANSYS/Ls-DYNA explicit code was used for analytical solution. Steel part of 0.3″ AP projectile and epoxy resin were modeled with MAT_PLASTIC_KINEMATIC, copper part of projectile and 6061-T6 aluminum were modeled with MAT_ELASTIC_PLASTIC_HYDRO and EOS_GRUNEISEN was used for copper part projectile and 6061-T6 aluminum. Ceramic was modeled with Johnson Holmquist (JH2). Numerical results were good agreement experimental study. It was shown that functionally graded Al_2O_3–ZrO_2 ceramics get better results compared to pure Al_2O_3 ceramics for almost every situation at ballistic performance.

In this study, ballistic performance of alumina ceramic front faced composites which are aramid/epoxy, hybrid carbon-aramid/epoxy, S2 glass/epoxy, hybrid S2 glass-aramid/epoxy were investigated numerically. Furthermore, alumina ceramic is used in three different thicknesses. Thus, the effect of the thickness of the ceramic and effect of different reinforced composites on the ballistic performance are investigated in four different velocities.

CHAPTER TWO
HISTORY OF ARMOR

All this time since the first human, exigency of armor usage is one of the most important issue due to mankind's desire of war. Even though only primitive materials like leather, wood and bone were used to make armor before Bronze Age, the backbone of today's modern armors dates back to then, which was 35 centuries ago.

Since the earliest of times, armors improved with the development of weapons and weapons improved with the development of armors as well. Armor started to be used as personal armors in pre-metal age against blade weapons, blunt weapons and ranged weapons. Primitive armors were durable enough to protect against stick and rocks at first but with the emergence of metal in weapons, these primitive armors were no longer capable to defend against attacks. Development in armor technology is not only due to the need to make the troops more capable in larger and longer battle scenarios, but it is also as a response to the emergence of new weapons. To resist the impact of more powerful sharpened weapons, blind attacks and arrows, metal armors were made to be used for complete body protection.

Bronze plate armors which were used to protect upper body and legs, were first known metal armors and these were used in Greek Mycenaean Era about 1400 BC. Later with the analogous armors, Corinthian-style bronze helmets and wood shields strengthened with bronze were widely used not only in Greek military but also in Macedonian and Egyptian as well. Meanwhile Greek soldiers were using plate armors. Greece separated to many states which at the time, were fighting each other. China was dealing with the same issues on a larger scale for about 2000 years. Big parts of Europe, northern Africa and Middle East were conquered by Rome. In this sense, Greek, Chinese and Romans managed to be the pioneer tribes in the field of armor improvement. Roman military gained great mobility and defense by using segmented armors instead of full body metal armor or leather like Greeks, Macedonians and Egyptians. After the collapse of Roman Empire, while the new countries were being built, they were producing various new kinds of armor. With the long term warfare

especially in Medieval Europe, new kind of body armors were found. These armors used metal as material and they were worn from head to toe that weighted around 30 kg. With that much armor on them, knights were nearly unstoppable from 14th to 17th century (Figure 2.1).



Figure 2.1 Armor for man and horse, Bavaria, Germany about 1480 (Plate armor, n.d.)

Those full body armors provided great protection against sharp and ranged weapons, but they weak against blunt weapons. Also they were very expensive to produce making these kinds of armors hard to obtain. Only a few selected knights had them. Later on, with the usage of crossbows and gunpowder weapons the supremacy of full body armors had ended. With the arrival of muskets, the armor used in the battlefield became insignificant. Because melee weapons were no longer used in battlefields and high powered guns were able to penetrate even the heaviest armor pieces. Various metal armors that were created all over the world until that time were outdated and practically fell into disuse (Figure 2.2).

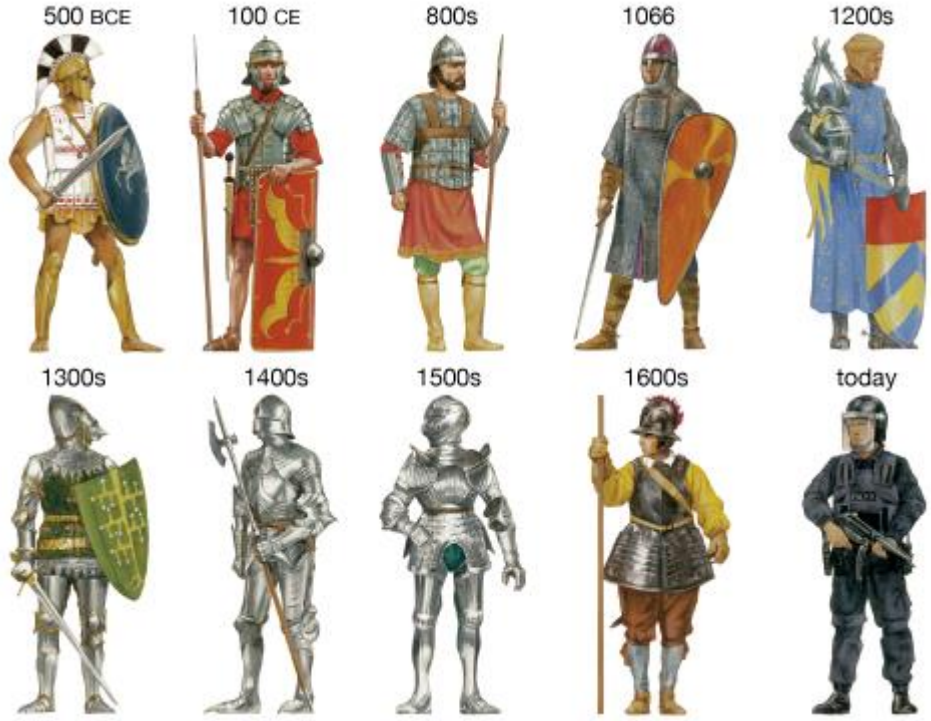


Figure 2.2 Development of armor in Europe through to centuries (Armor protective clothing, n.d.)

Importance of using personal body armors have gradually increased. This rise was slower during the course of World War I and it became a bit more in the course of World War II, but the real development was seen after advanced materials were produced industrially. Later on, resistant materials were used against bullets such as ceramic, plastic and Kevlar which are the representatives of these days' armor. Nowadays after having a body armor history which is more than 4000 years long, soldiers' and law enforcement members' primary purpose in using an armor piece is to prevent gunshot wounds. The secondary purpose is to prevent any damage from bladed weapons.

Armor development has been through ugh a big revolution in the past decades. There have been contributions from many different countries, mostly from Europe, the United States and Israel. The new, improved type of complex armors can be divided in to four categories. Reactive armor is made of blocks of explosives put between metal plates and are latched on the outer side of the vehicle. When a heavy attack such as a heat round hits the armor, the explosives will go off and reduce the effect of the attack. The opposite reaction of the explosives reduces the damage significantly. Applique

armor, on the other hand, is all about welding extra plated on top of a vehicle or the turret. The upside of this kind of armor is the reduced cost and work it requires. Laminated armor is made from layers of steel armor but it also has layers of ceramic, fiberglass and other materials. It is highly effective against any weapon, while the downside is the cost. Lastly, composite armor is made of some kind of ceramic. It is less effective than laminated armor yet it is easier to manufacture and less expensive (Armors, n.d.).

Composite armor is great at bringing a lighter and stronger option to the table. These types of armor consist of many different materials resulting in a hybrid much better than classic metal armor. For example, Chobham armor is a famous one. It is a composite armor that has ceramic between two plates of armor. This is a much more simplistic form of composite armor, yet still very effective. The Chobham armor was on the British Challenger tank and it was a huge success (Figure 2.3). While it was very successful on heavy vehicles like tanks, it is simply too heavy for lighter war machines.



Figure 2.3 British Challenger tank (Challenger 2, n.d.)

Weight is one of the four main considerations when building a protective case for war weaponry. The reduction of weight in armors almost always has a positive benefit. It reduces the strain on every part of the vehicle, making it more unlikely to malfunction. Also, some types of vehicles like aircraft, automobiles and boats require

being light in order to be fast. Hence, heavy armor would hinder the ability these vehicles are most known for, their speed. Cost and the compactness of the armor are also very important when designing the armor. Cost would be important because making the armor non-profitable would render all the other positive sides null. Compactness is also important mostly because if the armor is too large, it would make the vehicle an easy target.

Another consideration, which is most important when dealing with ceramic armor, is how the ceramic endures the first hit. The first hit is very important because it determines the vulnerability level of the composite armor. This is one of the most significant drawbacks of composite armors. The ceramic material lacks the tolerance against multiple hits. Thus, it is very important and necessary to progressively improve the formula of the ceramic materials. Ceramic materials are also nonmetallic, making them resistant against heat, abrasion, high rigidity. They are also chemically stable and low in weight. The advantage for using ceramic layers between steel armor plates is that when a high –caliber attack is made; the ceramic materials absorb the damage by fragmentation. To contain this fragmentation and reduce the deterioration rate of the armor, one or more containment layers are used. These containment layers absorb a bit of the damage and hold the fragmentation to a minimum.

While wanting to have a harder, stronger material makes sense in having a sturdy armor, it has contradictory results. The reason being is, if the material is higher in fracture toughness then it is more metal-like, meaning that it has less elasticity. Losing elasticity means the material will have a low fracture toughness value. In this matter, being prone to fractures makes the material less durable.

Armor-piercing rounds are known to be effective against hardened armors of modern day. These ammunition types have sharp hardened steel covered with a metal jacket that adds more mass for more power. The reason these armor-piercing rounds are very effective against modern armor is because composite armors simply do not have enough toughness to cause deformation on the hardened rounds. Thus, composite armors should be studied on and made to be cheaper and sturdier.

CHAPTER THREE
CLASSIFICATION OF MATERIALS AND METHOD

From the beginning of time, humankind has tried to use various materials within their own needs (Figure 3.1). When considering atomic structures of these materials, it can be classified into three categories which are metals, polymers and ceramics. Furthermore, combinations of at least two of these basic material classes create a new class which is called composite material, thus, making it easier to obtain a material with the desired properties.

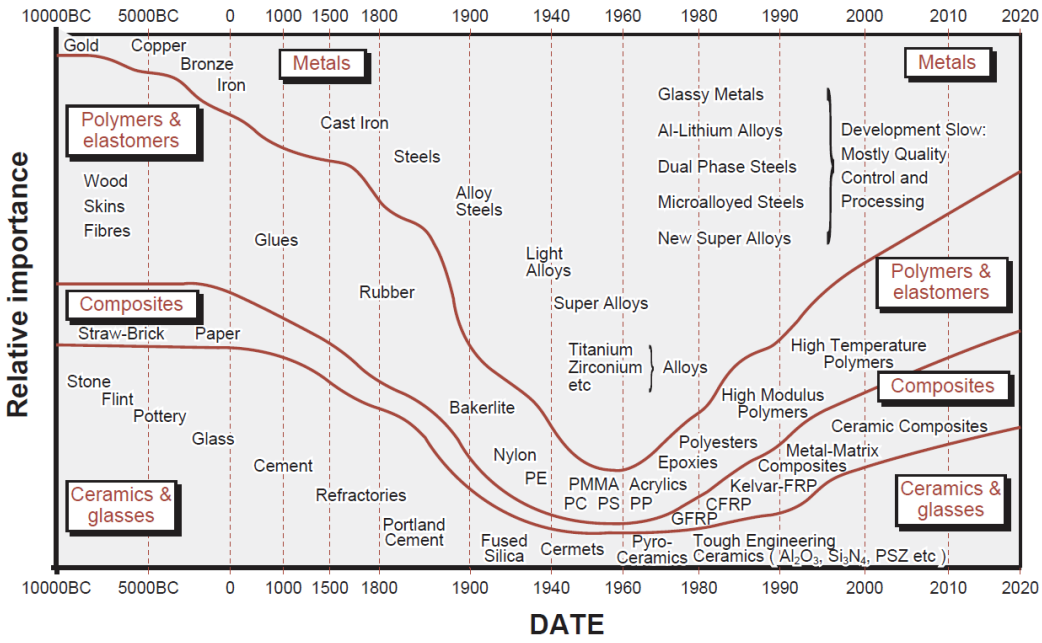


Figure 3.1 The importance of materials according to years (Ashby, 2005)

In this thesis, since ceramic and composite material classes are studied, a short brief summary of only these two material classes will be mentioned.

3.1 Ceramics

If the ceramics are defined in general, it is possible to say all materials that are not based on metallic or organic materials, are ceramics. The common characteristics of ceramic materials, bonding between of these materials atoms appear to be the covalent

and/ or ionic. Because of these strong bond classes, ceramics are commonly known as heat and corrosion resistant materials. However, this strong bonding makes material characterized in brittleness occurs, thus the smallest error in the microstructure material which can be formed, causing cracks to occur. Eventually the effect of stress, cracks leads to breakage of material (Richerson, 1992).

Ceramics are very often used in most of the engineering fields. However, most people believe that ceramics are only related to pottery and tiles. Depending on developments in manufacturing technology, especially in defense industry, mechanical and chemical industry for 40 years, ceramic materials have been used as alternative materials to metal materials (Figure 3.2). The interest in ceramics has increased so much that it has reached a market share of over 10 billion dollars.



(a) (b)

Figure 3.2 Usage of ceramics in industries (a) Silicon nitride ceramic bearing balls, (b) alumina electrical insulators (Reed, 1995)

Nowadays usage of ceramic materials is increased because of their superior properties (Reed, 1995):

High temperature resistance

High chemical stability

High Hardness

Lighter than metals

Generally cheaper than metals

No need for expensive and strategic metals

High Wear Resistance

High resistance to oxidation

Low coefficient of friction

High compressive strength

3.1.1 Classification of Ceramics

Ceramic materials can be categorized in three classes according to usage areas which are glasses traditional (conventional) ceramics and advanced (fine) ceramics (Figure 3.3).

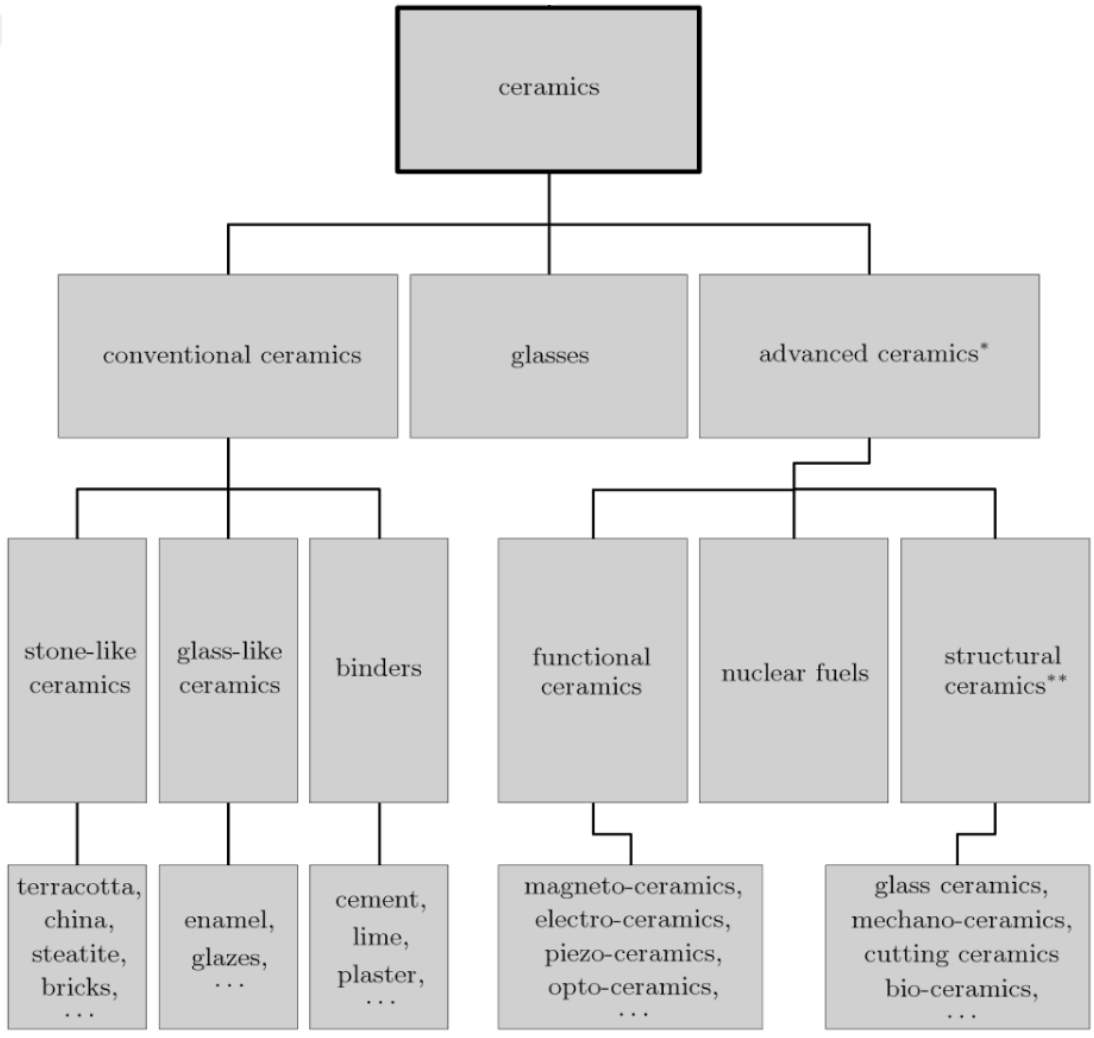


Figure 3.3 Classification and definition of ceramics *frequently noted as fine ceramics, ** frequently noted as engineering ceramics (Aldinger & Weberruss, 2010)

Traditional ceramics are based on mineral silicates, silica, and mineral oxides. They mostly consist of raw materials which are clay, cement and glass. These are clay products such as pottery and bricks, common abrasives, refractories and cement made of traditional ceramics. Glasses are based on silica and are distinguished by their non-crystalline structure. Glasses are inorganic, nonmetallic compounds that cool to a rigid condition without crystallizing. Window glasses, containers, light bulb glass, laboratory glassware are made of glasses.

3.1.1.1 Advanced ceramics

Advanced ceramics are based on oxides, carbides, etc. and generally possessing mechanical or physical properties superior or unique compared to traditional ceramics. Advanced ceramics, unlike traditional ceramics, contain purified ceramics of a kind that are purified, with well controlled internal structures and have the production process that can produce faultless microstructures (Groover, 2010). Examples of usage area of advanced ceramics are also given in Figure 3.4.

3.1.1.1.1 Structural ceramics. They are used for applications in engineering where structure is dealt with high mechanical, thermal, or chemical loads. Typical structural ceramics (Al2O3, ZrO2, Si3N4, SiC, B4C, CBN, TiC, TiB2, TiN, AlN) are used in: Wear-resistant synthetic yarn guides in textile industry, cutting ceramic tools, lightweight ballistic vest and armored vehicle protective covering, automotive engines, mining, heat exchangers (Heimann, 2010).

The structural ceramics attract everyone's attention in these days. Usage of the advanced structural ceramic increases day by day. So that market share of the advanced structural ceramic has been growing as a consequence of the increased demand for ceramic armor in personal protection and military vehicle industries. Since structural ceramics are so popular, a lot of research is being done to better understand and improve their properties. Also in this thesis, the ballistic performance of composites with front faced advanced structural ceramic Al_2O_3 will be performed with derivative thickness.

Application field	Component	Properties utilized	Advanced ceramics
Processing technology	Chemical apparatus	Corrosion resistance	Aluminum oxide
	Sliding rings	Wear resistance	Silicon carbide
	Thread guides		Titanium oxide
	Wire-drawing dies		Zirconium oxide
Shaping of materials	Cutting tools	Wear resistance	Aluminum oxide
	Grinding disks	Hardness	Silicon nitride
	Sand-blasting nozzles		Silicon carbide
			Boron carbide
High temperature	Burner nozzles	Heat resistance	Silicon nitride
	Welding nozzles	Corrosion resistance	Silicon carbide
	Heat exchanger	Heat conductivity	Aluminum oxide
	Crucibles		Carbon
	Heat pipes		Boron nitride
Engines	Valve seats	Heat resistance	Aluminum titanate
	Turbocharger	Corrosion resistance	Silicon carbide
	Gas turbine	Heat conductivity	Silicon nitride
	Catalyst support		Cordierite
	A-probe		Zirconium oxide
Electronics, electrical engineering, optics	Substrates	Special electrical and magnetic properties	Aluminum oxide
	Capacitors		Titanate perovskites
	Sensors		Ferrites
	Laser materials		
	Magnets		
Energy technology	Nuclear fuel	Radiation resistance	Uranium oxide
	Solid-state electrolyte	Ionic conductivity	Zirconium oxide
			β-Aluminum oxide
Medical technology	Hip joints	Mechanical resistance	Aluminum oxide
	Bone replacement	Surface finish	Calcium phosphate
		Biocompatibility	

Figure 3.4 Application fields of some advanced ceramics (Heimann, 2010)

3.2 Composites

Technology has come to such a state that the properties of traditional metal, polymer and ceramic materials that we used in the past, have become unable to meet the requirements in their places of use. This situation necessitated the development one of the advanced material which is composite material. Composite materials are called new materials that are consisted by combining at least two different materials in such a way that they do not dissolve in each other. The reason composite materials get such an important place in engineering is that we can obtain much better materials with a better combination of the properties of each material. Thus, thanks to the generated composite materials, many of the unused materials are now being used in extended and varied industries (Callister, 2007).

Composite means a mixture but it does not consist of solvated and solvent components. Composite components are chemically unaffected. If the mixture is at the level of particles at the nanometer level, such composites are called nanocomposites. Composite materials can be developed for each desired feature and property. So it is not possible to make a definite judgment on the properties of the composite material. However, the usage of composite materials can be generalized with some features (Zor, 2017):

High strength/density ratio (Specific Strength)
High stiffness/density ratio (Specific Stiffness)
Lightness
High Dielectric Resistance
High Corrosion resistance
Diversity
Easy molding
Color variety
Transparency Feature
Non-combustibility
Thermal resistance
Reparability

Flexibility

Impermeability

With developments in composite material technology, composites are beginning to be used increasingly in industry and technology applications. This technology is especially used in aircraft industry and in many other sectors which could be exemplified as aerospace industry, transportation, mechanical industry, sporting goods, automotive and construction industry. The development and research of composites in these industries have been continuing intensively (Figure 3.5). The usage of composite materials in the defense industry is increasing day after day. In the defense industry, traditionally used steel armor has slowly left its place to the lighter composite armor. Helmets, armor for light vehicles, spall liners and add-on armor for military vehicles can be given as examples.

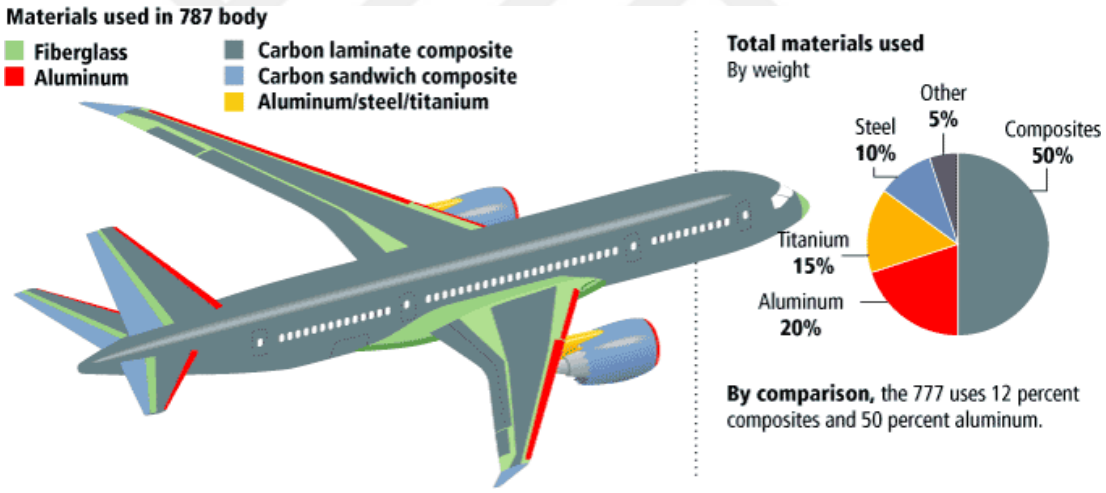


Figure 3.5 Material distribution used to construct the Boeing 787 Dreamliner (Boeing 787 Dreamliner, n.d.)

Generally, the composites consist of matrix and reinforcement elements and they can be classified as two different categories based on matrices and reinforcements.

3.2.1 Classification Based on Matrix Materials

Matrix materials have the adhesive and adhesive properties. The function of the matrix in a composite structure is to keep the fibers together and to transmit applied load between fibers. Composites are divided to four different categories according to matrix (Figure 3.6). In this thesis, polymer matrix composites will be examined. Hence, only polymer matrix composite will be explained in classification in matrices.

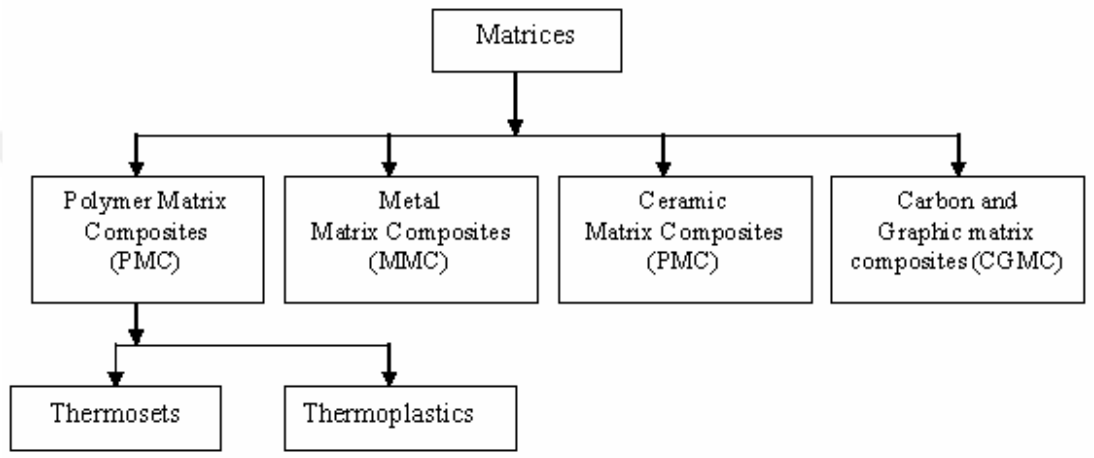


Figure 3.6 Classification composite materials based on Matrix Materials (Composite materials lecture notes, n.d.)

3.2.2.1 Polymer Matrix Composites

Nearly most of all the composite materials are polymer based matrices. Manufacturing of these polymer matrix composites are simpler and have lower production costs compared to other matrix composites which are ceramic and metal matrix composite. Polymers can be grouped as follows:

3.2.2.1.1 Thermosets. There are three-dimensional strong Vander Waals bonds between the molecules. So they are rigid structures. The thermosets after they have been formed and the material can no longer soften or deform with the effect of temperature. The most common thermosetting resins are: Polyester, Vinyl Ester, Epoxy, Phenolic and Silicone.

3.2.2.1.2 Thermoplastics. There is a weak Vander Waals bond between the molecules. For this reason, they are soft compared to thermoplastics. They can form new shapes with the effect of heat. The common thermoplastic resins are: polypropylene, polyethylene, polyether ether ketone and polycarbonate.

3.2.2 Classification Based on Reinforcements

Reinforcement materials determine the strength and load carrying capability of the composite structure. There are two different categories of composites according to reinforcements (Figure 3.7).

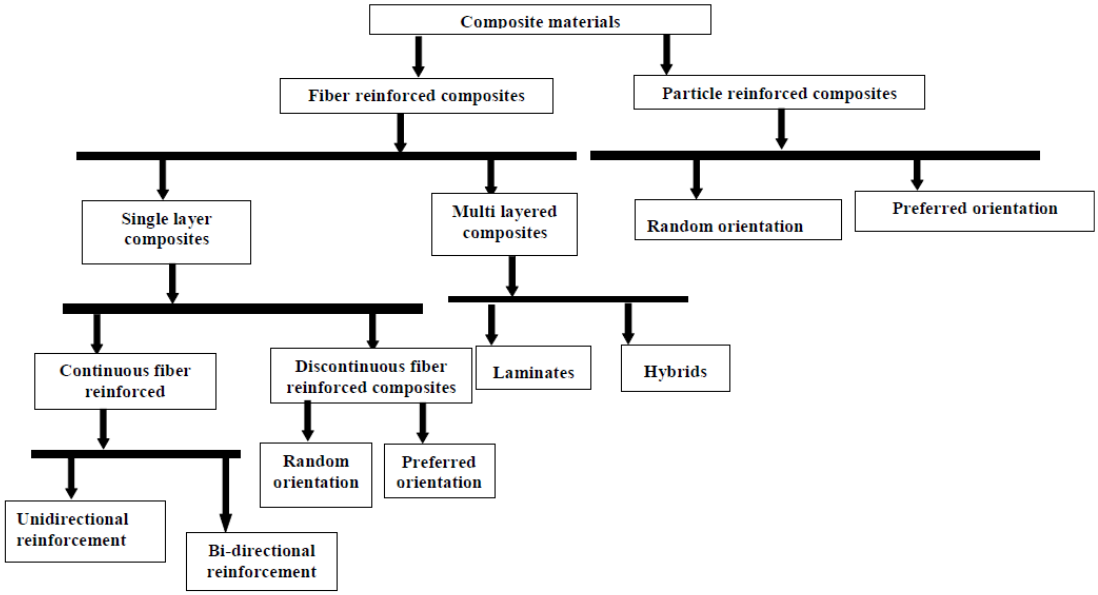


Figure 3.7 Classification of composite materials based on reinforcements (Mishra, 2011)

3.2.2.1 Fiber reinforced composites

Usually, fiber reinforced composites are prepared with thin circular shaped fibers. Fibrous composites are anisotropic materials. Properties of fibrous composites may change by desired feature due to direction, orientation, thickness and layers' number of fibers.

In this thesis, glass fibers, carbon fibers and aramid fiber were used as reinforcements. Also combination of these fibers that is hybrid reinforced fibers are formed with different methods.

3.2.2.1.1 Glass Fibers. Glass fibers are used more often than the other fibers mostly because of the reason that they are cheaper (Figure 3.8). Glass fibers are largely used in automotive and marine bodies, plastic pipes, containers. There are different types of glass fibers according to their properties and composition:

A-Glass: High Alkali Rate-Low Cost
C-Glass: Chemical Resistance
E-Glass: Electrical Specifications
L-Glass: Contains Lead Against Radiation
M-Glass: High Elastic Modulus
S2Glass: High Tensile Strength
W-2Glass: Semi Transparent For Panels
Ar-Glass :Alkali Resistance
R-Glass: High Tensile Strength



Figure 3.8 Glass fiber (DostKimya products, n.d.)

3.2.2.1.2 Carbon Fibers. Carbon fibers are widely used in advanced composite materials instead of glass fibers(Figure 3.9). The reason being is that carbon fibers have various advantages than glass fibers. It can be said that these advantages are higher tensile strength, higher thermal conductivity, higher wear resistance, higher fatigue strength. They are largely used in aerospace and automotive indusry.

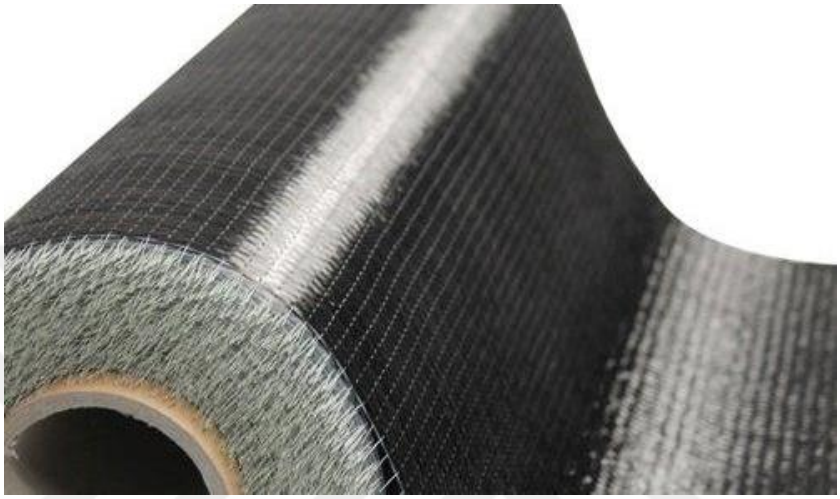


Figure 3.9 Carbon fiber (DostKimya products, n.d.)

3.2.2.1.3 Aramid Fibers. The aramid fibers have better properties which are high durability and high impact strength compared to glass fibers, and they are also 35% lighter than glass fibers (Figure 3.10). Aramid fibers are used in space, marine, automotive and especially defence industry.



Figure 3.10 Aramid fiber (DostKimya products, n.d.)

3.2.2.2 Hybrid composites

In general, hybrid composites can be practically described as: A single matrixed composite structure contains at least two different types of reinforcements or a single reinforced composite structure contains at least two different type of matrices. Even so, most commonly used ones are single matrixed and multiple reinforcement composites. As is understood, hybrid composites are complicated structures though it allows us to change many mechanical properties and make possible for the development of new types of composite structures (Figure 3.11).

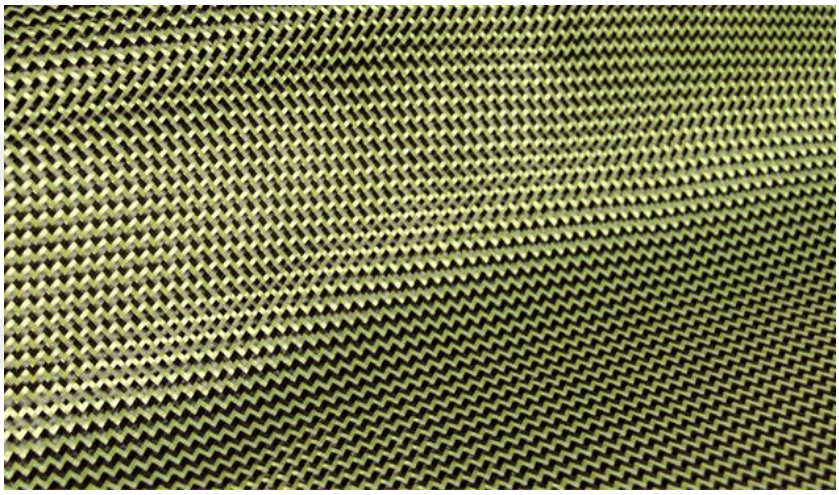


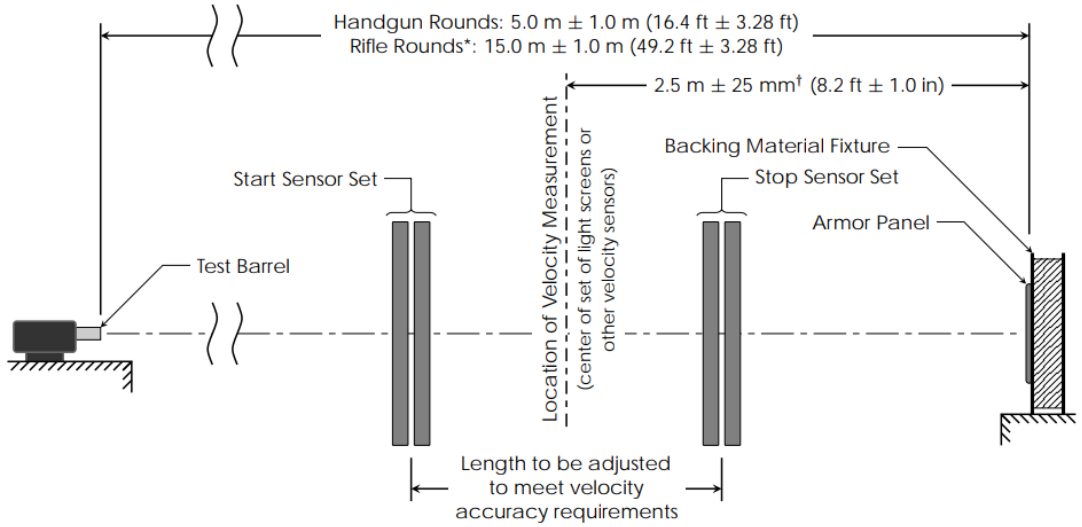
Figure 3.11 Carbon-aramid hybrid (DostKimya products, n.d.)

CHAPTER FOUR
NUMERICAL SIMULATION OF BALLISTIC IMPACT

4.1 Ballistic Impact Setup

Day after day, development of weapon industry, importance of the ballistic tests is rising. Purpose of the tests is examining response of ballistic impact loads of materials. Improvement of armor is a necessity due to developing and changing bullet kinds. There are many ammunition types. That's why there are various classifications. Among all, the most common is American NIJ (National Institute of Justice). There are experiments on different personal body armors with different bullet types as shown on Table 4.1 (I, II, IIA, III, IIIA and IV).

Generally, these tests are completed with distance adjustments according to used bullets types as shown in Figure 4.1.



*For rifle rounds the length may be further adjusted to minimize yaw at impact; however, in such cases the yaw at impact must be experimentally shown to be less than 5° and reasonably close to minimal.
†Tolerance for 0° shots. For 30° and 45° shots the tolerance shall be + 25 mm/- 190 mm (+ 1.0 in/- 7.5 in).

Figure 4.1 Test range configuration (NIJ Standard-0101.06 National Institute of Justice, 2005)

Table 4.1 Armor types and test ammunitions (NIJ Standard 0108.01 National Institute of Justice, 1985)

Armor Type	Test Ammunition	Nominal Bullet Mass	Suggested Barrel Length	Required Bullet Velocity	Required Hits Per Armor Specimen	Permitted Penetrations
I	22 LRHV Lead	2.6 g 40 gr	15 to 16.5 cm 6 to 6.5 in	320 ±12 m/s 1050 ±40 ft/s	5	0
	38 Special RN Lead	10.2 g 158 gr	15 to 16.5 cm 6 to 6.5 in	259 ±15 m/s 850 ±50 ft/s	5	0
II-A	357 Magnum JSP	10.2 g 158 gr	10 to 12 cm 4 to 4.75 in	381 ±15 m/s 1250 ±50 ft/s	5	0
	9 mm FMJ	8.0 g 124 gr	10 to 12 cm 4 to 4.75 in	332 ±12 m/s 1090 ±40 ft/s	5	0
II	357 Magnum JSP	10.2 g 158 gr	15 to 16.5 cm 6 to 6.5 in	425 ±15 m/s 1395 ±50 ft/s	5	0
	9 mm FMJ	8.0 g 124 gr	10 to 12 cm 4 to 4.75 in	358 ±12 m/s 1175 ±40 ft/s	5	0
III-A	44 Magnum Lead SWC Gas Checked	15.55 g 240 gr	14 to 16 cm 5.5 to 6.25 in	426 ±15 m/s 1400 ±50 ft/s	5	0
	9 mm FMJ	8.0 g 124 gr	24 to 26 cm 9.5 to 10.25 in	426 ±15 m/s 1400 ±50 ft/s	5	0
III	7.62 mm 308 Winchester FMJ	9.7 g 150 gr	56 cm 22 in	838 ±15 m/s 2750 ±50 ft/s	5	0
IV	30-06 AP	10.8 g 166 gr	56 cm 22 in	868 ±15 m/s 2850 ±50 ft/s	1	0

Abbreviations:

AP - Armor Piercing,

FMJ - Full Metal Jacket,

JSP - Jacketed Soft Point,

LRHV - Long Rifle High Velocity

RN - Round Nose,

SWC - Semi-Wad cutter

4.2 Finite Element Simulation

Finite element analysis provides less production and experiment costs in short time. Also with using finite element analysis, human errors can be prevented from production or experiments and more accurate results can be achieved.

In this study, 3D models are created and meshed by using ANSYS/LS-DYNA also LS-PREPOST preprocessor is used for make adjustments in model. Lastly, LS-DYNA explicit dynamic solver is used for processor.

4.2.1 Explicit Dynamic

Ballistic impacts are dynamic loads that occur large deformations in materials also they lead high strain rate behavior of materials. At this high strain rates, using finite element analysis (explicit dynamic code) is the best way to solve impact simulations of materials to save computational time.

4.2.1.1 Lagrangian Approach

In Lagrangian approach, coordinate system moves with material nodes. That allows no material transfer between elements when element gets deformed (Figure 4.2). Furthermore, Lagrangian approach takes shorter computational time when it compared with Eulerian. With these reasons, Lagrangian approach is the most common approach in the ballistic impact simulations and it will be used in this study too.

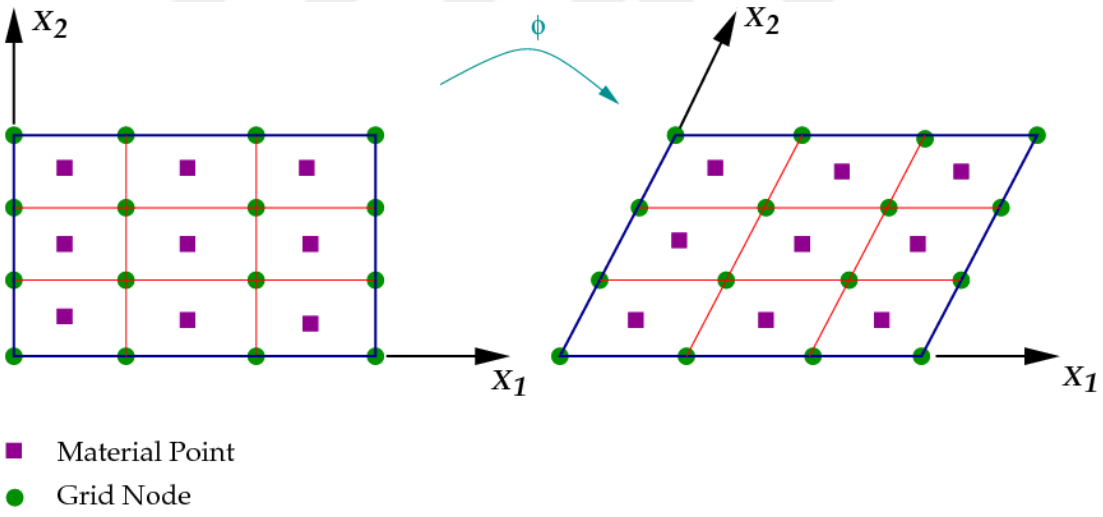


Figure 4.2 Lagrangian meshes of normal and deformed material (Lagrangian and Eulerian descriptions, n.d.)

4.2.2 Material Models

In this study, JH-2 material model is used for modelling ceramic on the front side of the target, Composite Failure Solid Model and Composite Damage Model are used

for modelling composites on the backside of the target. Johnson-Cook material model is used for modelling projectile.

4.2.2.1 Ceramic

The Johnson-Holmquist material model (JH-2) is commonly used to behavior of ceramics under ballistic impact. JH-2 material model is available in LS-DYNA explicit code as MAT 110 Johnson Holmquist Ceramics. JH-2 material model is shown in Figure 4.3. Corresponding relationships for JH-2 ceramics is demonstrated in the following equations (Ls-Dyna Keyword User's Manual, 2015).

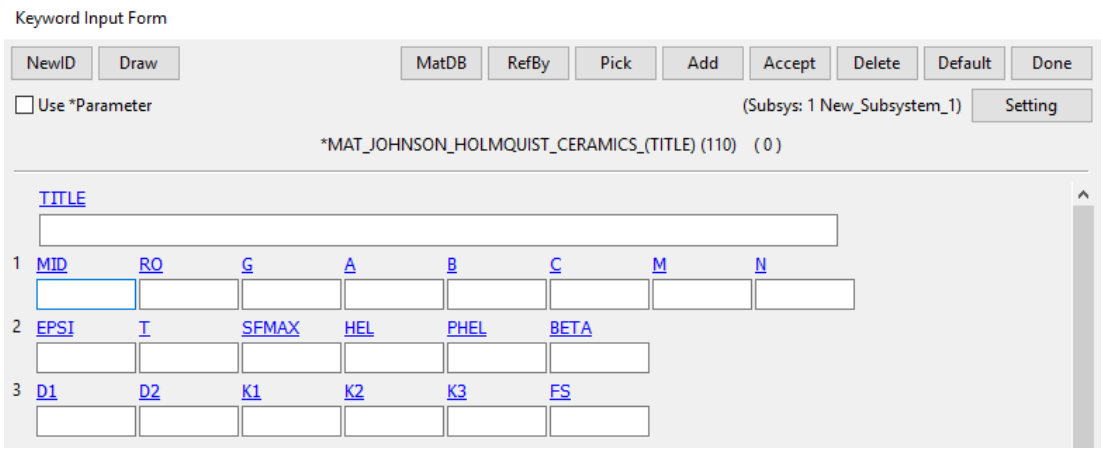


Figure 4.3 Display of JH-2 Model card (Mat 110) in LS-Dyna preprocessor

The equivalent stress is given by

$$\sigma^{*}=\sigma_i^{*}-D\left(\sigma_i^{*}-\sigma_f^{*}\right) \tag{4.1}$$

normalized effective stress equations are shown in equation (4.2) and equation (4.3)

$$\sigma_i^{*}=A\left(P^{*}+T^{*}\right)^{N}\left(1+C\ln\dot{\varepsilon}^{*}\right) \tag{4.2}$$

represents undamaged behavior,

$$\sigma_f^*=B\left(P^*\right)^M(1+C\ln\dot{\varepsilon})\leq SFMAX \tag{4.3}$$

represents the damaged behavior,

$$D=\sum\frac{\Delta\varepsilon^P}{\varepsilon_f^P} \tag{4.4}$$

represents the accumulated damage, based on plastic strain to fracture is given equation (4.5) and plastic strain in a given computational cycle which is $\Delta\varepsilon^P$,

$$\varepsilon_f^P=D_1\left(P^*+T^*\right)^{D_2} \tag{4.5}$$

where P^* is normalized pressure, T^* is normalized tensile strength, $\dot{\varepsilon}^*$ is normalized strain rate. SFMAX is Maximum normalized fractured strength, A, B, C, M, N, D_1 and D_2 are material constants.

The hydrostatic pressure is given by

$$P=K_1\mu+K_2\mu^2+K_3\mu^3 \tag{4.6}$$

in compression

$$P=K_1\mu \tag{4.7}$$

where μ is

$$\mu=\frac{\rho}{\rho_0}-1 \tag{4.8}$$

where ρ_0 is initial, ρ is present density. The Hugoniot elastic limit is given by

$$HEL=K_1\mu_{hel}+K_2\mu_{hel}^2+K_3\mu_{hel}^3+g\frac{4\mu_{hel}}{3\left(1+\mu_{hel}\right)} \tag{4.9}$$

and Pressure component at the Hugoniot elastic limit is given by

$$P_{hel}=K_1\mu_{hel}+K_2\mu_{hel}^2+(K_3\mu_{hel}^3)^3 \quad (4.10)$$

where K1, K2 and K3 are material constants. g and μ_{hel} can be found in given reference (G. McIntosh, 1998).

4.2.2.2 Composite

In this study, composites are modeled in MAT22 Composite Damage Model and MAT59 Composite Failure Solid Model. They were preferred because both model types are given good results in ballistic impact simulations when considering in previous studies have in good agreement between the experimental work.

4.2.2.2.1 Mat22. Composite Damage Model is also known as Chang-Chang composite failure model. Composite Damage Model is shown in Figure 4.4. Corresponding relationships for Composite Damage Model is demonstrated in the following equations (Berk, 2014)

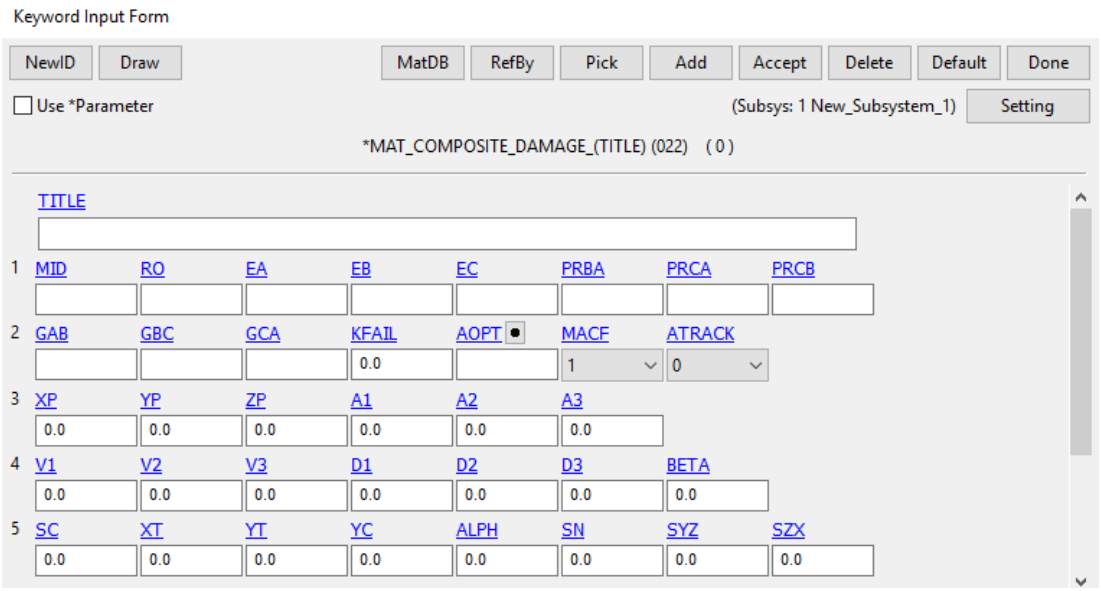


Figure 4.4 Display of Composite Damage Model card (Mat22) in LS-Dyna preprocessor

Longitudinal tension is given by

$$\left(\frac{\sigma_1}{X_t}\right)^2 + \bar{\tau} > 1, \ \sigma_1 > 0 \tag{4.11}$$

Transverse tension is given by

$$\left(\frac{\sigma_2}{Y_t}\right)^2 + \bar{\tau} > 1, \ \sigma_1 > 0 \tag{4.12}$$

Transverse compression is given by

$$\left(\frac{\sigma_2}{2S_{12}}\right)^2 + \left[\left(\frac{Y_c}{2S_{12}}\right)^2 - 1\right]\frac{\sigma_2}{Y_c} + \bar{\tau} > 1 \tag{4.13}$$

Where σ_1,σ_2 are stresses in longitudinal and transverse direction respectively, X_t,Y_t are tensile strengths in longitudinal and transverse direction respectively, X_c,Y_c are compressive strengths in longitudinal and transverse direction respectively, S_{12} is inplane shear strength.

$$\bar{\tau} = \frac{\frac{\tau_{12}^2}{2G_{12}} + \frac{3}{4}\alpha\tau_{12}^4}{\frac{S_{12}^2}{2G_{12}} + \frac{3}{4}\alpha\tau_{12}^4} \tag{4.14}$$

Where τ_{12} is inplane shear stress, G_{12} is inplane shear modulus, α is nonlinear shear stress coefficients. Stress-strain equations are given by

$$\varepsilon_1 = \frac{1}{E_1}(\sigma_1 - \nu_{12}\sigma_2) \tag{4.15}$$

$$\varepsilon_2 = \frac{1}{E_2}(\sigma_2 - \nu_{12}\sigma_1) \tag{4.16}$$

$$\varepsilon_{12}=\frac{\tau_{12}}{2G_{12}}+\frac{\alpha\tau_{12}^{3}}{2} \tag{4.17}$$

where $\varepsilon_1,\varepsilon_2$ are longitudinal and transverse direction strains.

4.2.2.2.2 Mat59. Composite Failure Solid Model is based on the Composite Damage Model described by Cheng. Composite Damage Model is shown in Figure 4.5. Corresponding relationships for Composite Failure Solid Model is demonstrated in the following equations (Berk, 2014).

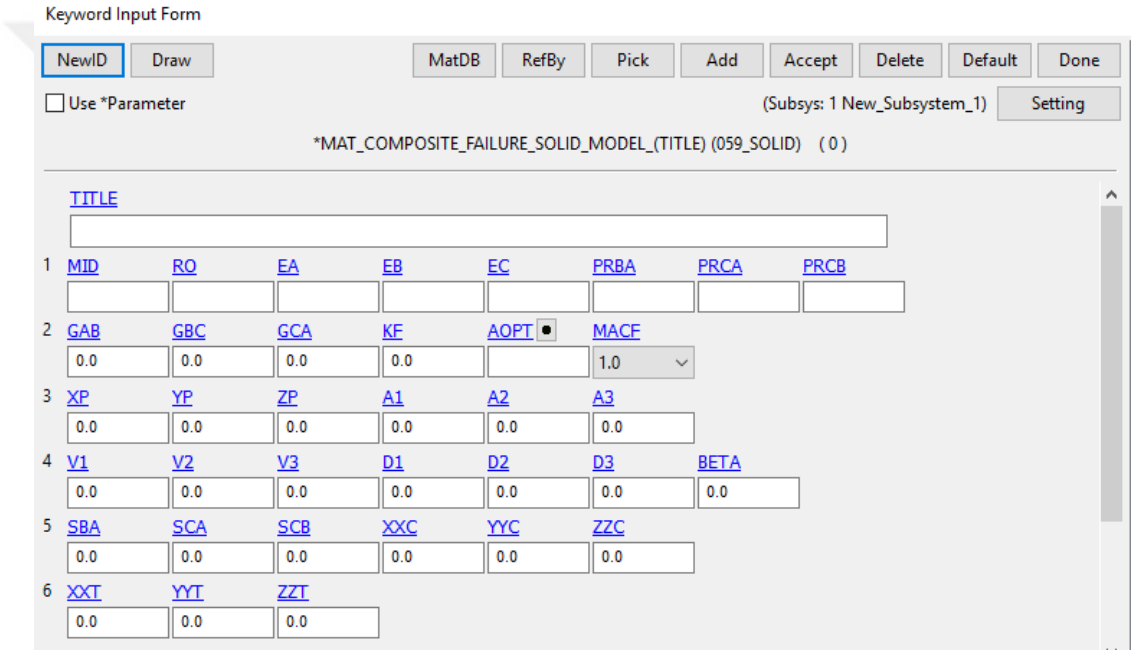


Figure 4.5 Display of Composite Failure Solid Model card (Mat59) in LS-Dyna preprocessor

Longitudinal tension is given

$$\frac{\sigma_1^2}{X_t^2}+\frac{\tau_{12}^2}{S_{12}^2}+\frac{\tau_{31}^2}{S_{31}^2}>1,\ \sigma_1>0 \tag{4.18}$$

Transverse tension is given

$$\frac{\sigma_2^2}{Y_t^2}+\frac{\tau_{12}^2}{S_{12}^2}+\frac{\tau_{23}^2}{S_{23}^2}>1,\ \sigma_2>0 \tag{4.19}$$

Through-thickness shear with longitudinal tension is given

$$\frac{\sigma_1^2}{X_t^2}+\frac{\tau_{31}^2}{S_{31}^2}>1,\ \sigma_1>0 \tag{4.20}$$

Delamination is given

$$\frac{\sigma_3^2}{Z_t^2}+\frac{\tau_{23}^2}{S_{23}^2}+\frac{\tau_{31}^2}{S_{31}^2}>1,\ \sigma_3>0 \tag{4.21}$$

Through-thickness shear with transverse tension is given

$$\frac{\sigma_2^2}{Y_t^2}+\frac{\tau_{23}^2}{S_{23}^2}>1,\ \sigma_2>0 \tag{4.22}$$

Longitudinal compression is given

$$\frac{\sigma_1^2}{X_c^2}>1,\ \sigma_1<0 \tag{4.23}$$

Transverse compression is given

$$\frac{\sigma_2^2}{(S_{12}+S_{23})^2}+\frac{\sigma_2}{Y_c}\left[\left(\frac{Y_c^2}{(S_{12}+S_{23})^2}-1\right)\right]+\frac{\tau_{12}^2}{S_{12}^2}+\frac{\tau_{31}^2}{S_{31}^2}>1,\ \sigma_2<0 \tag{4.24}$$

Through-thickness compression is given

$$\frac{\sigma_3^2}{(S_{31}+S_{23})^2}+\frac{\sigma_3}{Z_c}\left[\left(\frac{Z_c^2}{(S_{31}+S_{23})^2}-1\right)\right]+\frac{\tau_{31}^2}{S_{31}^2}+\frac{\tau_{23}^2}{S_{23}^2}>1,\ \sigma_3<0 \tag{4.25}$$

where X_t,Y_t, Z_t are tensile strength in longitudinal, transverse and normal direction respectively, X_c,Y_c, Z_c are compressive strength in longitudinal, transverse and normal direction respectively, τ_{12} is inplane shear stress, τ_{23},τ_{31} are transverse shear stresses, S_{12} is inplane shear strength, S_{31},S_{23} are transverse shear strengths.

4.2.2.3 Projectile

Projectile material is chosen hard steel. Thus The Johnson-Cook material model can be used for projectile. Johnson-Cook model is shown in Figure 4.6. Corresponding relationships for Johnson-Cook model is demonstrated in the following equations (Ls-Dyna Keyword User's Manual, 2015).

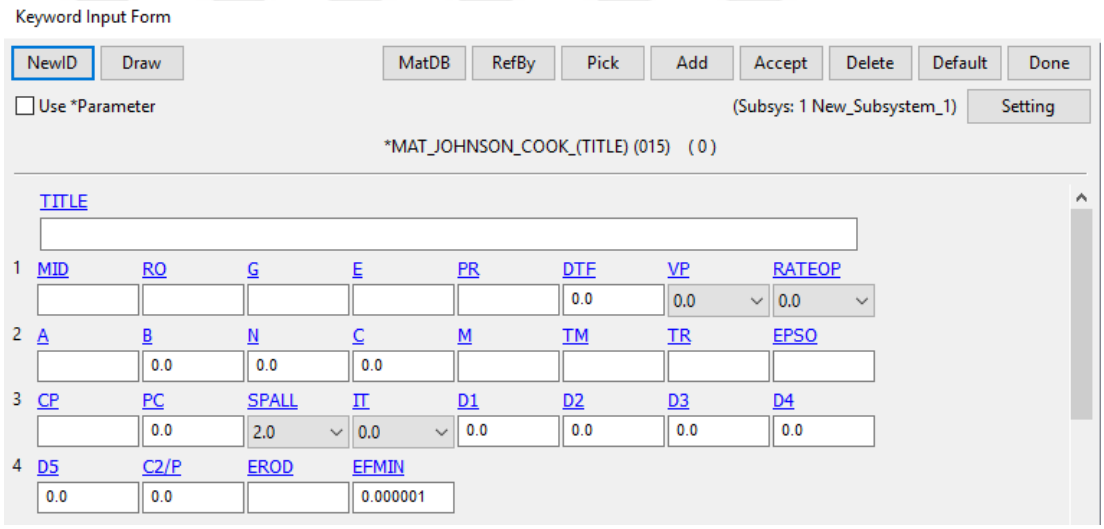


Figure 4.6 Display of Johnson Cook Model card (Mat15) in LS-Dyna preprocessor

stress is given by

$$\sigma_y=(A+B\bar{\varepsilon}^{pn})\left(1+C\ln\dot{\varepsilon}^{*}\right)(1-T^{*m}) \tag{4.26}$$

Homologous temperature is given by

$$T^{*}=\frac{T-T_{room}}{T_{melt}-T_{room}} \tag{4.27}$$

where A, B ,C, N and M are material constants, $\dot{\varepsilon}^*$ is changes with viscoplastic formulation, $\bar{\varepsilon}^p$ is effective plastic strain, T is temperature.

In this study Simplified Johnson-Cook Model is used instead of using normal Johnson-Cook Model. Unlike the Johnson-Cook Model is consisted thermal effects, thermal softening and damage are neglected in Simplified Johnson-Cook Model. It works 50% faster than Full Johnson-Cook Model and it doesn't require to use the EOS (Equations of State) parameters compared to Full Johnson-Cook Model. Simplified Johnson-Cook model is shown in Figure 4.7. Corresponding relationships for Simplified Johnson-Cook model is demonstrated in the following equations (Ls-Dyna Keyword User's Manual, 2015).

In Simplified Johnson Cook Model, stress is given by

$$\sigma_y=(A+B\bar{\varepsilon}^{p^n})\left(1+C\ln\dot{\varepsilon}^*\right) \tag{4.28}$$

Where all above constants are the same in equation (4.26).

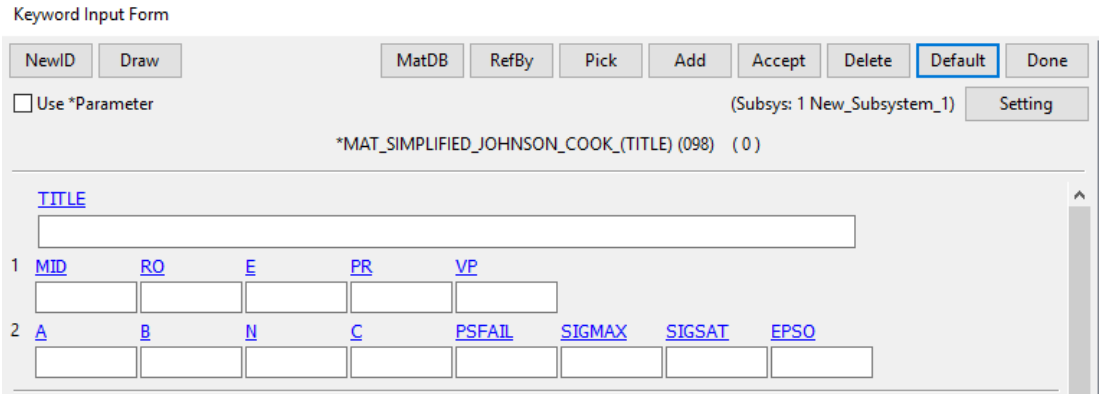


Figure 4.7 Display of Simplified Johnson Cook Model card (Mat98) in LS-Dyna preprocessor

4.2.3 Mechanical Properties and Model Parameters of Structures

4.2.3.1 Ceramic

Mechanical properties of Al_2O_3 ceramic are taken from Feli and Asgari's study. (Feli & Asgari, 2011). Mechanical properties are demonstrated in Table 4.2 with JH-2 model parameters.

Table 4.2 Mechanical parameters for 99.5% purity Alumina ceramic in JH-2 (Feli & Asgari, 2011)

Parameter	**Symbol**	**Value**	**Unit**
Density	ρ_0	3700	kg/m^3
Shear modulus	G	90.16	GPa
Intact strength coefficient	A	0.93	-
Fractured strength coefficient	B	0.31	-
Strain rate coefficient	C	0	s^{-1}
Fractured strength exponent	M	0.6	-
Intact strength exponent	N	0.6	-
Normalized maximum fractured strength	σ^f_{max}	0.2	-
Hugoniot elastic limit	HEL	19	GPa
Pressure at Hugoniot elastic limit	P_{HEL}	1460	MPa
Bulking factor	β	1	-
Elastic bulk modulus	$K=K_1$	130.95	GPa
Coefficient for 2nd degree term in EOS	K_2	0	GPa
Coefficient for 3rd degree term in EOS	K_3	0	GPa
Damage coefficient	D_1	0.005	-
Damage exponent	D_2	1	-

4.2.3.2 Composite

Mechanical properties of Aramid, S2 glass and hybrid Carbon-aramid reinforced epoxy composite materials are taken from Berk et al. (Berk, 2014, 2016, 2017). Through-thickness mechanical properties of composite materials are obtained from a multiplication of 0.6 times of in-plane mechanical properties. Thus parameters of composite materials can be used in Mat59 Composite Failure Solid Model and Mat22 Composite Damage model parameters. Mechanical properties with derived mechanical parameters are shown in Table 4.3.

In addition to these reinforced epoxy composites, a new hybrid type of composite is created. Aramid and S2 glass reinforcements are united with different thickness ratio in same composite. It will be explained in more detailed in Topic 4.2.6 Combination of Target Placing.

Table 4.3 Mechanical parameters for composite materials (Berk et al., 2014, 2016, 2017)

		Aramid Epoxy	**S2 glass Epoxy**	**Carbon-aramid Epoxy**	
Parameter	**Symbol**		**Value**		**Unit**
Density	ρ	1117	1750	1148	kg/m^3
Elastic Modulus-Longitudinal	E_1	17230	20256	47700	MPa
Elastic Modulus-Transverse	E_2	17230	30310	47700	MPa
Elastic Modulus-Normal	E_3	10340	15170	28620	MPa
Poisson's Ratio	ν_{12}	0.2	0.17	0.1	-
Poisson's Ratio	ν_{23}	0.12	0.11	0.06	-
Poisson's Ratio	ν_{31}	0.12	0.11	0.06	-
Tensile Strength-Longitudinal	X_t	425	630	552	MPa
Compressive Strength-Longitudinal	X_c	88	397	273	MPa
Tensile Strength-Transverse	Y_t	425	590	552	MPa
Compressive Strength-Transverse	Y_c	88	426	273	MPa
Tensile Strength-Normal	Z_t	255	366	331	MPa
Compressive Strength-Normal	Z_c	53	247	164	MPa
Shear Modulus-Inplane	G_{12}	5510	4300	2245	MPa
Shear Modulus-Transverse	G_{23}	3300	2580	1407	MPa
Shear Modulus-Transverse	G_{31}	3300	2580	1407	MPa
Shear Strength-Inplane	S_{12}	66	99	82	MPa
Shear Strength-Transverse	S_{23}	40	60	49	MPa
Shear Strength-Transverse	S_{31}	40	60	49	MPa

4.2.3.3 Projectile

M61 Type 7.62 x 51mm AP (Armor Piercing) Projectile is used as impactor. 4340 Steel is chosen for projectile material. Material properties are taken from ANSYS 17 Engineering Data Material Model (ANSYS Inc., 2016). Mechanical parameters of 4340 Steel are shown in Table 4.4 with the Simplified Johnson-Cook Model.

Table 4.4 Mechanical parameters for 4340 Steel (ANSYS 17 Engineering Data Material Model, 2016)

Parameter	Symbol	Value	Unit
Density	ρ	7830	kg/m^3
Elastic Modulus	E	209.5	GPa
Poisson's Ratio	ν	0.28	-
Static Yield Strength	A	792	MPa
Strain Hardening Modulus	B	510	MPa
Strain Hardening Parameter	N	0.26	-
Strain Hardening Parameter	C	0.014	-

4.2.4 Geometry of Structures

Geometry of ballistic test model is demonstrated in Figure 4.8. In numerical model, quarter of model is preferred to save computational time. X and Y axis are symmetry planes which will be demonstrated in next sections. Quarter of model is shown in Figure 4.9.

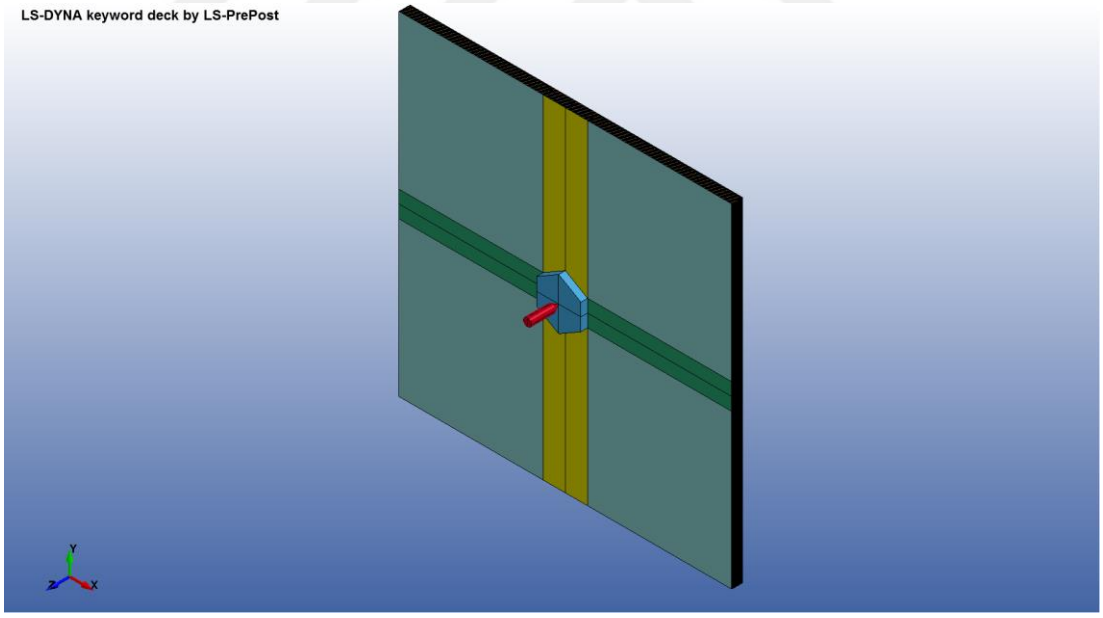


Figure 4.8 Isometric view of Ballistic Test Model Geometry

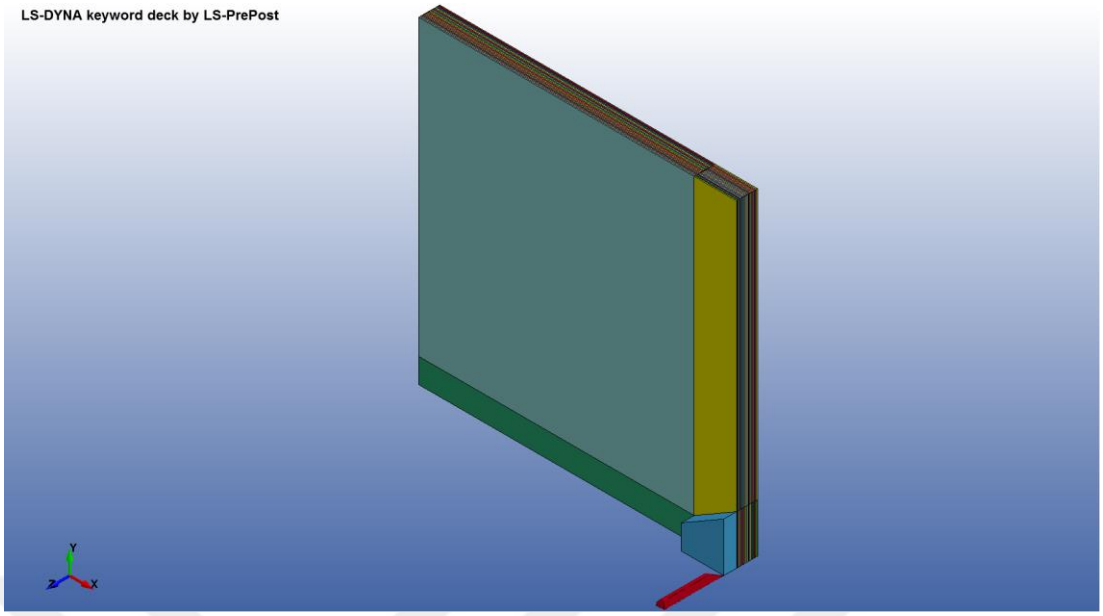


Figure 4.9 Isometric view of quarter Geometry model

4.2.4.1 Ceramic Front Layer

Hexagonal Alumina ceramic was modeled in the dimensions of 40 mm x 40 mm with different three different thicknesses. Thicknesses are set 6mm, 8mm and 10mm. Front view of quarter ceramic geometry is shown in Figure 4.10.

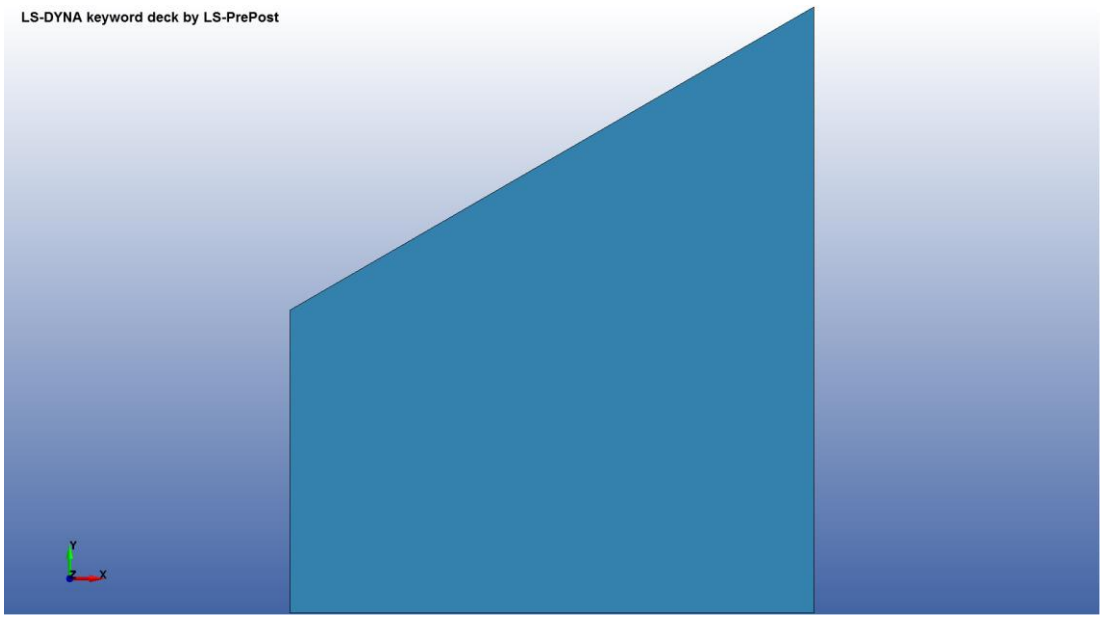


Figure 4.10 Front view of quarter ceramic geometry

4.2.4.2 Backing Plate Composites

Composites were modeled in the dimensions of 300 mm x 300 mm x 10 mm for aramid/epoxy, S2 glass/epoxy, Hybrid carbon-aramid/epoxy, hybrid S2 glass-aramid/epoxy. Layer numbers of composite materials with 10 mm thickness are given in Table 4.5. Front view of quarter composite geometry is shown in Figure 4.11. In numerical simulation, all composite materials are modeled in 20 layers and 4 parts for overlapping with ceramic shape to set matched mesh on it.

Table 4.5 Layer numbers of composite materials in 10 mm thickness

	Aramid/epoxy	S2 glass/epoxy	Carbon-aramid/epoxy
Layer Number	20	80	40

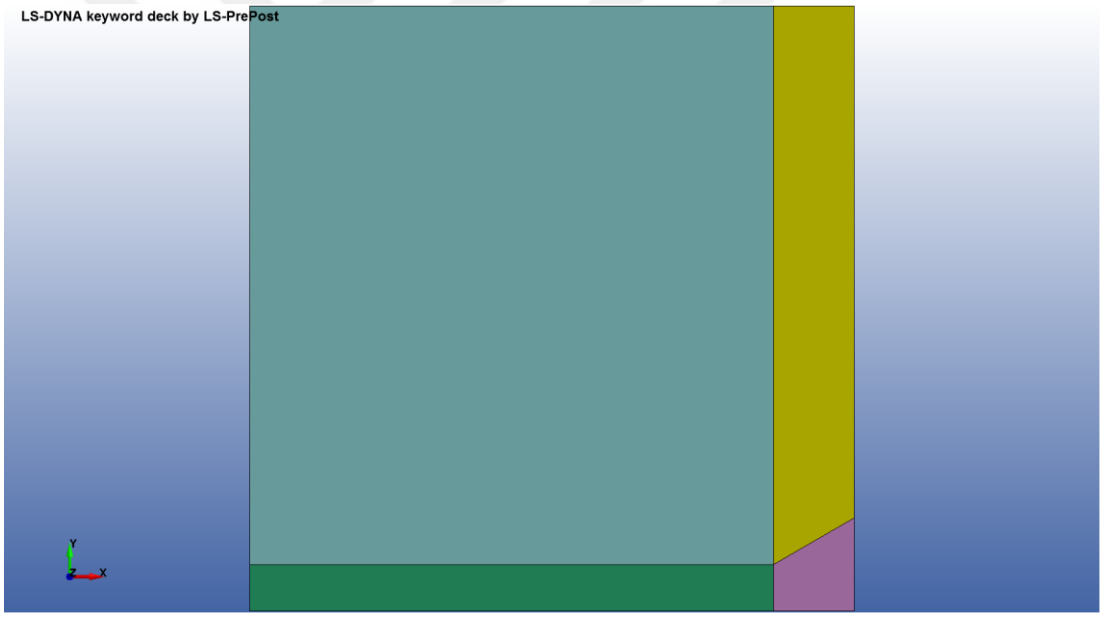


Figure 4.11 Front view of quarter composite geometry

4.2.4.3 Projectile

M61 type AP projectile is modeled in 60^{o} conical–cylindrical and dimensions of 7.62 mm diameter and 28.1 mm length. Performance of this model was found analogous with M61 Type 7.62 x 51mm AP (Armor Piercing) Projectile (Fawaz et al., 2004). Isometric view of quarter composite geometry is shown in Figure 4.12.

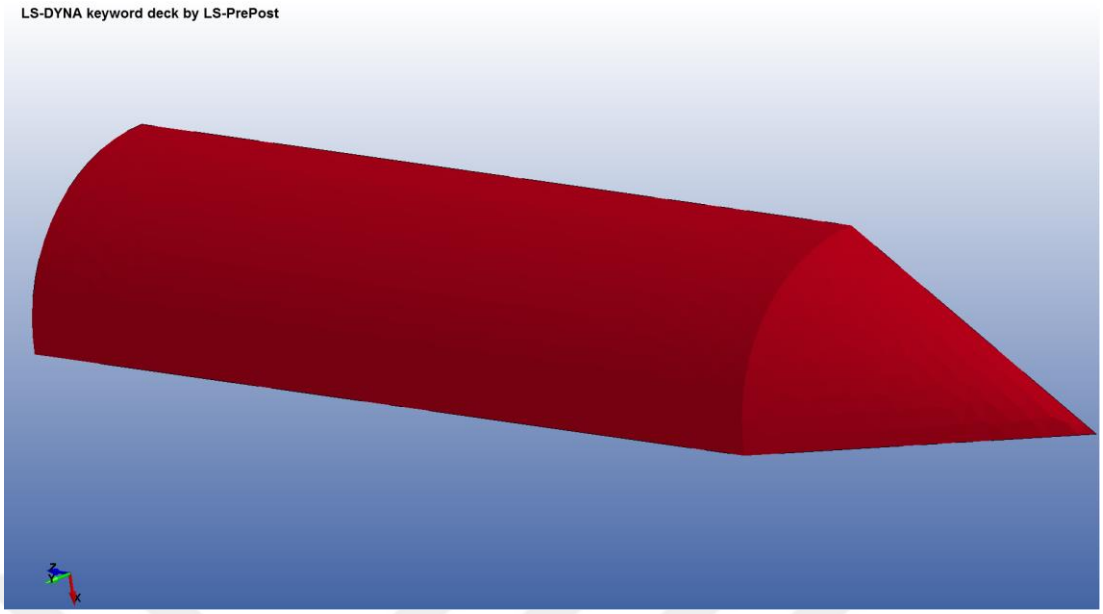


Figure 4.12 Isometric view of quarter composite geometry

4.2.5 Element Types and Meshes

Ceramic and composite materials were modeled with eight-node hexahedron solid elements. Six-node tetrahedron solid elements were used for model of projectile (Fawaz et al., 2004).

When the total target thickness is set 16mm, 296184 elements were determined in total model. When the total target thickness is set 18mm 310359 elements were determined in total model. When the total target thickness is set 20mm 324534 elements were determined in total model. General views of quarter geometry mesh are seen in Figure 4.13-16 when the total target thickness is set 16mm (ceramic thickness is 6 mm and composite is 10 mm).

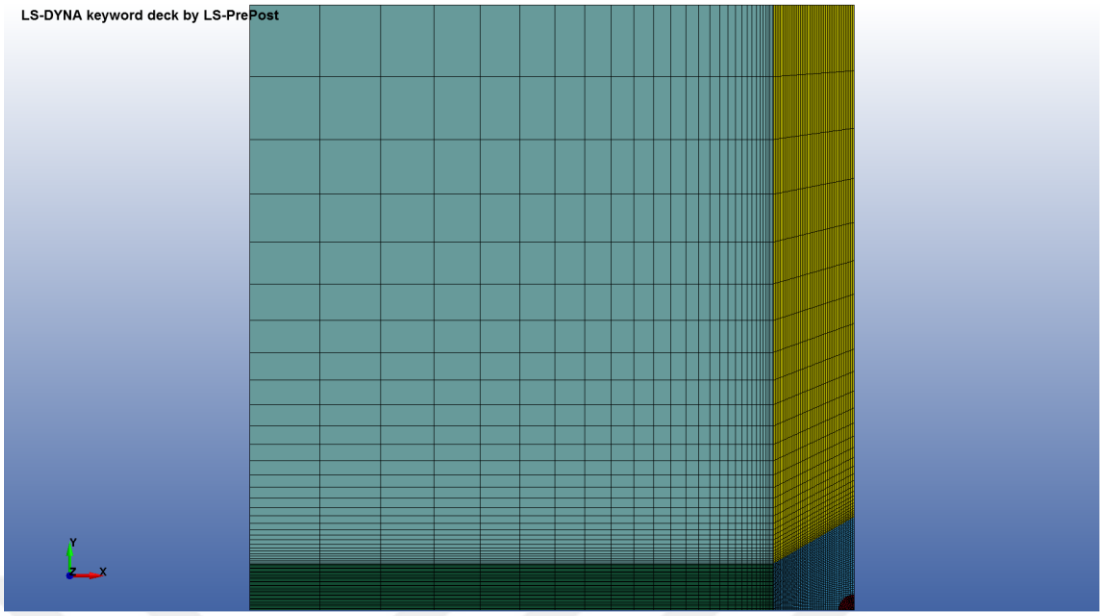


Figure 4.13 Front view of quarter geometry mesh

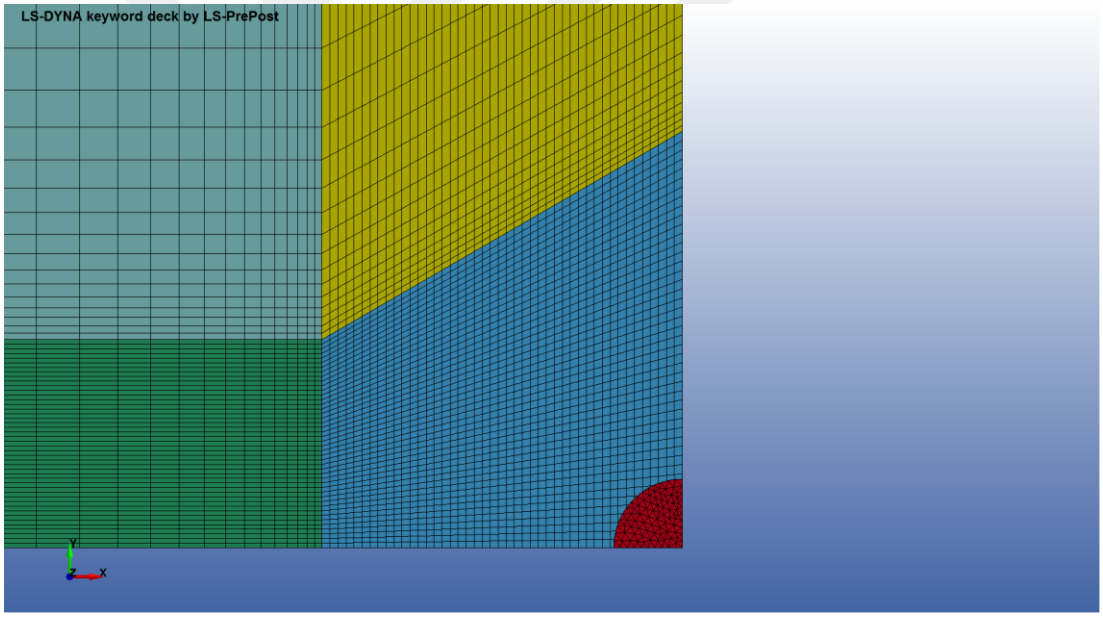


Figure 4.14 Zoomed in ceramic front view of quarter geometry mesh

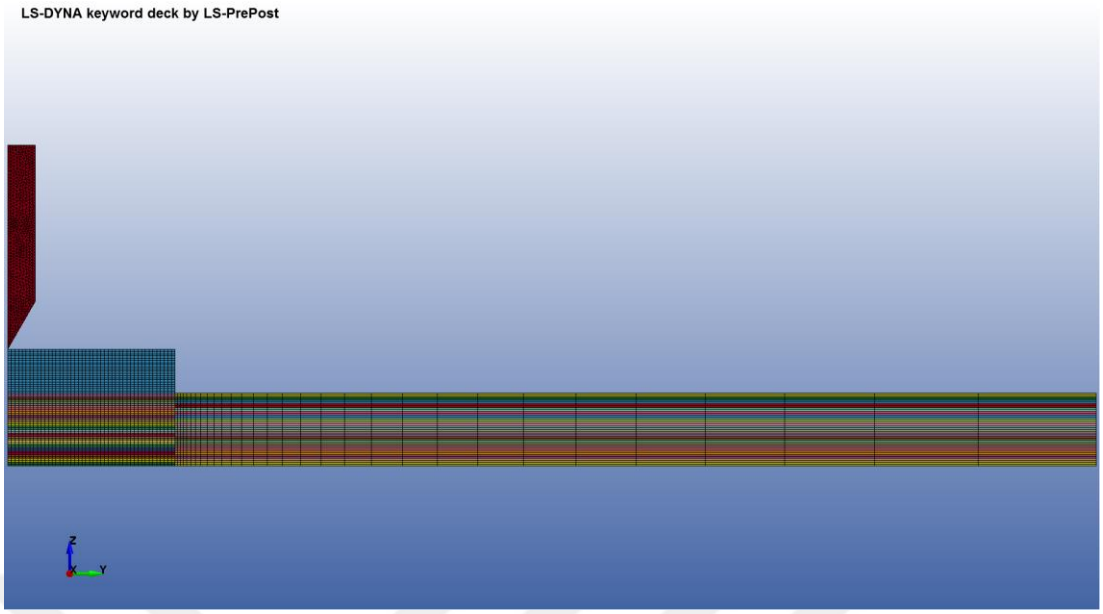


Figure 4.15 Right view of quarter geometry mesh

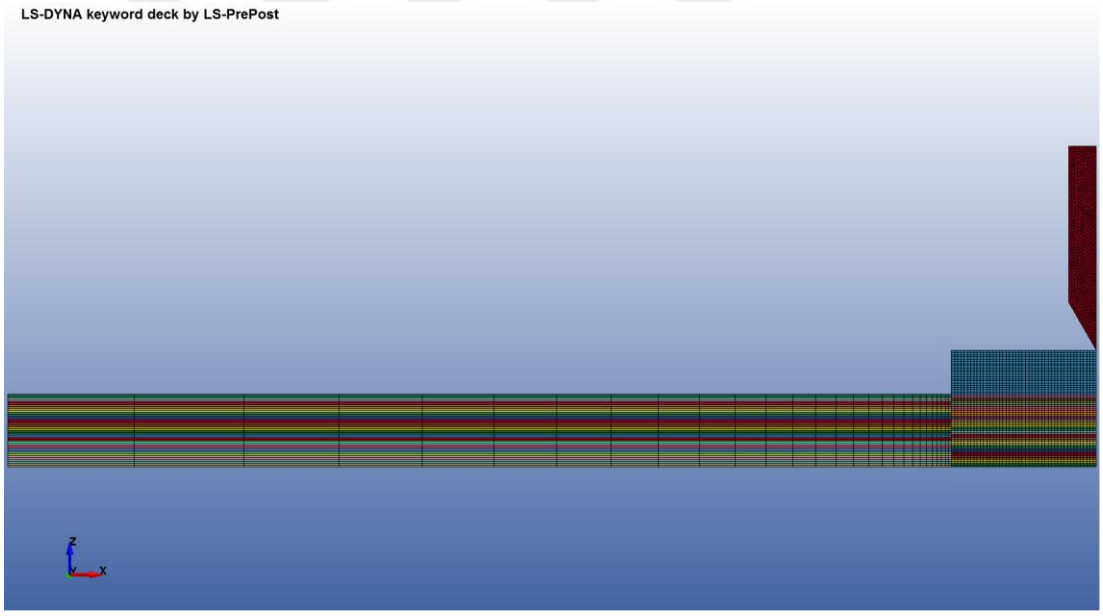
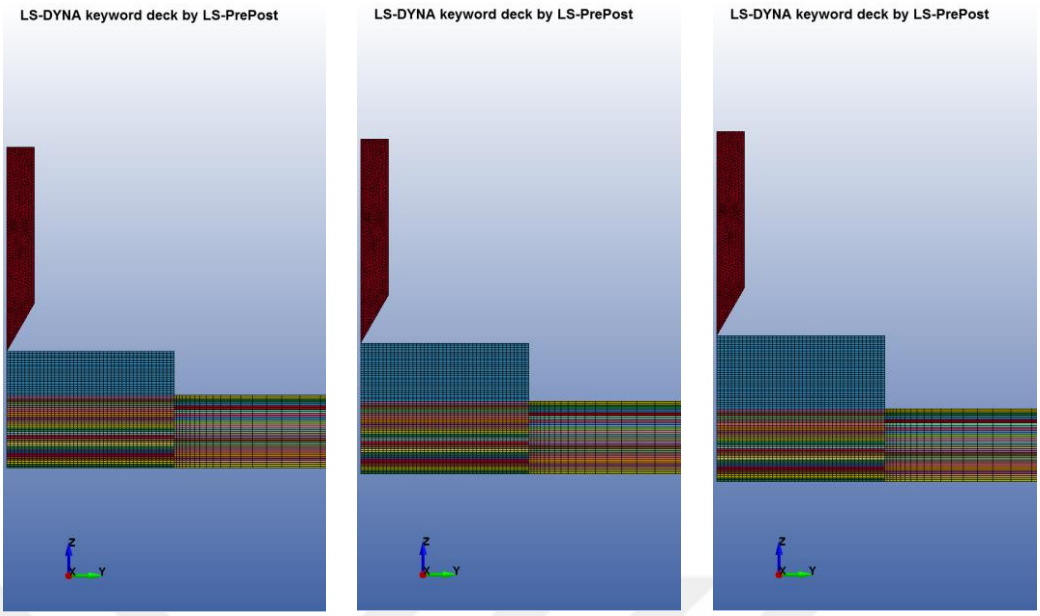


Figure 4.16 Bottom view of quarter geometry mesh

4.2.6 Combination of Target Placing

There are 3 different case in combinations of targets. Cases change with ceramic layer thicknesses which are 6mm, 8mm and 10mm (Figure 4.17). Also each case has 6 different condition in itself (Table 4.6).



(Case 1) (Case 2) (Case 3)

Figure 4.17 View of the 3 different ceramic thickness, (Case 1) 6 mm, (Case 2) 8 mm, (Case 3) 10 mm

Table 4.6 All combination of targets

Target			Case 1	Case 2	Case 3	
Condition	**Placing**	**Material**	**Thickness**			**Unit**
Fixed	Front side	Al_2O_3 ceramic	6	8	10	mm
1	Back side	Aramid/epoxy	10	10	10	mm
2	Back side	Aramid/epoxy	10	10	10	mm
3	Back side	Carbon-aramid/epoxy	10	10	10	mm
4	Back side	Hybrid 1*	10	10	10	mm
		S2 glass/epoxy	3	3	3	mm
		Aramid/epoxy	7	7	7	mm
5	Back side	Hybrid 2*	10	10	10	mm
		S2 glass/epoxy	5	5	5	mm
		Aramid/epoxy	5	5	5	mm
6	Back side	Hybrid 3*	10	10	10	mm
		S2 glass/epoxy	7	7	7	mm
		Aramid/epoxy	3	3	3	mm

To make new hybrid S2 glass-aramid/epoxy composites, following parameters are created:

Hybrid 1: 3 mm S2 glass/epoxy - 7 mm Aramid/epoxy
Hybrid 2: 5 mm S2 glass/epoxy - 5 mm Aramid/epoxy
Hybrid 3: 7 mm S2 glass/epoxy - 3 mm Aramid/epoxy

As it seen in Table 4.6, 18 different combinations of target are modeled in this study.

4.2.7 Boundary Conditions

X and Y axis are set as symmetry planes. Symmetry planes are seen in Figure 4.18. All nodes are fixed in every direction at the top 20 mm of the composite (Figure 4.19).

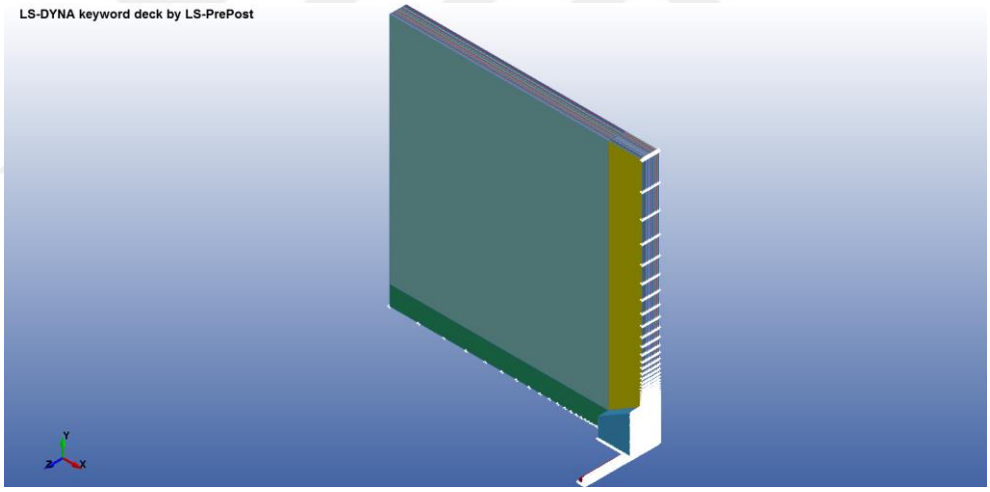


Figure 4.18 Isometric view of quarter geometry's symmetry planes

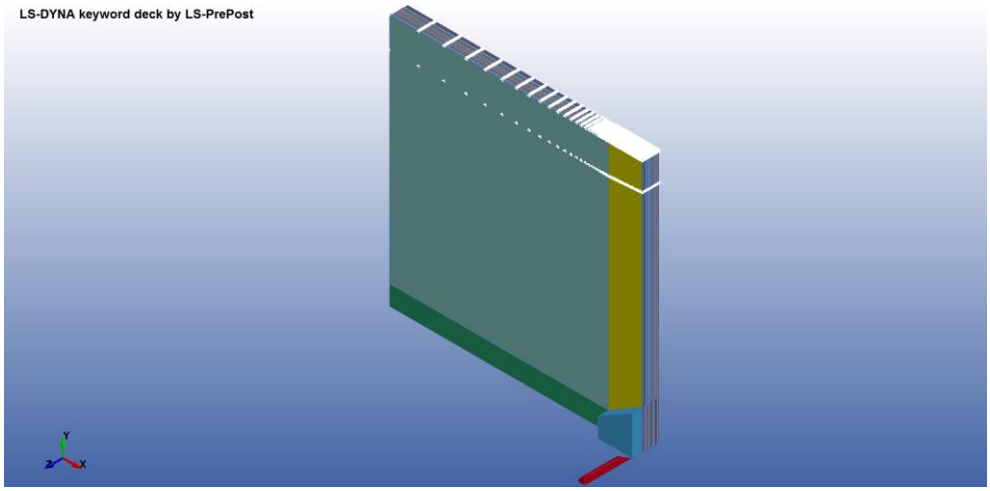


Figure 4.19 Isometric view of quarter geometry's fixed nodes

4.2.8 Initial Conditions

Projectile hits to targets at 4 different strike velocities (Table 4.7). Thus, it was done 72 different simulations with 18 different target combination and 4 different strike velocities.

Table 4.7 Initial velocity of projectile for each combinations

	CASE 1 (Ceramic thickness is 6 mm)						
Projectile	**Cond. 1**	**Cond. 2**	**Cond. 3**	**Cond. 4**	**Cond. 5**	**Cond. 6**	**Unit**
Strike Velocity 1	850	850	850	850	850	850	m/s
Strike Velocity 2	800	800	800	800	800	800	m/s
Strike Velocity 3	750	750	750	750	750	750	m/s
Strike Velocity 4	700	700	700	700	700	700	m/s
	CASE 2 (Ceramic thickness is 8 mm)						
Projectile	**Cond. 1**	**Cond. 2**	**Cond. 3**	**Cond. 4**	**Cond. 5**	**Cond. 6**	**Unit**
Strike Velocity 1	850	850	850	850	850	850	m/s
Strike Velocity 2	800	800	800	800	800	800	m/s
Strike Velocity 3	750	750	750	750	750	750	m/s
Strike Velocity 4	700	700	700	700	700	700	m/s
	CASE 3 (Ceramic thickness is 10 mm)						
Projectile	**Cond. 1**	**Cond. 2**	**Cond. 3**	**Cond. 4**	**Cond. 5**	**Cond. 6**	**Unit**
Strike Velocity 1	850	850	850	850	850	850	m/s
Strike Velocity 2	800	800	800	800	800	800	m/s
Strike Velocity 3	750	750	750	750	750	750	m/s
Strike Velocity 4	700	700	700	700	700	700	m/s

4.2.9 Contacts

Segment based Eroding Surface to Surface card is chosen between for all contacts, including between interfaces in composite. Eroding Surface card features deleting failed elements from calculations. The coefficients of friction between interfaces in composite also between projectile-ceramic and ceramic–composite are considered 0.3 and 0.28 respectively (Feli & Asgari, 2011)

4.2.10 Hourglass

Hourglass Type 4 which is Flanagan-Belytschko stiffness form is used for composite. Hourglass Type 3 Flanagan-Belytschko viscous form is used for rest of Other components were hourglass type 3 (Tunusoğlu, 2011). Both Hourglass coefficients are set as default which is 0.1.

4.2.11 Time Step

Ls-Dyna calculates the Time Step by its own according to the material types. Although it is allowed users to change parameters by inputs, it is not recommended. In this study, all scale factors for computed time step are lowered to 0.67 from 0.9 by default.

CHAPTER FIVE
NUMERICAL RESULTS

5.1 Verification of Model

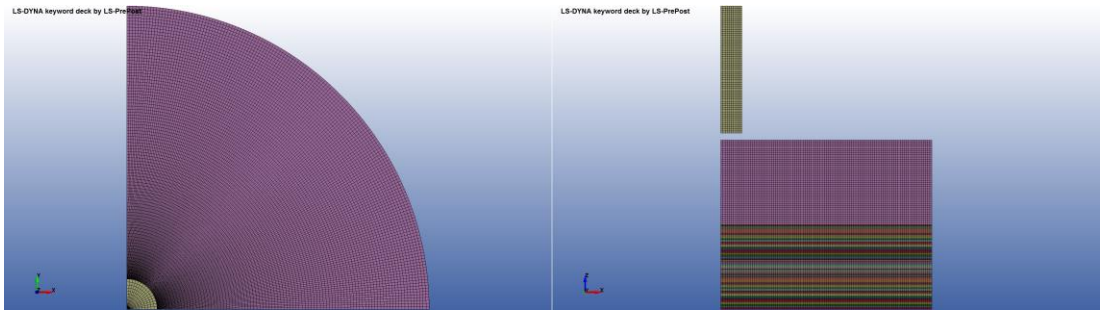
In this section, two different studies were simulated again for validation of present study.

5.1.1 Reference 1: Finite Element Simulation of Ceramic/Composite Armor under Ballistic Impact (S. Feli, M.R. Asgari, 2011)

5.1.1.1 Preparation

Simulation is modeled in Ls-Dyna 3D instead of 2D. Composite, ceramic and tungsten projectile are modeled in Eight-node hexahedron solid elements. Al_2O_3 ceramic is modeled in JH-2 Model card, Twaron composite which is similar properties Kevlar49 is modeled in Composite Damage Model card, tungsten alloy projectile is modeled in Johnson-Cook Model card (Table 5.1-2). Mechanical parameters for 99.5% purity Alumina ceramic were shown in Table 4.2 before.

Projectile is modeled in cylindrical and dimensions of 10 mm diameter and 30 mm length. Ceramic is modeled in cylindrical and dimensions of 100 mm diameter and 20 mm length. Each composite ply is cylindrical and dimensions of 100 mm diameter and 0.4 mm length. 50 composite plies are set as backing plate. Projectile and ceramic are given in 0.5 mm x 0.5 mm element size and composite is 0.5 mm x 0.2 mm element size (Figure 5.1). Quarter of model is modeled to save time. 2206024 elements were determined in quarter model. Outer edge nodes of both ceramic and composite plies are fixed in all directions.



(a) (b)

Figure 5.1 View of Feli and Asgari's quarter model, (a) front view, (b) bottom view

Table 5.1 Mechanical properties of Twaron (CT1000, 1680dtex/1000f) composite (Feli & Asgari, 2011)

Parameter	**Symbol**	**Value**	**Unit**
Density	ρ	1230	kg/m^3
Elastic Modulus-Longitudinal	E_1	20440	MPa
Elastic Modulus-Transverse	E_2	8900	MPa
Elastic Modulus-Normal	E_3	8900	MPa
Poisson's Ratio	ν_{12}	0.31	-
Poisson's Ratio	ν_{23}	0.31	-
Poisson's Ratio	ν_{31}	0.49	-
Tensile Strength-Longitudinal	X_t	1145	MPa
Tensile Strength-Transverse	Y_t	130	MPa
Compressive Strength-Transverse	Y_c	65	MPa
Shear Modulus-Inplane	G_{12}	1640	MPa
Shear Modulus-Transverse	G_{23}	3030	MPa
Shear Modulus-Transverse	G_{31}	1640	MPa
Shear Strength-Inplane	S_{12}	340	MPa
Non-linear parameters of shear stress	α	0	-
Bulk modulus	E_{Bulk}	20400	MPa

Table 5.2 Mechanical parameters for tungsten alloy projectile in Johnson–Cook Model and the Mie–Gruneisen equation of state (Feli & Asgari, 2011)

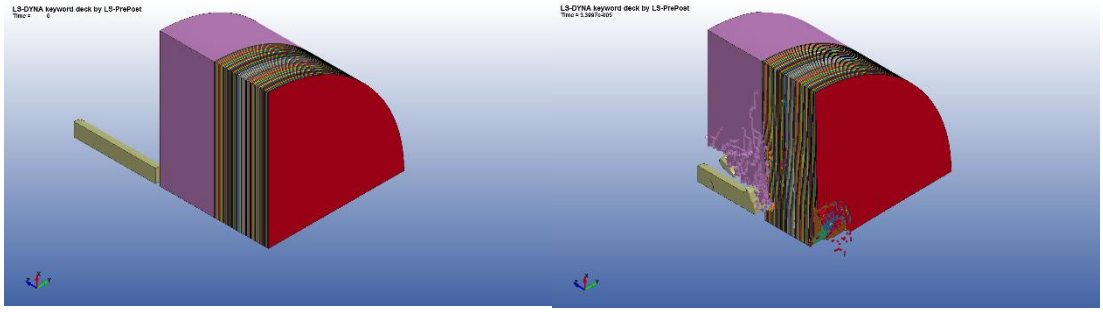
Parameter	**Symbol**	**Value**	**Unit**
Density	g	17600	kg/m^3
Young's Modulus	E	314	GPa
Shear modulus	G	122	GPa
Poison ratio	ν	0.29	-
Static yield stress	A	1506	MPa
Strain hardening modulus	B	177	MPa
Strain hardening exponent	n	0.12	-
Strain rate coefficient	C	0.016	-
Thermal softening exponent	m	1	-
Initial reference temperature	T_0	300	^oK
Melting temperature	T_m	1723	^oK
Slope in Us versus Up diagram	S	S1 = 1.23	-
Slope in Us versus Up diagram	S	S2 = S3 = 0	-
Gruneisen coefficient	γ_0	1.54	-
Elastic wave speed	C_0	4029	m/s

5.1.1.2 Results and Comparison

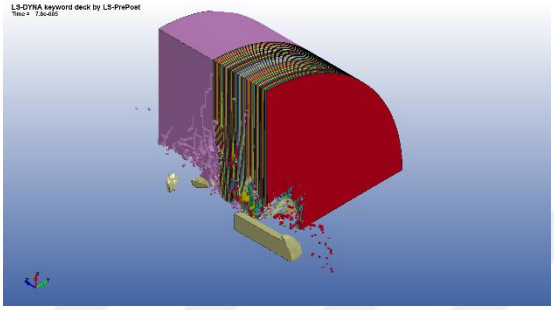
The results are found similar with Reference. Comparison between residual velocities of reference versus residual velocity of present are seen in Table 5.3. In addition to demonstration of validation study at 1250 m/s strike velocity is seen in Figure 5.2, Velocity versus Time curve for 1250 m/s strike velocity is seen in Figure 5.3.

Table 5.3 Comparison between residual velocities of reference versus residual velocity of present study

Initial impact velocity (m/s)	**1400**	**1250**	**1100**	**900**	**800**	**600**	**500**
Reference residual velocity (m/s)	995	721	630	550	470	285	175
Present residual velocity (m/s)	940	732	595	526	489	300	160



(a) (b)



(c)

Figure 5.2 View of Feli and Asgari's quarter model after 1200m/s strike velocity, (a) t=0 ms, (b) t=0.04 ms, (c) t=0.078 ms

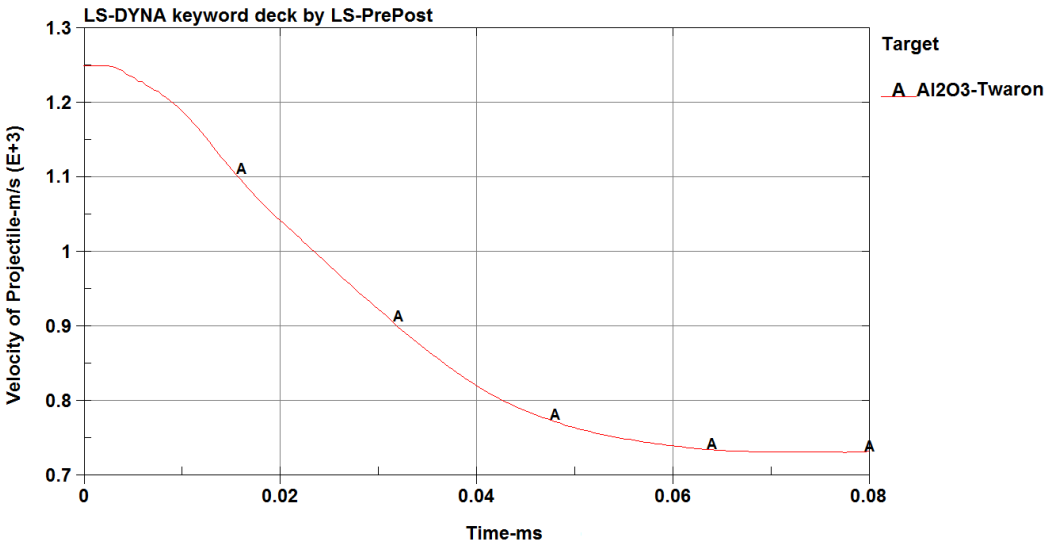


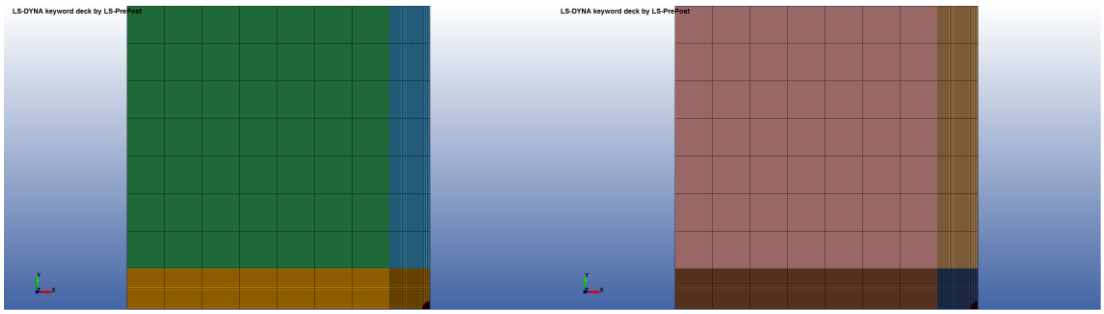
Figure 5.3 Velocity versus Time curve for 1250 m/s strike velocity of validation study

5.1.2 Reference 2: Finite Element Simulation of Ballistic Impact on Composite Plates (Berk, 2014)

5.1.2.1 Preparation

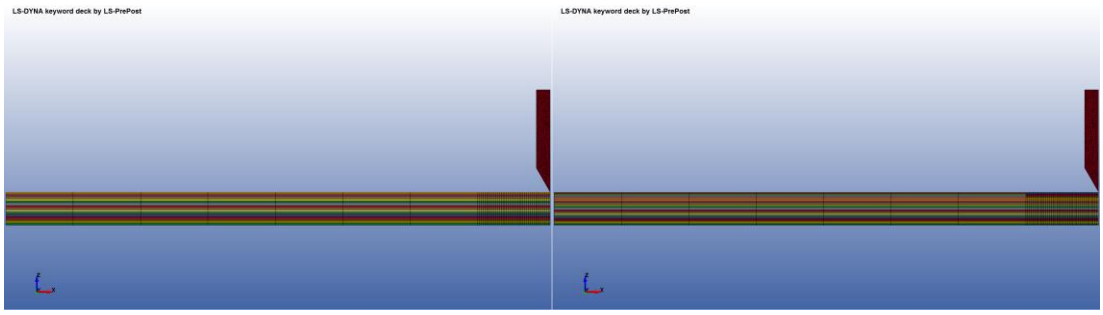
Simulation is modeled in Ls-Dyna same as the reference. 7.62 M61 projectile type is modeled in Simplified Johnson Cook Model card instead of Rigid cart. Composites were modeled in the dimensions of 300 mm x 300 mm x 9 mm for and Aramid/epoxy and hybrid Carbon-aramid/epoxy by using Composite Failure Solid Model cart. Mechanical parameters for Aramid/epoxy and Carbon-aramid/epoxy were given in Table 4.3 before. Projectile is modeled in 60^{o} conical–cylindrical and dimensions of 7.62 mm diameter and 28.1 mm length. Mechanical parameters for projectile are shown in Table 5.4. Composite materials are modeled with eight-node hexahedron solid elements. Six-node tetrahedron solid elements were used for model of projectile.

Aramid/epoxy is 15 layers and Carbon-aramid/epoxy is 38 layers in 9 mm target thickness. Quarter of model is modeled to save time. Finer mesh is set at where the projectile hit same as the reference. 102940 elements in Aramid/epoxy, 120612 elements in Carbon-aramid/epoxy were determined in quarter models (Figure 5.4-5). Composite is fixed in all directions from 40 mm of top side.



(a) (b)

Figure 5.4 Front view of Berk's quarter model, (a) Aramid/epoxy, (b) Carbon-aramid/epoxy



(a) (b)

Figure 5.5 Bottom view of Berk's quarter model, (a) Aramid/epoxy, (b) Carbon-aramid/epoxy

Table 5.4 Mechanical parameters for 4340 Steel (ANSYS 17 Engineering Data Material Model, 2016)

Parameter	**Symbol**	**Value**	**Unit**
Density	ρ	7830	kg/m^3
Elastic Modulus	E	209.5	GPa
Poisson's Ratio	ν	0.28	-
Static Yield Strength	A	792	MPa
Strain Hardening Modulus	B	510	MPa
Strain Hardening Parameter	N	0.26	-
Strain Hardening Parameter	C	0.014	-

5.1.2.2 Results and Comparison

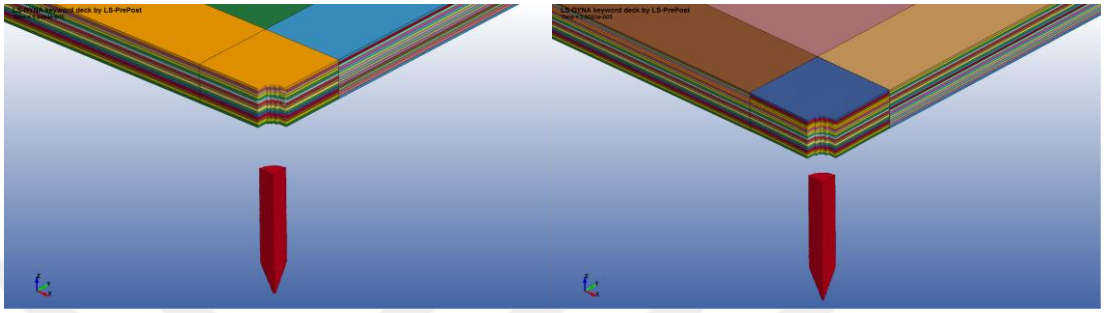
The results are found similar with Reference. Comparison between experimental residual velocities of reference versus residual velocity of present are seen in Table 5.5-6. Demonstrations of validation study at 852 m/s strike velocity for Aramid/epoxy and 850 m/s strike velocity for Carbon-aramid/epoxy are seen in same Figure 5.6, velocity versus time curve for 852 m/s strike velocity for Aramid/epoxy and 850 m/s strike velocity for Carbon-aramid/epoxy are seen in same Figure 5.7.

Table 5.5 Comparison between residual velocities of reference versus residual velocity of present study for Carbon-aramid/epoxy

Initial impact velocity (m/s)	**852**	**790**	**713**	**619**	**543**	**333**
Reference experimental residual velocity (m/s)	817	742	657	579	498	259
Present residual velocity (m/s)	816	752	678	587	514	313

Table 5.6 Comparison between residual velocities of reference versus residual velocity of present study for Aramid/epoxy

Initial impact velocity (m/s)	**850**	**840**	**764**	**652**	**540**	**381**
Reference experimental residual velocity (m/s)	820	805	724	626	489	353
Present residual velocity (m/s)	818	803	728	621	513	358



(a) (b)

Figure 5.6 View of Berk's quarter model after impact (a) 852 m/s strike velocity for Aramid/epoxy, (b) 850 m/s strike velocity for Carbon-aramid/epoxy

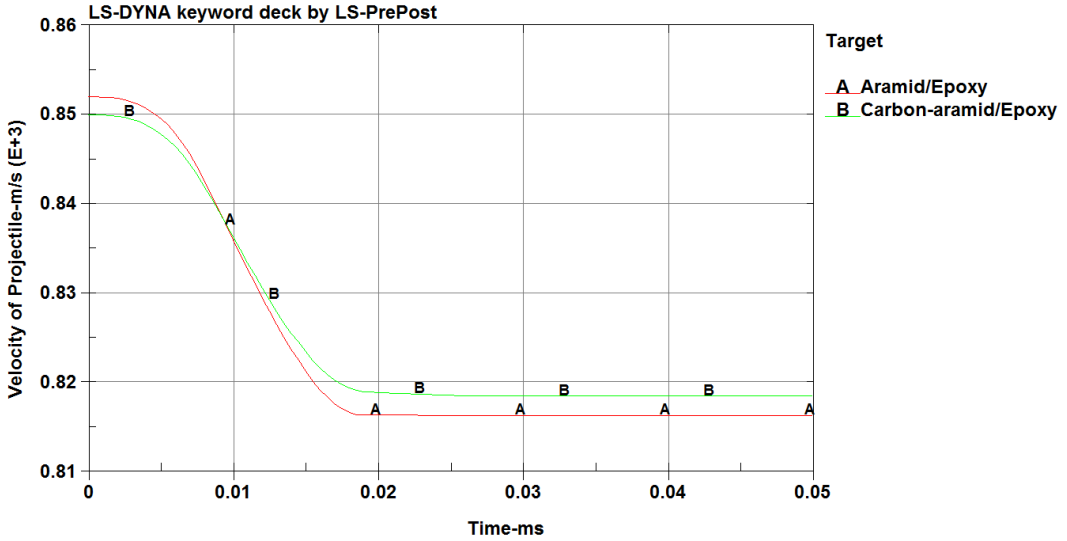


Figure 5.7 Velocity versus Time curve for 852 m/s strike velocity for Aramid/epoxy and 850 m/s strike velocity for Carbon-aramid/epoxy of validation study

5.2 Numerical Results for Present Study

After solving total 72 different target-impact combination in numerically, residual velocities of projectile are found for every target combination.

New Hybrid backing plate composite placements are formed as following:

In the first instance, we used S2 glass/epoxy stationed on the front side of the composite while using Aramid/epoxy on the back side. Later on, in the second instance we reversed the components, using Aramid/epoxy on the front side and S2 glass/epoxy on the back side. These instances were analyzed in numerical order. However, since the results are almost the same after the modified placement sequences, only hybrid sorts with front face S2 glass/epoxy and back face Aramid/epoxy are given as results. In this case, it can be said that the displacement of the hybrid composites which placed behind the ceramic, does not affect the results.

5.2.1 Numerical Results of Case 1: 6 mm Alumina Ceramic Front Faced Targets

In Case 1, six different target combinations are shot by four different velocities. Strike velocity versus residual velocity of projectile on 16 mm thickness target model with all used backing plates are demonstrated in Table 5.7 and Figure 5.8

Table 5.7 Strike velocities and residual velocities of projectile on 16 mm thickness target model with all used backing plates

	Backing Plates				
Strike velocity of projectile (m/s)		**850**	**800**	**750**	**700**
Residual velocity of projectile (m/s)	Aramid/epoxy	652	612	562	496
	Carbon-aramid/epoxy	670	616	556	512
	S2 glass/epoxy	607	563	539	469
	Hybrid 1	646	603	558	481
	Hybrid 2	637	592	560	493
	Hybrid 3	635	577	555	478

Where:

All Hybrid 1, 2 and 3 composite types are the same in this study. And,

Hybrid 1: 3 mm S2 glass/epoxy - 7 mm Aramid/epoxy

Hybrid 2: 5 mm S2 glass/epoxy - 5 mm Aramid/epoxy

Hybrid 3: 7 mm S2 glass/epoxy - 3 mm Aramid/epoxy

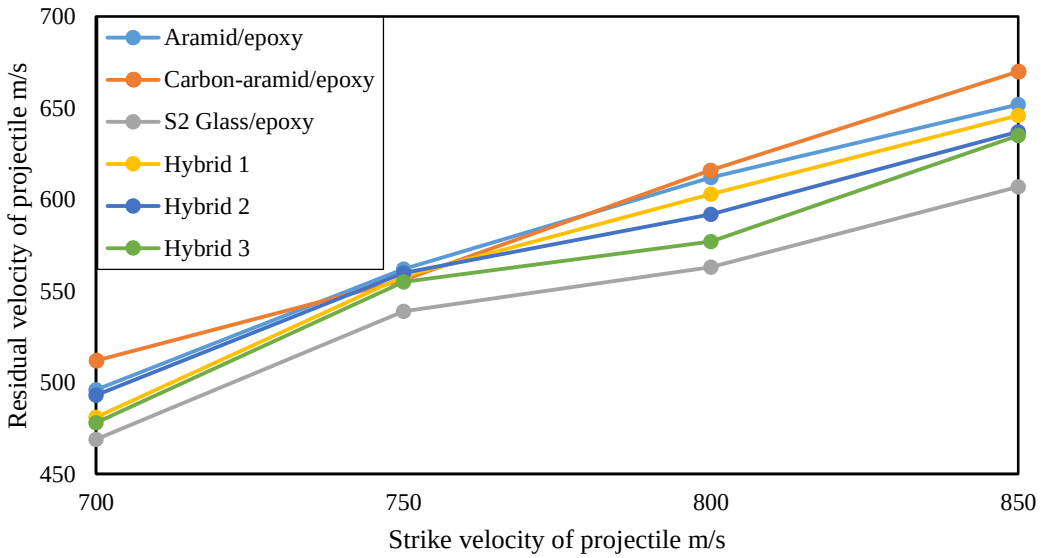
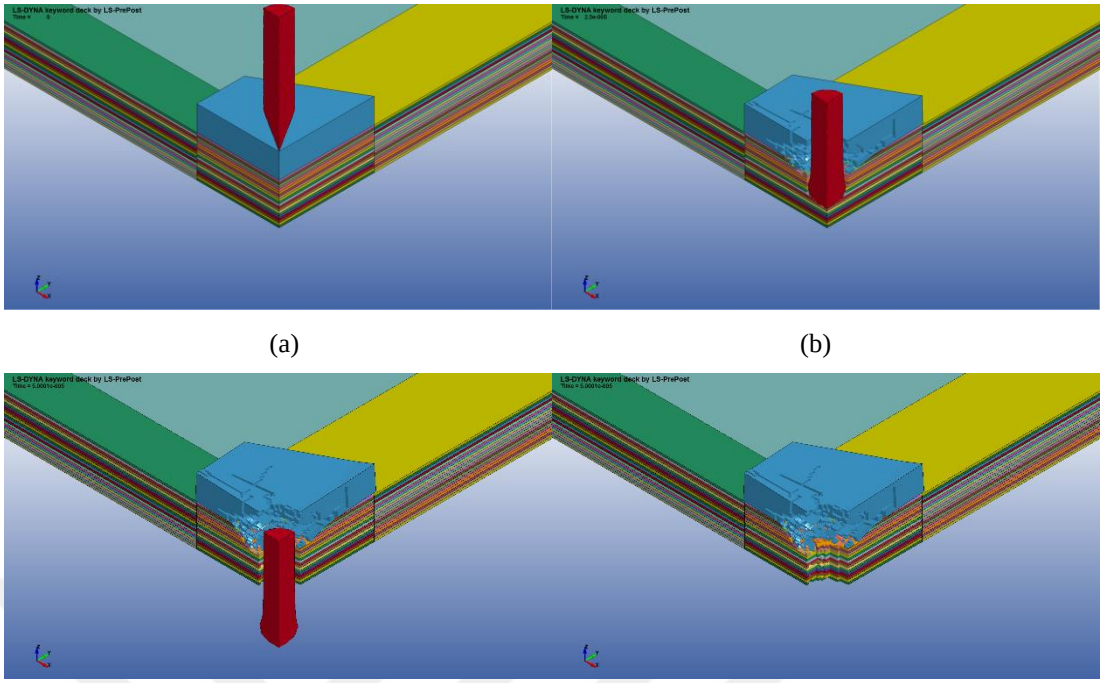


Figure 5.8 Strike velocity versus residual velocity of projectile on 16 mm thickness target model with all used backing plates

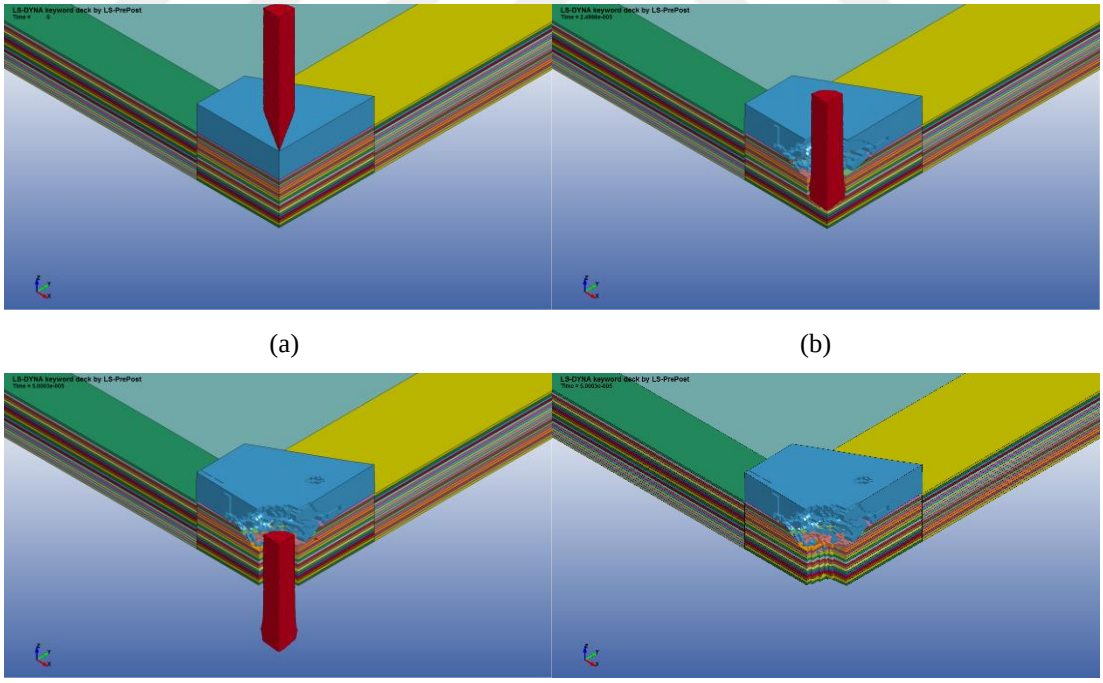
Views of 16 mm thickness target model with all backing plate types after 800 m/s strike velocity can be seen in Figure 5.9-14. Comparison of velocity versus time curve of 16 mm thickness target model with all used backing plates at 800 m/s strike velocity is given in Figure 5.15. Other velocity versus time curves of 16 mm thickness target model can be found in Appendix A.



(a) (b)

(c) (d)

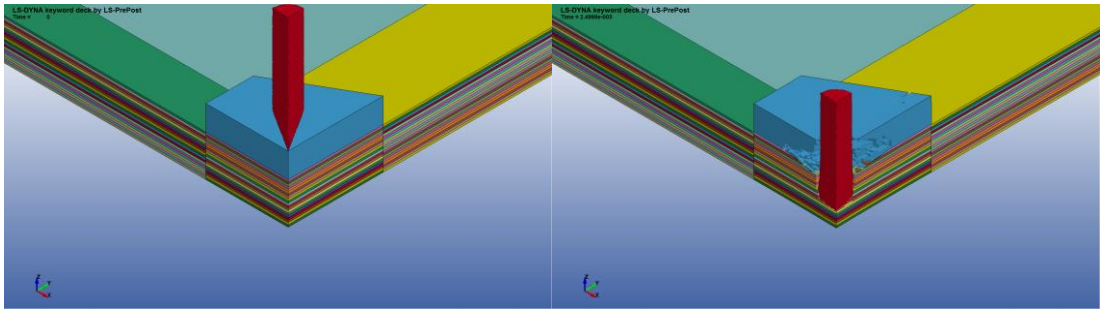
Figure 5.9 Views of 16 mm thickness target model with Aramid/epoxy backing plate after 800 m/s strike velocity, (a) t=0 ms, (b) t=0.025 ms, (c) t=0.05 ms, (d) t= 0.05 ms without projectile view



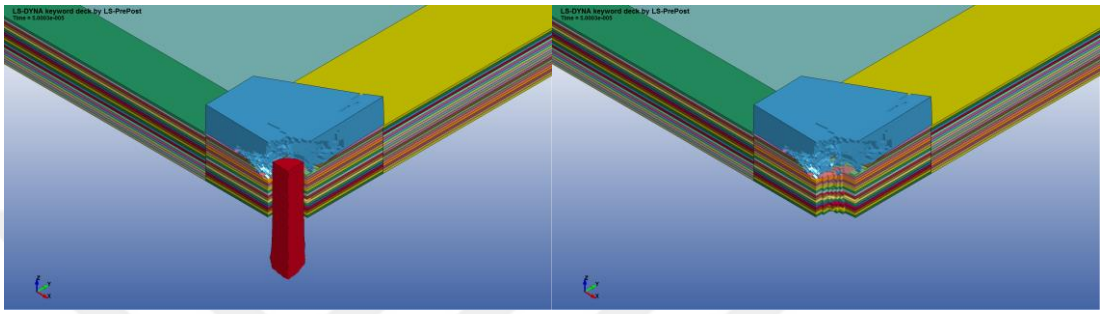
(a) (b)

(c) (d)

Figure 5.10 View of 16 mm thickness target model with Carbon-aramid/epoxy backing plate after 800 m/s strike velocity, (a) t=0 ms, (b) t=0.025 ms, (c) t=0.05 ms, (d) t= 0.05 ms without projectile view

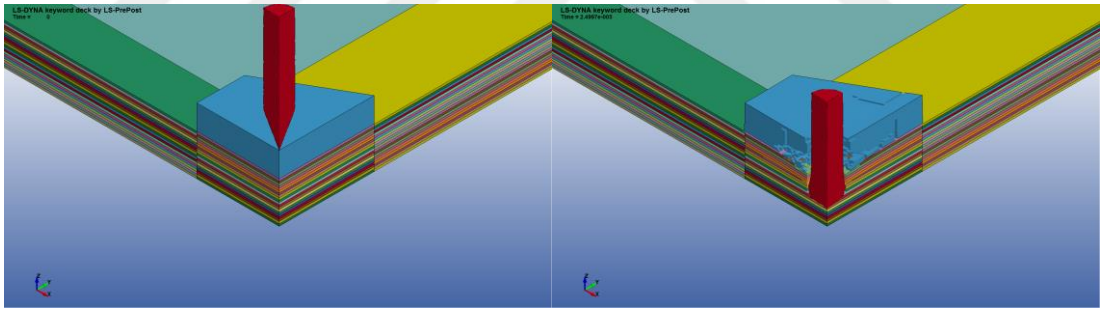


(a) (b)

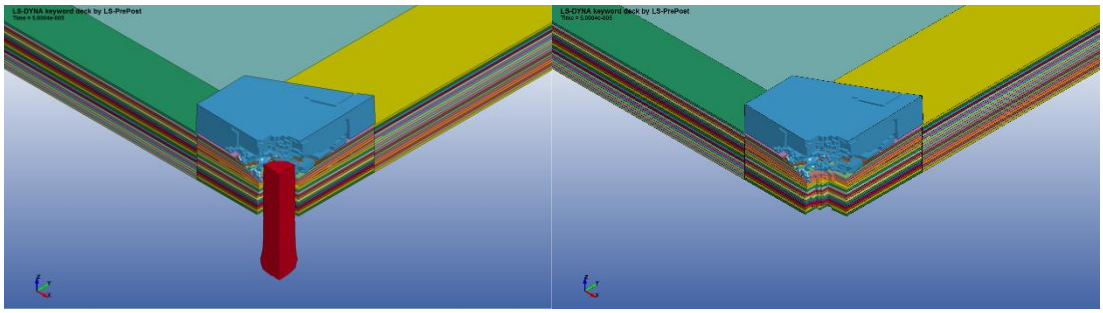


(c) (d)

Figure 5.11 View of 16 mm thickness target model with S2 glass/epoxy backing plate after 800 m/s strike velocity, (a) t=0 ms, (b) t=0.025 ms, (c) t=0.05 ms, (d) t= 0.05 ms without projectile view

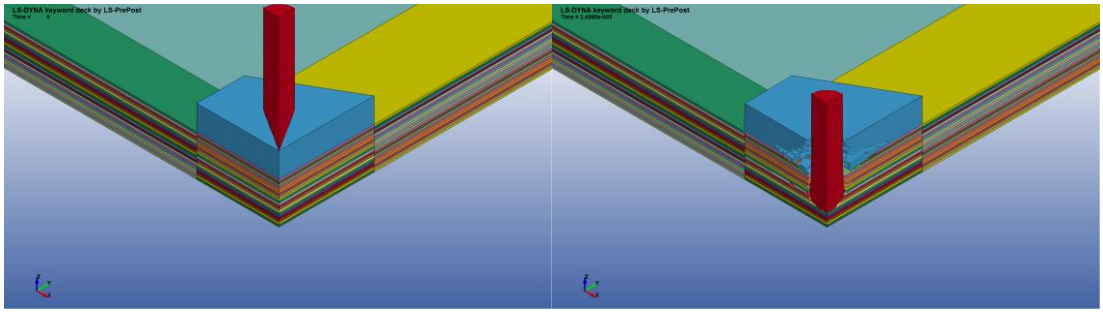


(a) (b)

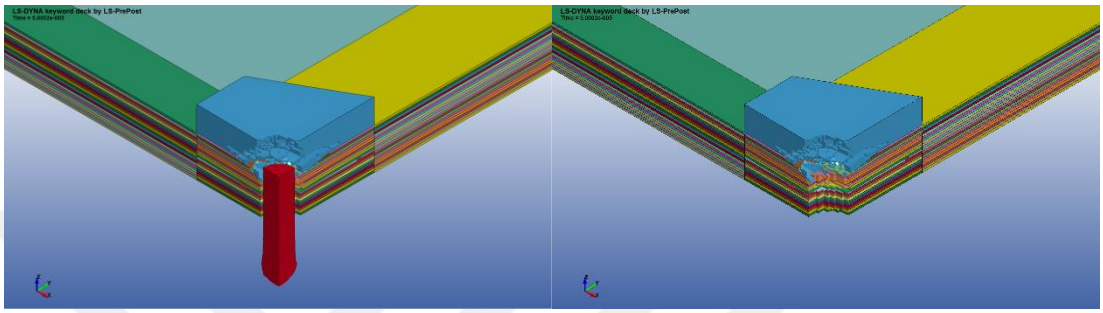


(c) (d)

Figure 5.12 View of 16 mm thickness target model with Hybrid 1 backing plate after 800 m/s strike velocity, (a) t=0 ms, (b) t=0.025 ms, (c) t=0.05 ms, (d) t= 0.05 ms without projectile view

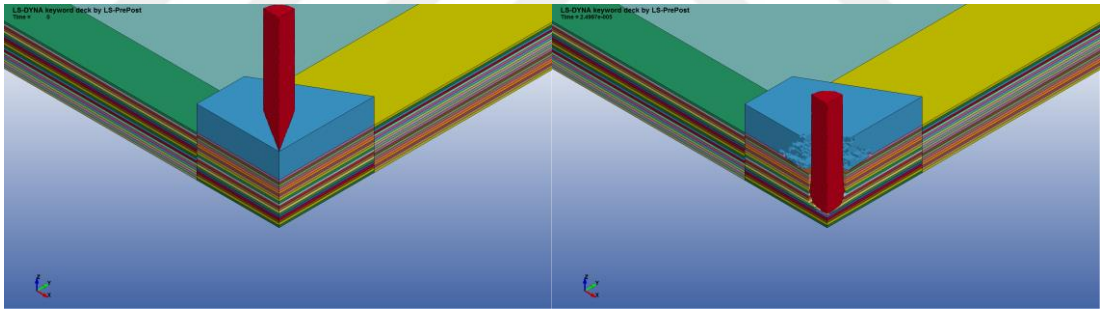


(a) (b)

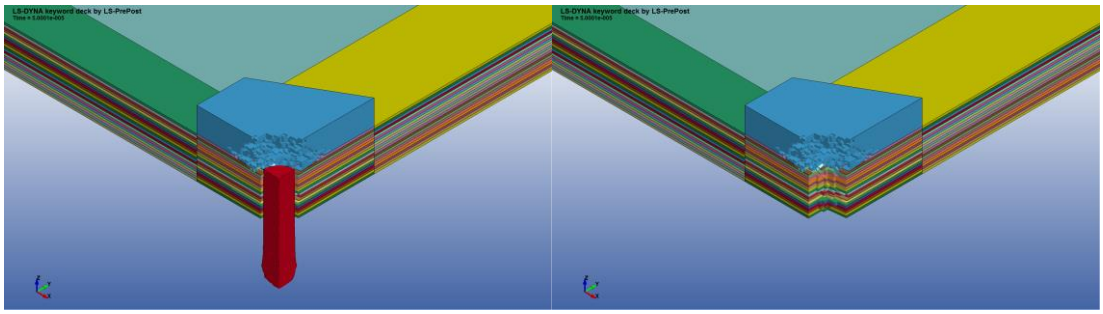


(c) (d)

Figure 5.13 View of 16 mm thickness target model with Hybrid 2 backing plate after 800 m/s strike velocity, (a) t=0 ms, (b) t=0.025 ms, (c) t=0.05 ms, (d) t= 0.05 ms without projectile view



(a) (b)



(c) (d)

Figure 5.14 View of 16 mm thickness target model with Hybrid 3 backing plate after 800 m/s strike velocity, (a) t=0 ms, (b) t=0.025 ms, (c) t=0.05 ms, (d) t= 0.05 ms without projectile view

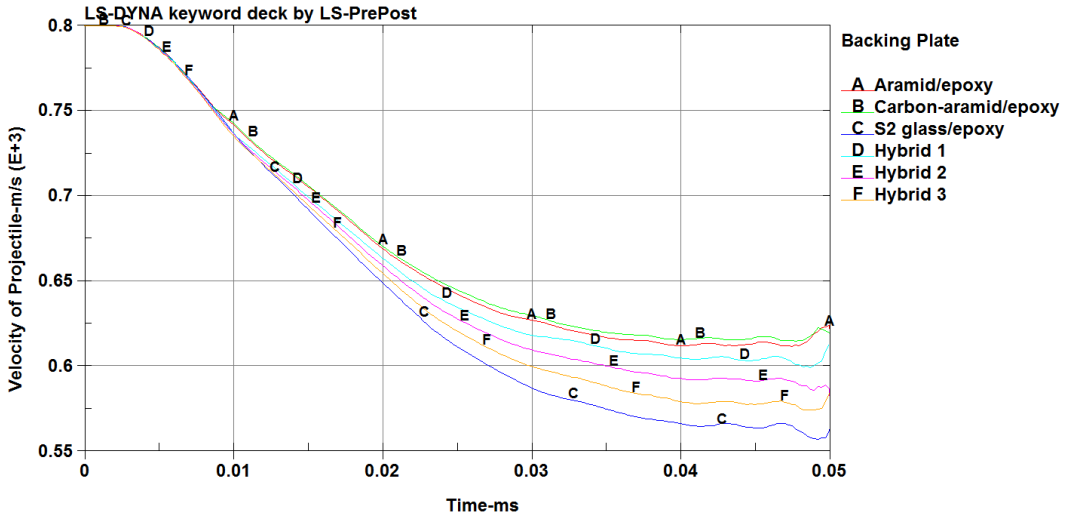


Figure 5.15 Comparison of Velocity versus Time curve of 16 mm thickness target model with all used backing plates at 800 m/s strike velocity

In this thickness, ballistic performance of target with S2 glass/epoxy backing plate gives better results than others, at all four different strike velocities. Respectively, Hybrid 3, Hybrid 2, Hybrid 1, Aramid/epoxy and Carbon-aramid/epoxy give the best results after S2 glass/epoxy. At 750 m/s strike velocity, the ballistic performance of all composites except the S2 glass/epoxy are found nearly same. The ballistic performances of Hybrid 1, Hybrid 2 and Hybrid 3, formed by the combination of Aramid/epoxy and S2 glass/epoxy, were found to match the combined thickness ratios of S2 glass/epoxy and Aramid/epoxy.

As it seen, at all strike velocities, when the backing plate is Aramid/epoxy, the damage is spread out to a larger area on ceramic front face after impact compared to other backing plate composites. The least damaged area occurs when the backing plate is also S2 glass/epoxy. It is observed that when the backing plates are different, damaged area of the ceramic after the impact did not affect the ballistic performance of the target at the same time.

It was found that the deformation increased on the projectile when the same backing plate is used on the target and as the impact velocity increases. As the impact velocity increases, the further blunting on the projectile is observed and the effect of mushrooming is observed to increase.

It was observed that ceramic and composite surfaces were separated by the impact in all ceramic-composite combinations. In high strike velocities of the projectile, the connection between composite and ceramic was more stable.

When compared to the response of targets with all the used composite backing plates to projectile, at the same strike velocity, it was found that it was directly proportional to their ballistic performances. As a result, when using S2 glass/epoxy backing plate, it was observed that the deformation of the projectile was at its highest value and when using Carbon-aramid/epoxy backing plate, it was observed that the deformation of the projectile was at its lowest. Moreover, there was no difference between the appearance of the projectile after it had penetrated the ceramics, and the appearance of the projectile after it had penetrated the composite.

Displacement of the hybrid composites placed behind the ceramic has no effect on the results. Crushing and/or delamination between the surfaces of S2 glass/epoxy and Aramid/epoxy composites were observed in the armor used with the hybrid backing plate.

5.2.2 Numerical Results of Case 2: 8 mm Alumina Ceramic Front Faced Targets

In Case 2, six different target combinations are shot by four different velocities. Strike velocity versus residual velocity of projectile on 18 mm thickness target model with all used backing plates are seen in Table 5.8 and Figure 5.16.

Table 5.8 Strike velocities and residual velocities of projectile on 18 mm thickness target model with all used backing plates

	Backing Plates				
Strike velocity of projectile (m/s)		**850**	**800**	**750**	**700**
Residual velocity of projectile (m/s)	Aramid/epoxy	538	498	440	396
	Carbon-aramid/epoxy	573	502	429	408
	S2 glass/epoxy	495	435	387	375
	Hybrid 1	531	465	404	393
	Hybrid 2	528	473	402	379
	Hybrid 3	527	456	395	378

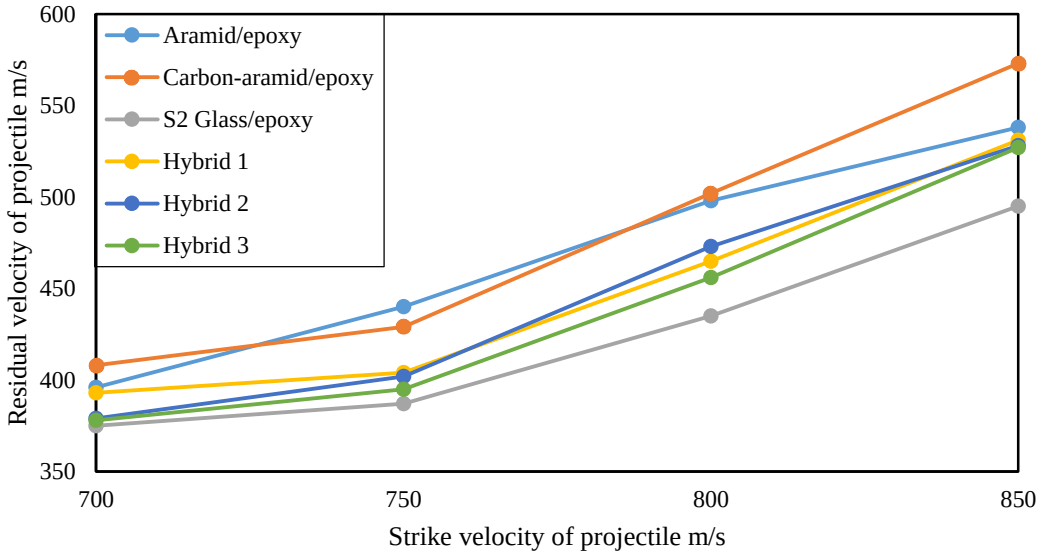
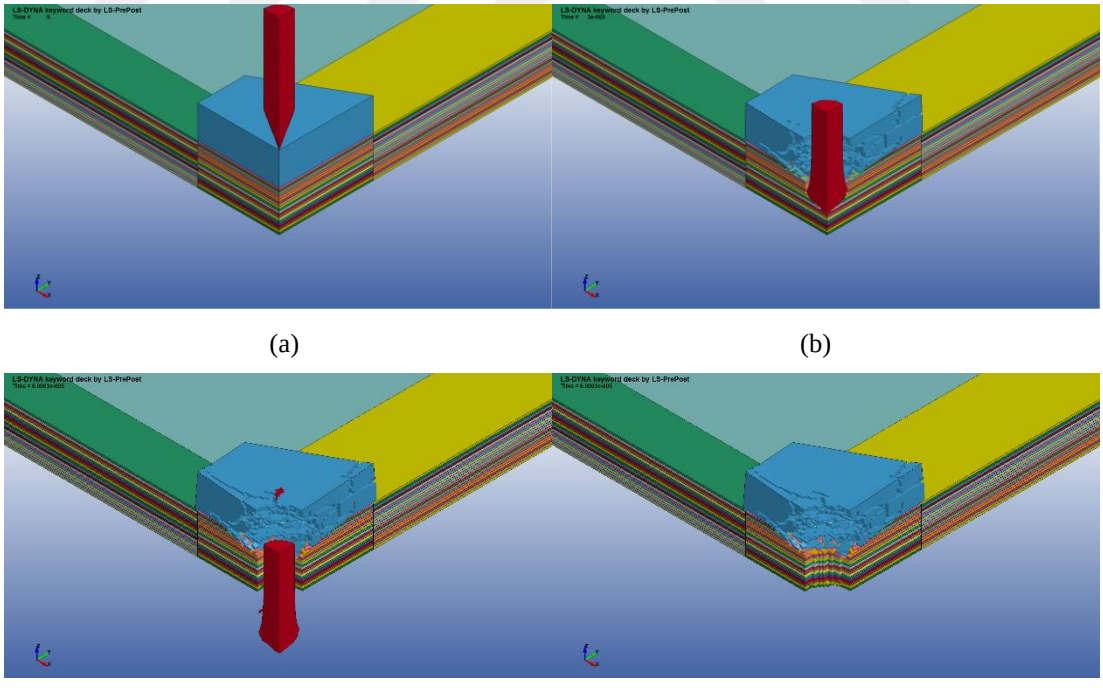


Figure 5.16 Strike velocity versus residual velocity of projectile on 18 mm thickness target model with all used backing plates

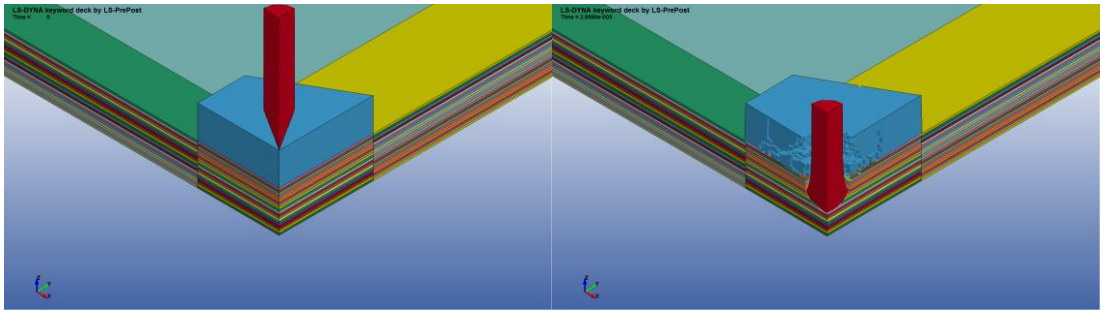
Also views of 18 mm thickness target model with all backing plate types after 800 m/s strike velocity can be seen in Figure 5.17-22.



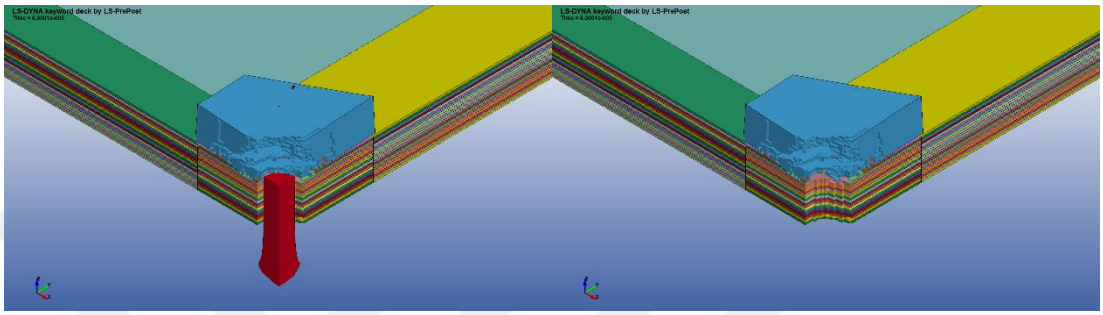
(a) (b)

(c) (d)

Figure 5.17 View of 18 mm thickness target model with Aramid/epoxy backing plate after 800 m/s strike velocity, (a) t=0 ms, (b) t=0.03 ms, (c) t=0.06 ms, (d) t= 0.06 ms without projectile view

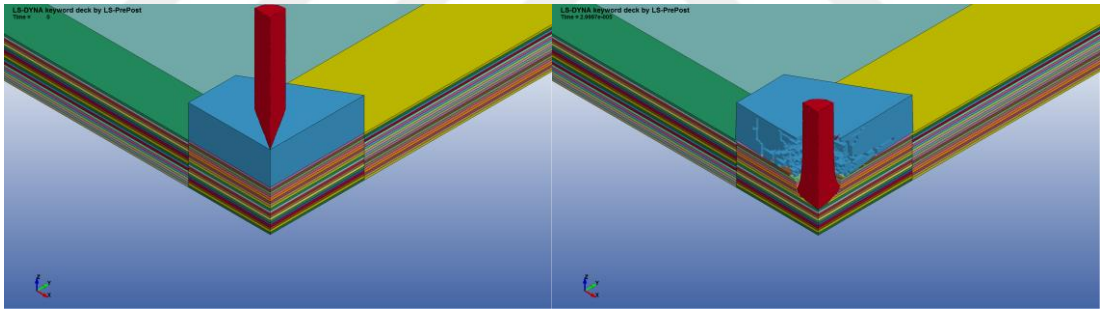


(a) (b)

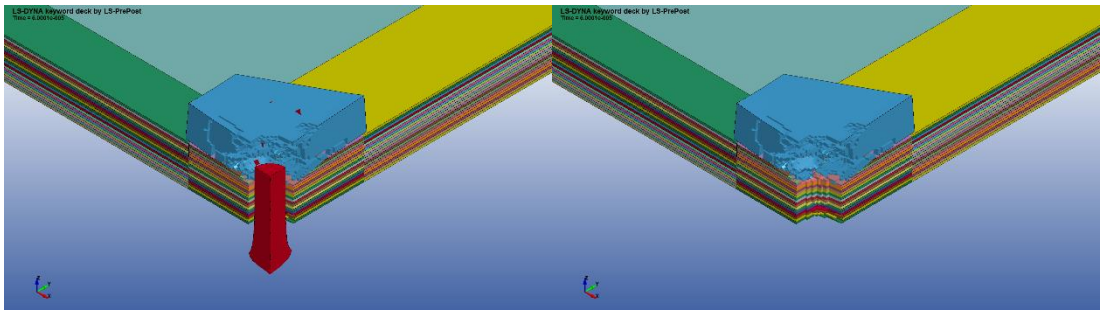


(c) (d)

Figure 5.18 View of 18 mm thickness target model with Carbon-aramid/epoxy backing plate after 800 m/s strike velocity, (a) t=0 ms, (b) t=0.03 ms, (c) t=0.06 ms, (d) t= 0.06 ms without projectile view

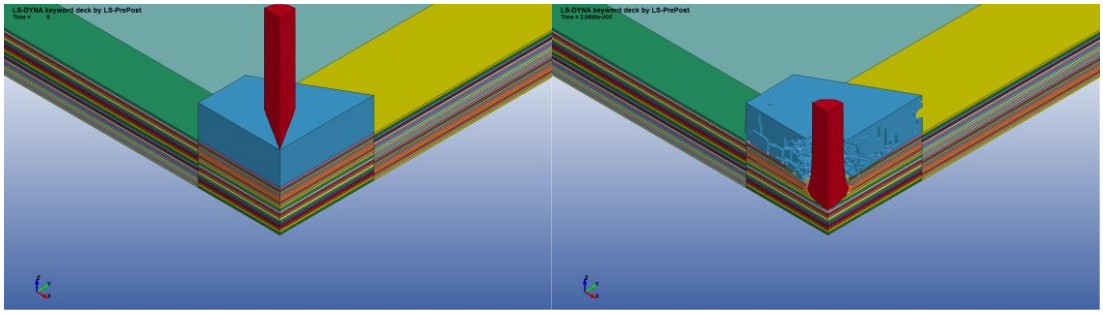


(a) (b)

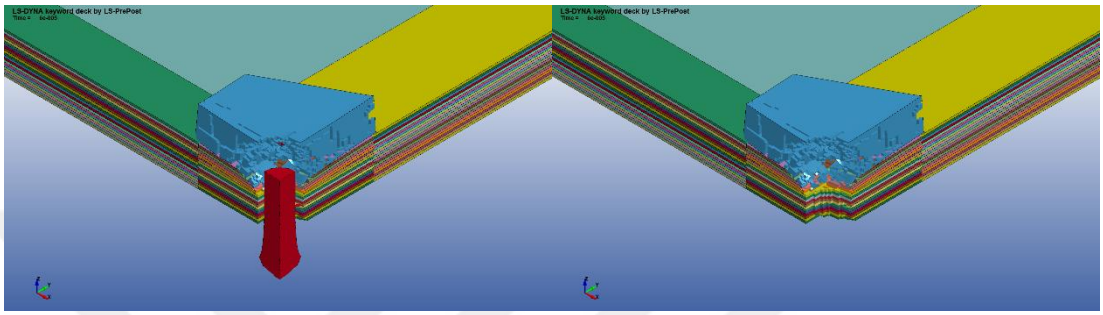


(c) (d)

Figure 5.19 View of 18 mm thickness target model with S2 glass/epoxy backing plate after 800 m/s strike velocity, (a) t=0 ms, (b) t=0.03 ms, (c) t=0.06 ms, (d) t= 0.06 ms without projectile view

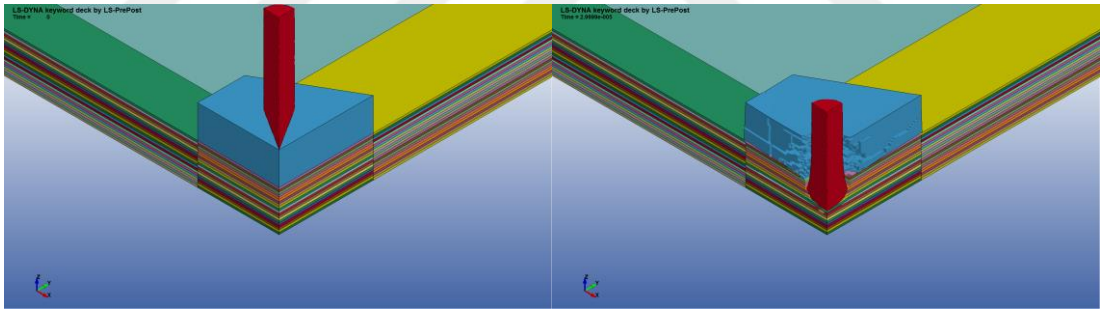


(a) (b)

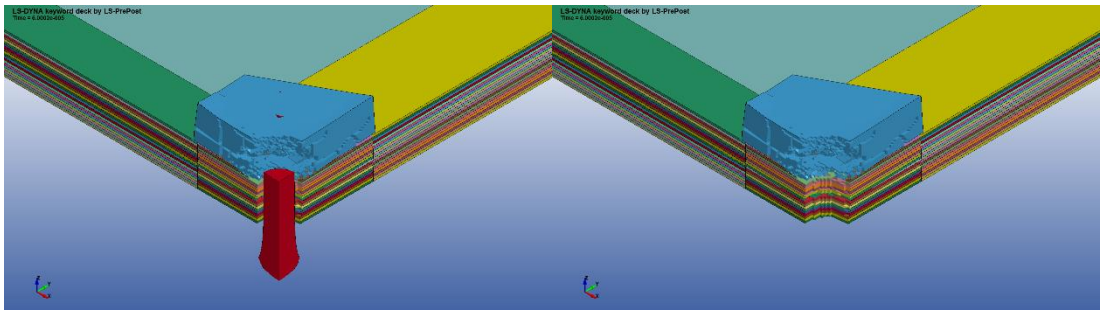


(c) (d)

Figure 5.20 View of 18 mm thickness target model with Hybrid 1 backing plate after 800 m/s strike velocity, (a) t=0 ms, (b) t=0.03 ms, (c) t=0.06 ms, (d) t= 0.06 ms without projectile view

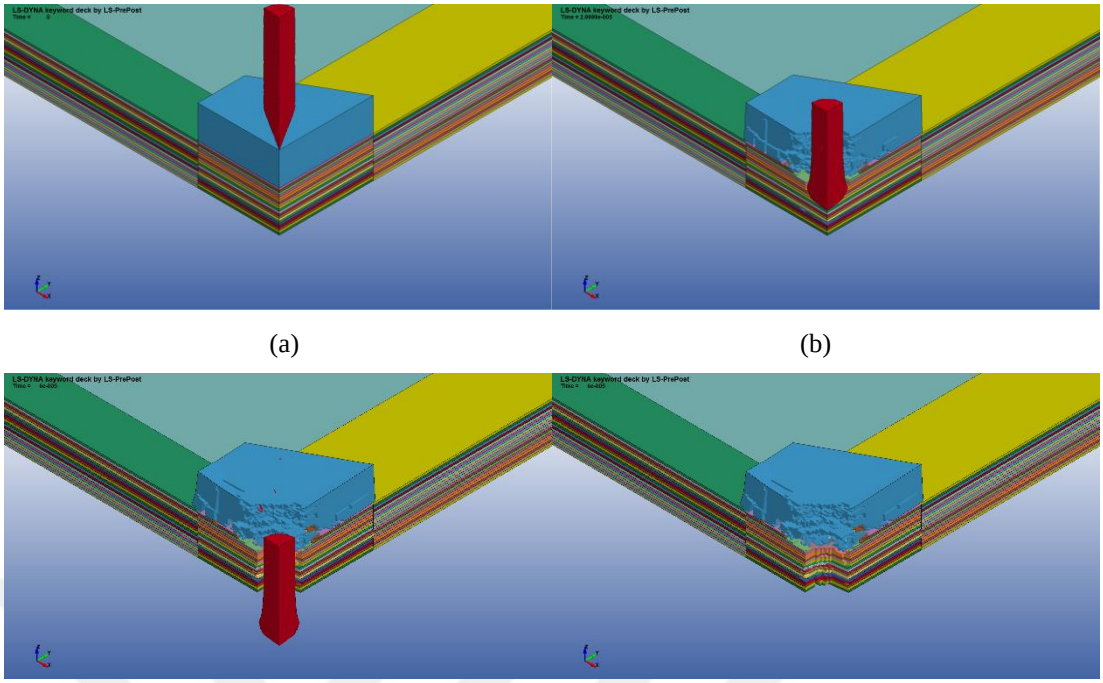


(a) (b)



(c) (d)

Figure 5.21 View of 18 mm thickness target model with Hybrid 2 backing plate after 800 m/s strike velocity, (a) t=0 ms, (b) t=0.03 ms, (c) t=0.06 ms, (d) t= 0.06 ms without projectile view



(a) (b)

(c) (d)

Figure 5.22 View of 18 mm thickness target model with Hybrid 3 backing plate after 800 m/s strike velocity, (a) t=0 ms, (b) t=0.03 ms, (c) t=0.06 ms, (d) t= 0.06 ms without projectile view

Comparison of velocity versus time curve of 18 mm thickness target model with all used backing plates at 800 m/s strike velocity is given in Figure 5.23. Other velocity versus time curves of 18 mm thickness target model can be found in Appendix B.

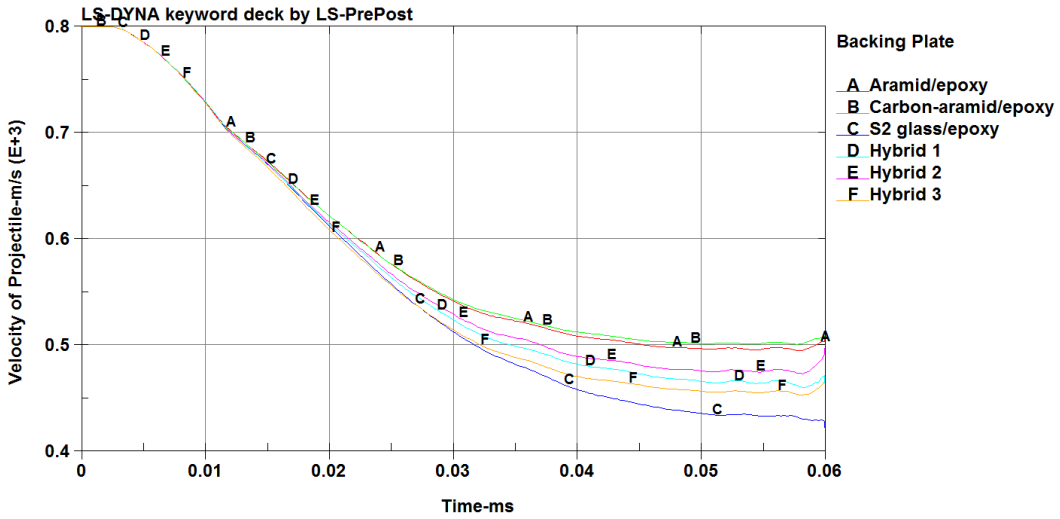


Figure 5.23 Comparison of Velocity versus Time curve of 18 mm thickness target model with all used backing plates at 800 m/s strike velocity

In this thickness, ballistic performance of target with S2 glass/epoxy backing plate gives better results than others, at all four different strike velocities. Respectively, Hybrid 3, Hybrid 2, Hybrid 1, Aramid/epoxy and Carbon-aramid/epoxy give the best results after S2 glass/epoxy. The difference in the ballistic performance between the Aramid/epoxy and the Carbon-aramid/epoxy was slightly reduced. Even at 750 m/s strike velocity, the ballistic performance of Carbon-aramid/epoxy is better than the ballistic performance of Aramid/epoxy. Differences between the ballistic performances of Hybrid 1, Hybrid 2 and Hybrid 3, formed by the combination of Aramid/epoxy and S2 glass/epoxy, were found to match the combined thickness ratios of S2 glass/epoxy and Aramid/epoxy.

As it is seen, at all strike velocities, when the backing plate is Aramid/epoxy, the damage is spread out to a larger area on ceramic front face after impact compared to other backing plate composites. The damaged area was determined to be almost the same on the other backing plate composites. It is observed that when the backing plates are different, damaged area of the ceramic after the impact did not affect the ballistic performance of the target at the same time.

It was found that there are no deformation differences on the projectile when the same backing plate was used on the target and as the impact velocity increases. At four different strike velocities, it was seen that it was almost the same deformation on projectile. After the impact, blunting on the projectile is observed and the effect of mushrooming is observed.

It was observed that ceramic and composite surfaces were separated by the impact in all ceramic-composite combinations. In high strike velocities of the projectile, the connection between composite and ceramic was more stable.

When compared to the response of targets with all the used composite backing plates to projectile, at the same strike velocity, it was found that it was directly proportional to their ballistic performances. As a result, when using S2 glass/epoxy backing plate, it was observed that the deformation of the projectile was at its highest

value and when using Carbon-aramid/epoxy backing plate, it was observed that the deformation of the projectile was at its lowest. Moreover, there was no difference between the appearance of the projectile after it had penetrated the ceramics, and the appearance of the projectile after it had penetrated the composite.

Displacement of the hybrid composites placed behind the ceramic has no effect on the results. Crushing and/or delamination between the surfaces of S2 glass/epoxy and Aramid/epoxy composites were observed in the armor used with the hybrid backing plate.

5.2.3 Numerical Results of Case 3: 10 mm Alumina Ceramic Front Faced Targets

In Case 3, six different target combinations are shot by four different velocities. Strike velocity versus residual velocity of projectile on 20 mm thickness target model with all used backing plates are given in Table 5.9 and Figure 5.24.

Table 5.9 Strike velocities and residual velocities of projectile on 20 mm thickness target model with all used backing plates

	Backing Plates				
Strike velocity of projectile (m/s)		**850**	**800**	**750**	**700**
Residual velocity of projectile (m/s)	Aramid/epoxy	473	366	281	250
	Carbon-aramid/epoxy	461	361	303	220
	S2 glass/epoxy	399	316	265	207
	Hybrid 1	460	362	287	230
	Hybrid 2	445	351	299	225
	Hybrid 3	427	349	268	231

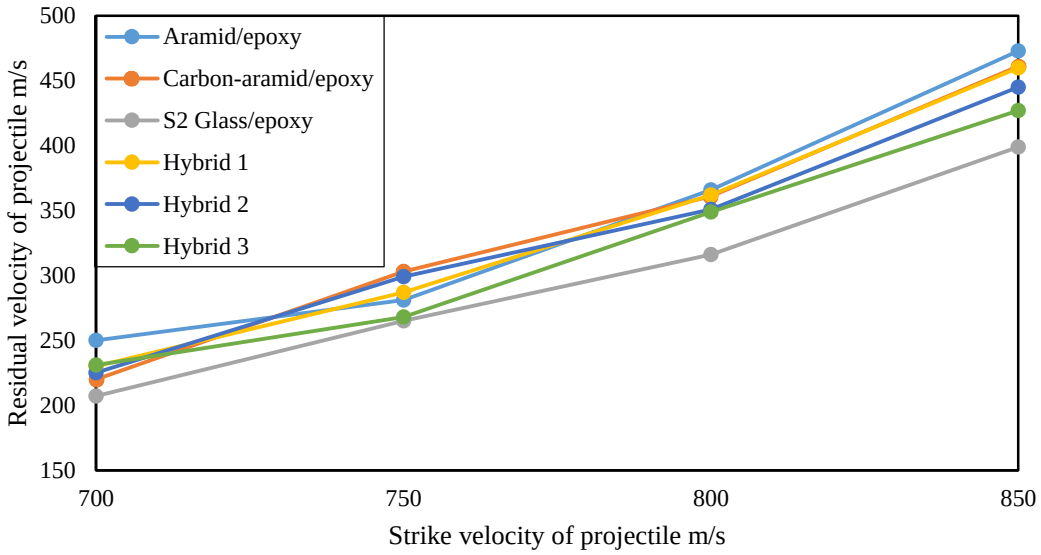
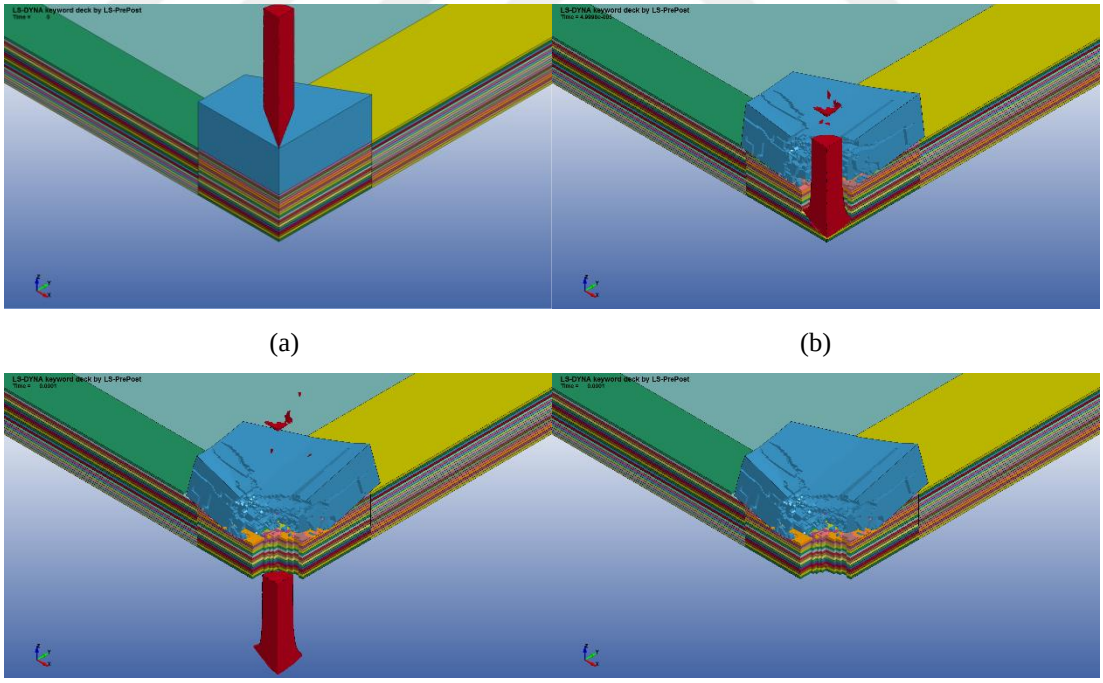


Figure 5.24 Strike velocity versus residual velocity of projectile on 20 mm thickness target model with all used backing plates

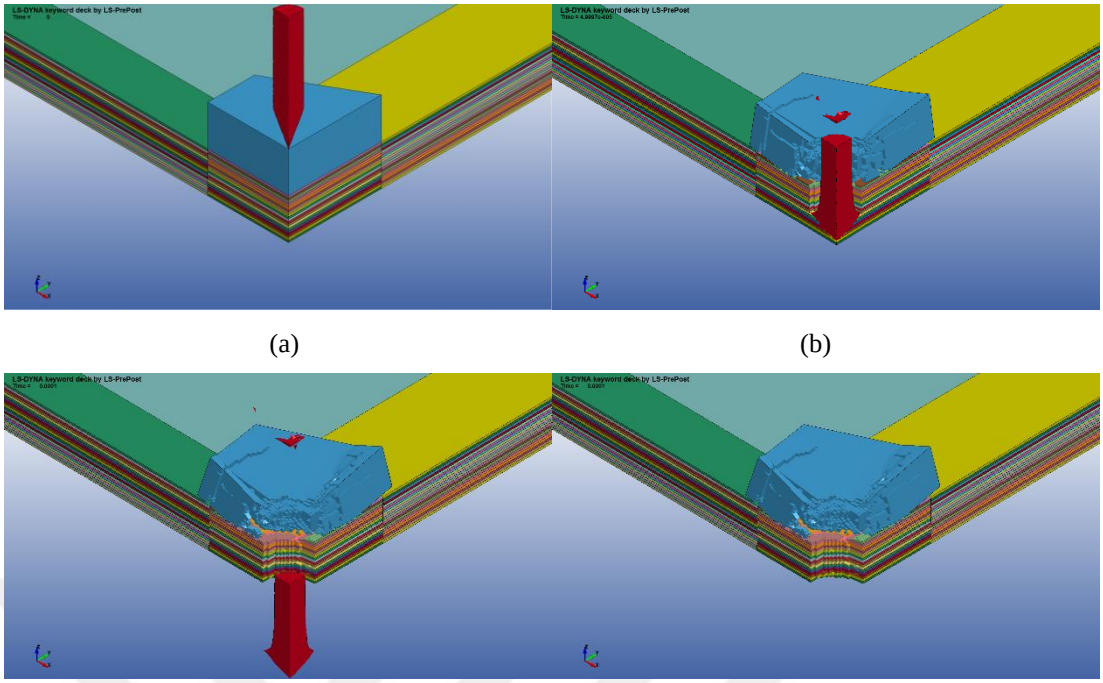
Also views of 20 mm thickness target model with all backing plate types after 800 m/s strike velocity can be seen in Figure 5.25-30.



(a) (b)

(c) (d)

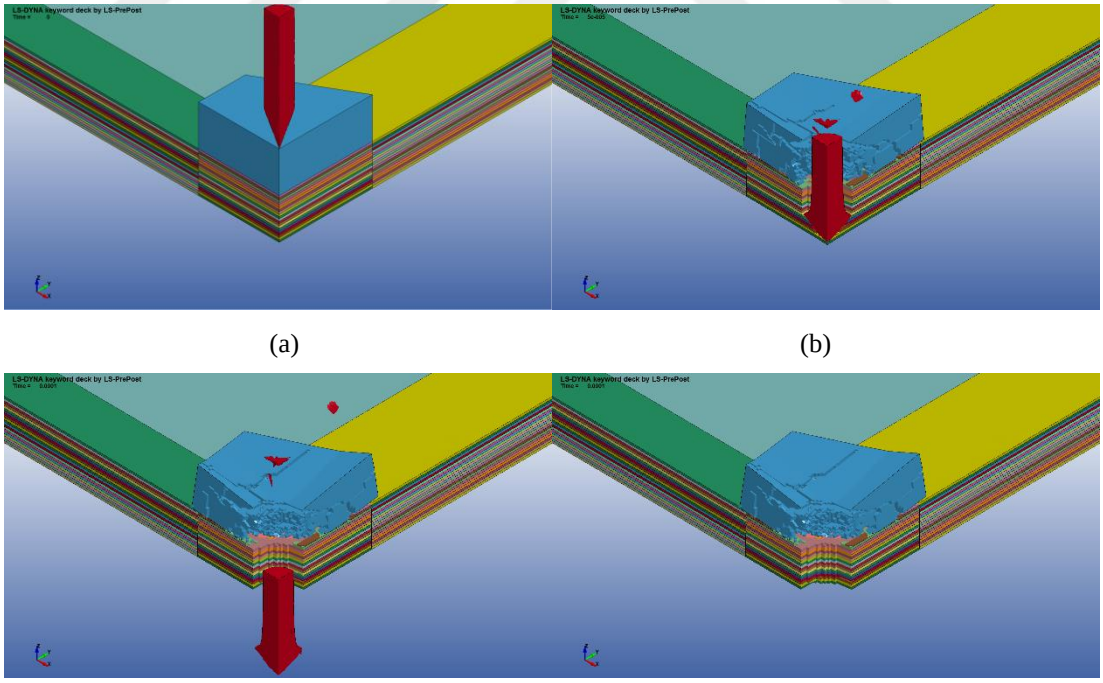
Figure 5.25 View of 20 mm thickness target model with Aramid/epoxy backing plate after 800 m/s strike velocity, (a) t=0 ms, (b) t=0.05 ms, (c) t=0.1 ms, (d) t= 0.1 ms without projectile view



(a) (b)

(c) (d)

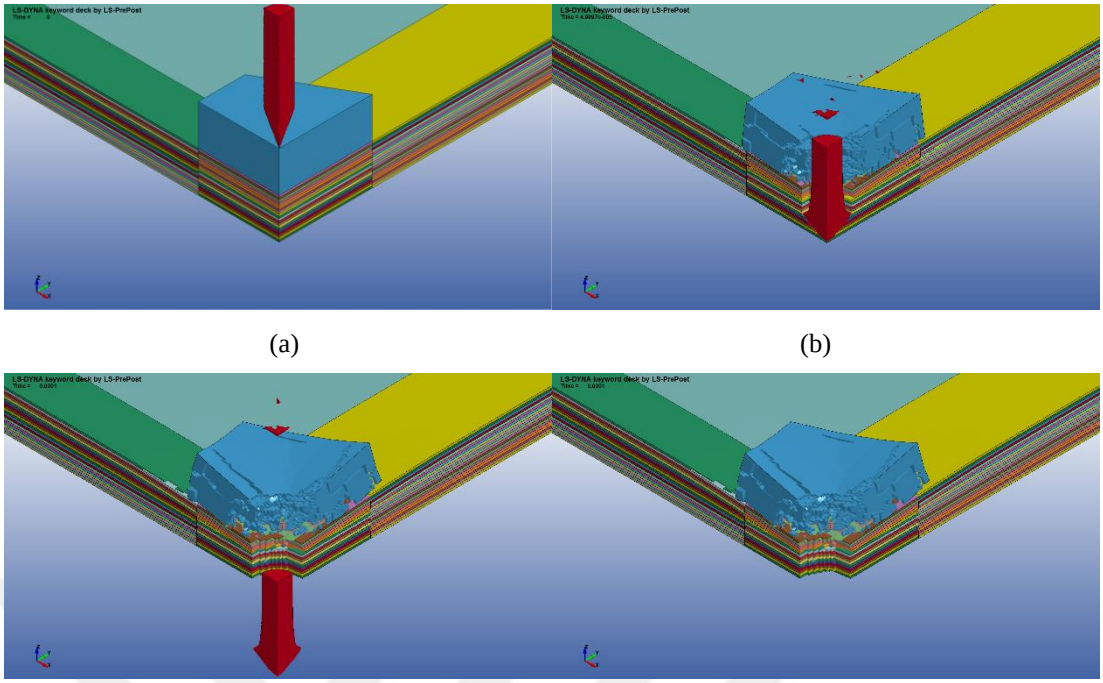
Figure 5.26 View of 20 mm thickness target model with Carbon-aramid/epoxy backing plate after 800 m/s strike velocity, (a) t=0 ms, (b) t=0.05 ms, (c) t=0.1 ms, (d) t= 0.1 ms without projectile view



(a) (b)

(c) (d)

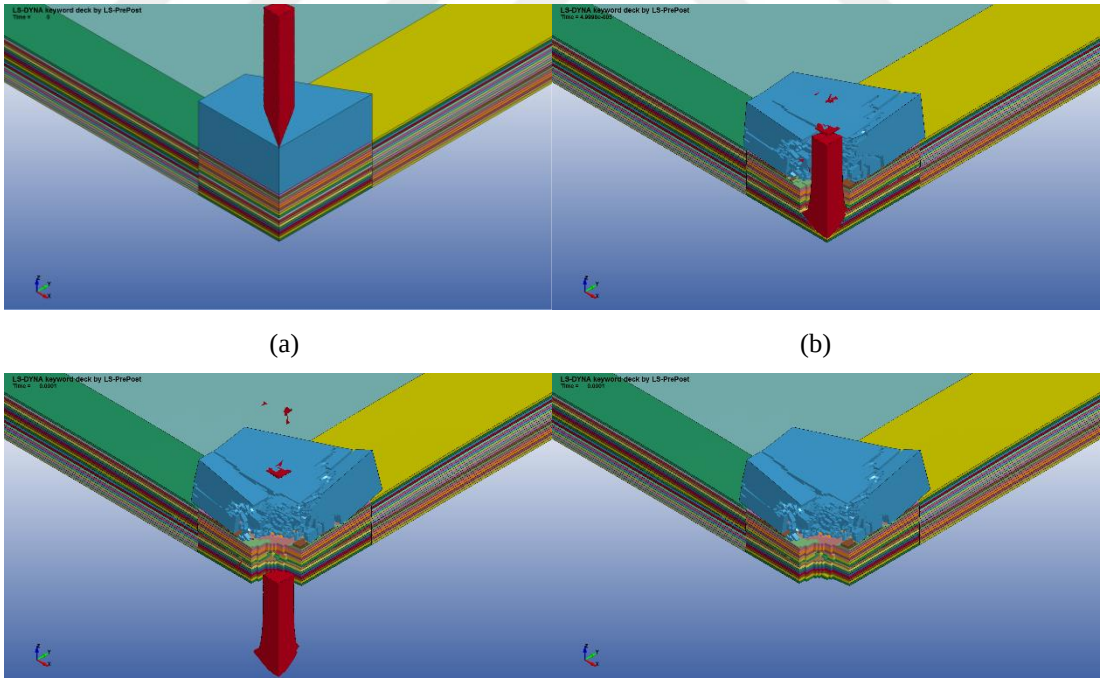
Figure 5.27 View of 20 mm thickness target model with S2 glass/epoxy backing plate after 800 m/s strike velocity, (a) t=0 ms, (b) t=0.05 ms, (c) t=0.1 ms, (d) t= 0.1 ms without projectile view



(a) (b)

(c) (d)

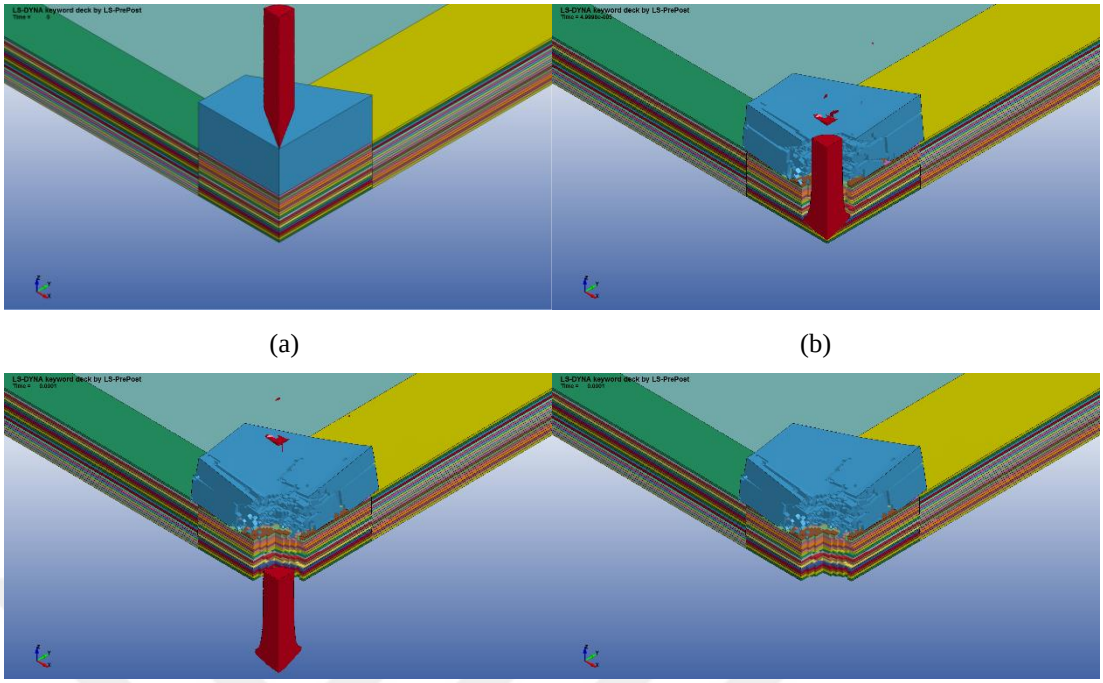
Figure 5.28 View of 20 mm thickness target model with Hybrid 1 backing plate after 800 m/s strike velocity, (a) t=0 ms, (b) t=0.05 ms, (c) t=0.1 ms, (d) t= 0.1 ms without projectile view



(a) (b)

(c) (d)

Figure 5.29 View of 20 mm thickness target model with Hybrid 2 backing plate after 800 m/s strike velocity, (a) t=0 ms, (b) t=0.025 ms, (c) t=0.05 ms, (d) t= 0.05 ms without projectile view



(a) (b)

(c) (d)

Figure 5.30 View of 20 mm thickness target model with Hybrid 3 backing plate after 800 m/s strike velocity, (a) t=0 ms, (b) t=0.05 ms, (c) t=0.1 ms, (d) t= 0.1 ms without projectile view

Comparison of velocity versus time curve of 20 mm thickness target model with all used backing plates at 800 m/s strike velocity is given in Figure 5.31. Other velocity versus time curves of 20 mm thickness target model can be found in Appendix C.

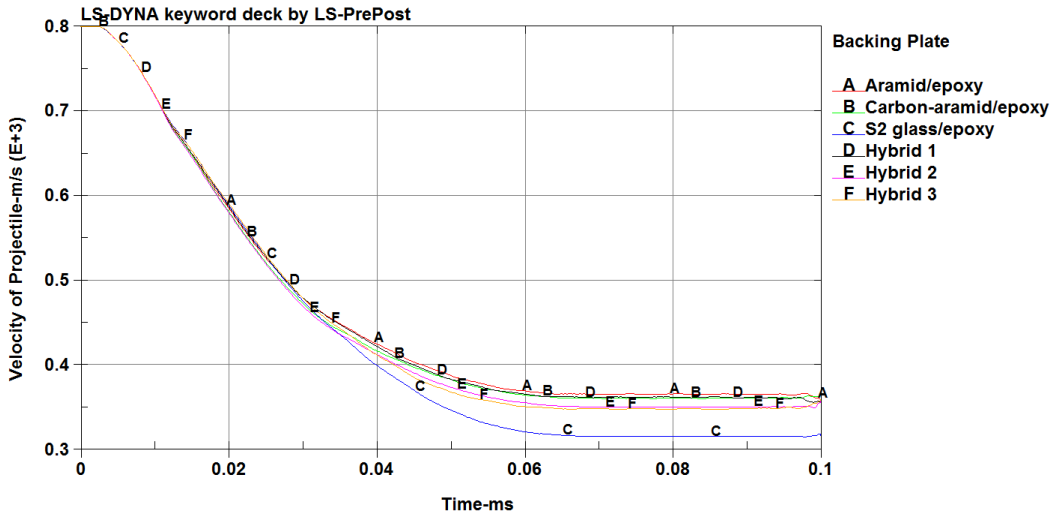


Figure 5.31 Comparison of Velocity versus Time curve of 20 mm thickness target model with all used backing plates at 800 m/s strike velocity

In this thickness, ballistic performance of target with S2 glass/epoxy backing plate gives better results than others, at all four different strike velocities. Respectively, Hybrid 3, Hybrid 2, Hybrid 1, Carbon-aramid/epoxy and Aramid/epoxy give the best results after S2 glass/epoxy. Only at 750 m/s strike velocity, the ballistic performance of Aramid/epoxy is better than the ballistic performance of Carbon-aramid/epoxy. Generally, the ballistic performances of Hybrid 1, Hybrid 2 and Hybrid 3, formed by the combination of Aramid/epoxy and S2 glass/epoxy, were found to match the combined thickness ratios of S2 glass/epoxy and Aramid/epoxy. However, at 750 m/s strike velocity, the ballistic performances of Hybrid 1 and Hybrid 2 are even worse than the ballistic performance of Aramid/epoxy.

It was found that the damaged area was determined to be almost the same on the all backing plate composites after all strike velocities.

It was found that the deformation increased on the projectile when the same backing plate is used on the target and as the impact velocity decreases. As the impact velocity increases, the further blunting on the projectile is observed and the effect of mushrooming is observed to decrease.

It was observed that ceramic and composite surfaces were separated by the impact in all ceramic-composite combinations. In high strike velocities of the projectile, the connection between composite and ceramic was more stable.

When compared to the response of targets with all the used composite backing plates to projectile, at the same strike velocity, it was found that it was directly proportional to their ballistic performances. As a result, when using S2 glass/epoxy backing plate, it was observed that the deformation of the projectile was at its highest value and when using Aramid/epoxy backing plate, it was observed that the deformation of the projectile was at its lowest. Moreover, there was no difference between the appearance of the projectile after it had penetrated the ceramics, and the appearance of the projectile after it had penetrated the composite.

Displacement of the hybrid composites placed behind the ceramic has no effect on the results. Crushing and/or delamination between the surfaces of S2 glass/epoxy and Aramid/epoxy composites were observed in the armor used with the hybrid backing plate.

When these three cases are compared with each other, the effect of the ceramic thickness change on ballistic performance can be seen more clearly. It can also be demonstrated that residual velocity of projectile versus thickness of ceramic with all used backing plates is shown in Figure 5.32-35. It is seen that even a slight change in the thickness of the ceramic how effective it is on the residual velocity of projectile. Generally, according to other strike velocities, the ballistic performance of all composites are found close at 700 m/s strike velocity in their same ceramic thicknesses.

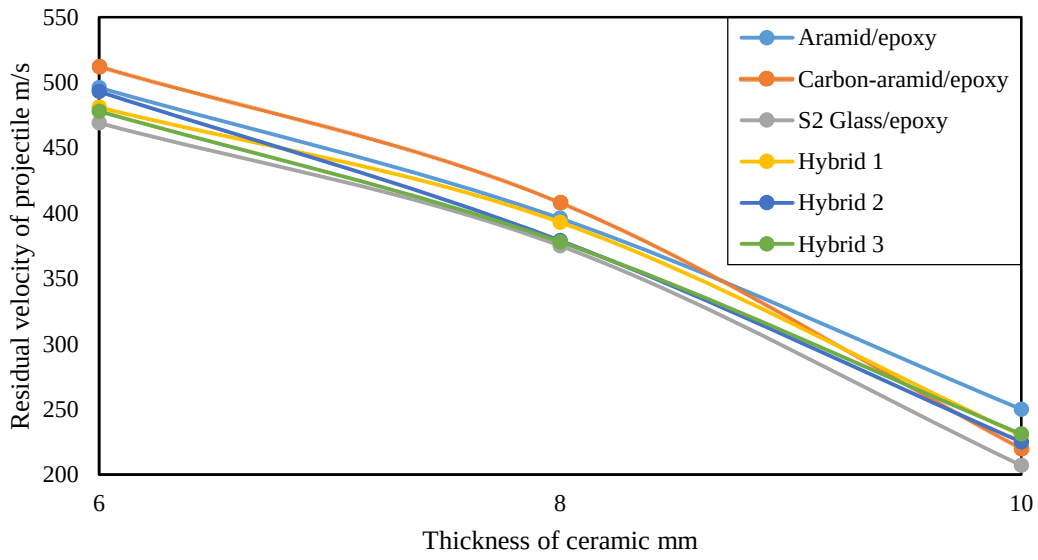


Figure 5.32 Residual velocity of projectile versus thickness of ceramic curve with all used backing plates at 700 m/s strike velocity

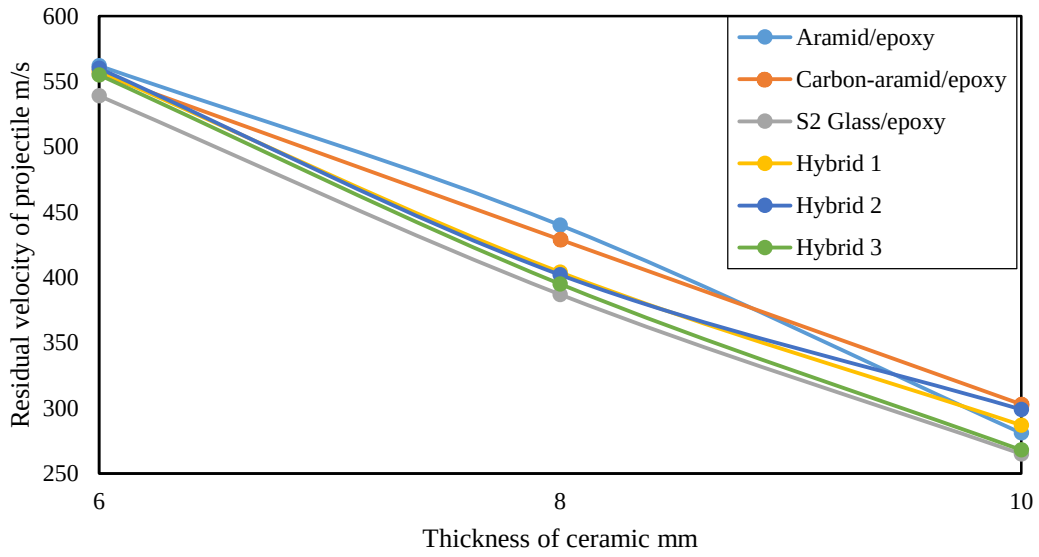


Figure 5.33 Residual velocity of projectile versus thickness of ceramic curve with all used backing plates at 750 m/s strike velocity

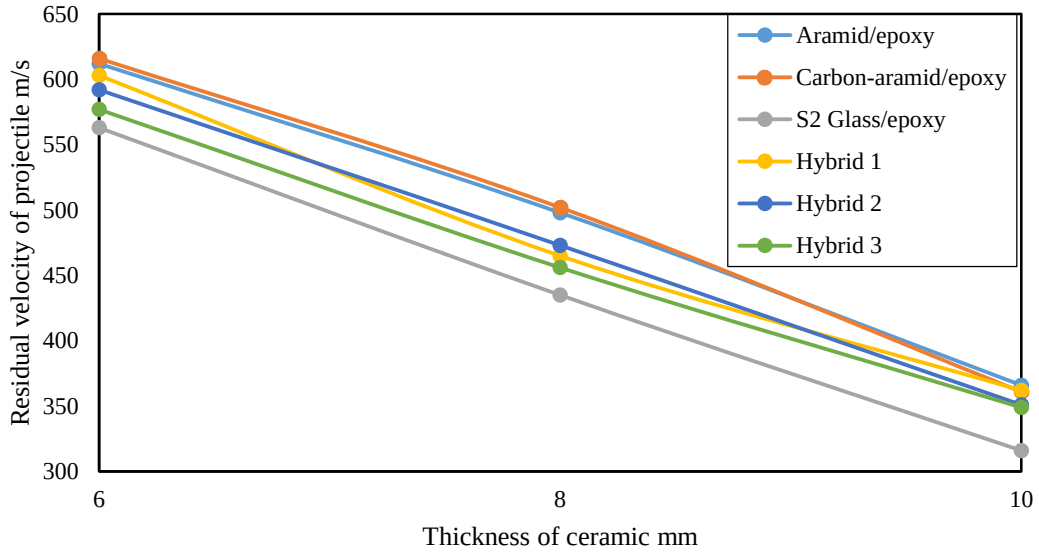


Figure 5.34 Residual velocity of projectile versus thickness of ceramic curve with all used backing plates at 800 m/s strike velocity

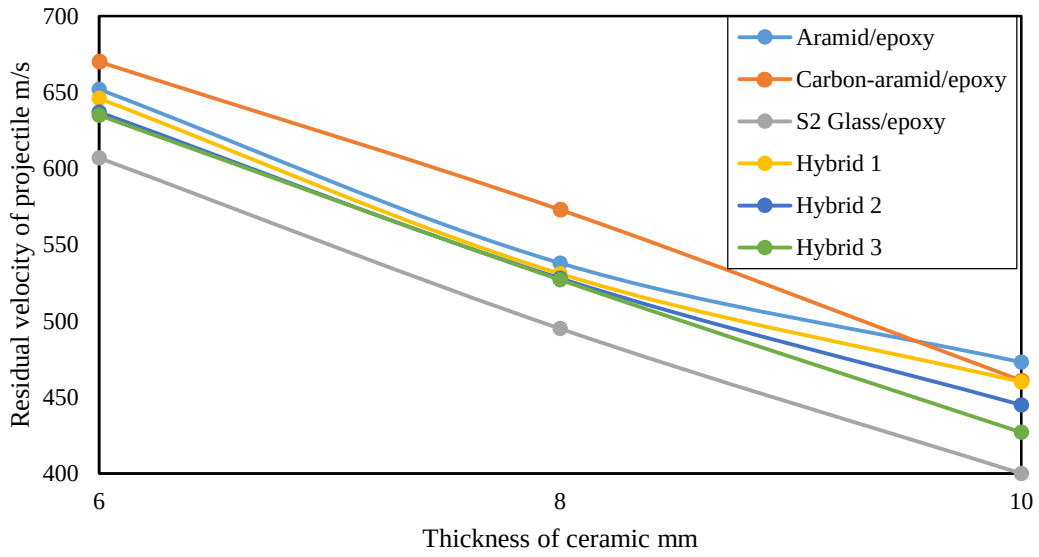


Figure 5.35 Residual velocity of projectile versus thickness of ceramic curve with all used backing plates at 850 m/s strike velocity

Lastly, when the ballistic performance/areal density ratio is considered, it can be said that the highest possible ceramic thickness should be preferred. Furthermore, S2 glass/epoxy had the best ballistic performance at 6 mm ceramic thickness, Hybrid 1 had the best ballistic performance at 8 mm ceramic thickness and Carbon-aramid/epoxy had the best ballistic performance at 10 mm ceramic thickness.

When the all ceramic thicknesses and areal density of armors are considered, aramid/epoxy backing plate had a higher ballistic performance than the others. Respectively, Hybrid 1, S2 glass/epoxy, Carbon-aramid/epoxy, Hybrid 2 and Hybrid 3 give the best results after Aramid/epoxy.

CHAPTER SIX
CONCLUSIONS AND RECOMMENDATIONS

In this study, the effect of the thickness values of variable ceramics on the structure of the armor and the effect of different reinforcement type as backing plates on fixed thickness was investigated. Also ballistic performances of 72 different combination armor types are carried out in this thesis. From the results, the following conclusions can be drawn:

For projectile:

As the impact velocity increases at low ceramic thickness, the blunting on the projectile is observed and the effect of mushrooming is observed to increase. When the ceramic thickness and the impact velocity are increased, blunting of the projectile is observed and the effect of mushrooming is observed to decrease.

The deformation on the projectile changes depending on the change of the composites used as the backing plate. Also, as the thickness of the ceramic increases, the projectile deformation also increases.

However, as the thickness of the ceramics increases, the effect of the backing plate substitution on the deformation of the projectile reduces and the deformation of the projectile remains mostly unchanged.

For armors:

As the thickness of the ceramics decreases and the velocity of the projectiles increases, the damage area in the armor decreases.

When the thickness of the ceramics increases, it becomes more apparent that the ceramic tends to break in a conical shape and the separation of ceramics and

composites seems to increase significantly. In the high strike velocities of projectile, the connection between composite and ceramic seems to be more stable.

It is found that the damaged area differences on ceramic that is caused by impact is smaller when the ceramic thickness is increased for different backing plates. However, crushing and/or delamination between the surfaces of S2 glass/epoxy and aramid/epoxy composite was observed in the armor with the hybrid backing plate.

As the thickness of the ceramics in the front side increases, it is seen that the residual velocity difference of projectile between the hybrid carbon-aramid/ epoxy and other type of composites diminishes.

It is observed that the armor that has S2 glass/epoxy as backing plate, in every possible combination it has the best ballistic performance when the areal density of armors is not considered. The armor with Hybrid 3 gives better ballistic performance than ones with Hybrid 2. It is observed that the results are very similar when Hybrid 1 or aramid/epoxy is used as the backing plate.

As the ceramic gets thicker, it is observed that ballistic performance of the armor with aramid/epoxy diminishes compared to other armors.

When the all ceramic thicknesses and areal density of armors are considered, aramid/epoxy backing plate had a higher ballistic performance than the others.

The effect of the thickness of the epoxy adhesive used for bonding the ceramic front plate and composite backing plate can be examined on the ballistic performance.

Multiple ceramic can be used instead of putting a single piece of ceramic on the surface of the composite. The ballistic performance of these two different armor models can be compared after the impact. Also the widths of the damaged areas formed on the ceramics and composites can be compared.

Optimum thickness ratios can be calculated by changing the ceramic and composite thickness ratios while keeping the armor thickness constant.

REFERENCES

Abu Talib, A. R., Abbud, L. H., Ali, A., & Mustapha, F. (2012). Ballistic impact performance of Kevlar-29 and Al2O3 powder/epoxy targets under high velocity impact. *Materials and Design, 35*, 12–19

Aldinger, F. & Weberruss, V. A. (2010). *Advanced Ceramics and Future Materials*. Weinheim: Wiley-VCH.

Ansys 17 engineering data material model (2016). Software Product, ANSYS

Armor protective clothing, (n.d.). Retrieved October 1, 2017, from https://www.britannica.com

Armors, (n.d.). Retrieved October 1, 2017, from https://www.globalsecurity.org

Ashby, M. F. (2005). *Materials Selection in Mechanical Design* (3rd ed.). Oxford: Butterworth-Heinemann

Azevedo, R., & Alves, M. (2009). Numerical simulation of soft-body impact on GFRP laminate composites: mixed SPH-FE and pure SPH approaches. *Mechanics of Solids in Brazil*. Retrieved October 1, 2017, from http://www.abcm.org.br/symposium-series/SSSM_Vol2/Contents/SSSM_02.pdf

Benloulo, I. S. C., & Sanchez-Galvez, V. (1998). A new analytical model to simulate impact onto ceramic/composite armors. *International Journal of Impact Engineering, 21*(6), 461-671

Berk, B. (2014). *Finite element simulation of ballistic impact on composite plates*. M.sc Thesis, Dokuz Eylül University, Turkey

Berk, B., Karakuzu, R., Icten, B. M., Arikan, V., Arman, Y., et al. (2016). An experimental and numerical investigation on low velocity impact behavior of composite plates. *Journal of Composite Materials, 50*(25), 3551–3559

Berk, B., Karakuzu, R., & and Toksoy, A. K. (2017). An experimental and numerical investigation on ballistic performance of advanced composites. *Journal of Composite Materials, 51*(25), 3467–3480

Boeing 787 Dreamliner, (n.d.). Retrieved October 1, 2017, from http://www.modernairliners.com/boeing-787-dreamliner/boeing-787-dreamliner-specs

Callister, W. D. Jr. (2007). *Materials Science and Engineering: An Introduction* (7th ed.). USA: John Wiley & Sons

Carpenter, A. J., Anderson, C. E. Jr., & Chocron, S. (2015). Mesoscale Simulations of High-Velocity Impact on Plain-Weave and 3-D Weave S-2 Glass Targets. *Procedia Engineering, 103,* 60 – 67

Challenger 2, (n.d.). Retrieved October 1, 2017, from https://en.wikipedia.org

Composite Materials Lecture Notes, (n.d.). Retrieved October 1, 2017, from http://nptel.ac.in/courses/Webcourse-contents/IISc-BANG/Composite%20Materials/pdf/Lecture_Notes/LNm1.pdf

Cortés, R., Navarro, C., Martínez, M.A., Rodríguez, J., & Sánchez-Gálvez V. (1992). Numerical modelling of normal impact on ceramic composite armours. *International Journal of Impact Engineering, 12*, 639–651

DostKimya products, (n.d.). Retrieved October 1, 2017, from http://www.kompozit.net/

Fawaz, Z., Zheng, W., & Behdinan, K. (2004). Numerical simulation of normal and oblique ballistic impact on ceramic composite armours. Composite Structures, *63*, 387–395

Feli, S., & Asgari M. R. (2011). Finite element simulation of ceramic/composite armor under ballistic impact. *Composites: Part B, 42*, 771–780

Feli, S., Yas, M. H., & Asgari, M. R. (2011). An analytical model for perforation of ceramic/multi-layered planar woven fabric targets by blunt projectiles. *Composite Structures, 93*, 548–556

Gama, B. A., Bogetti, A., Fink, B. K., Yu, C., Claar, T. D., Eifert H. H., et al. (2001). Aluminum foam integral armor: a new dimension in armor design. *Composite Structures, 52*, 381-395

Groover, M. P. (2010). *Fundamentals of Modern Manufacturing* (4th ed.). USA: John Wiley & Sons

Hajheydari, M., & Eftekhari, S. A. (2014). Simulation and numerical analysis of optimized ceramic-composite armor under vertical ballistic impact. *International Journal of Basic Sciences & Applied Research, 3*, 184-199

Heimann, R. B. (2010). *Classic and Advanced Ceramics*. Weinheim: Wiley-VCH Verlag GmbH & Co.KGaA.

Hetherington, J. G. (1992). The optimization of two-component composite armors. *International Journal of Impact Engineering, 12*, 229–259

Huang, C., & Chen, Y. (2016). Design and impact resistant analysis of functionally graded Al2O3–ZrO2 ceramic composite. *Materials and Design, 91*, 294–305

Kim, Y. A., Woo, K., Cho, H., Kim, I., & Kim, J. (2015). High-velocity impact damage behavior of carbon/epoxy composite laminates. *Int'l J. of Aeronautical & Space Sci.*, *16*(2), 190–205

Lagrangian and Eulerian descriptions, (n.d.). Retrieved October 1, 2017, from https://en.wikiversity.org/wiki/Nonlinear_finite_elements/Lagrangian_and_Eulerian_descriptions

Lee, M., & Yoo, Y. H. (2001). Analysis of ceramic/metal armour systems. *International Journal of Impact Engineering, 25*, 819–829

Liaghat, GH., Shanazari, H., Tahmasebi, M., Aboutorabi, A., & Hadavinia, H. (2013). A modified analytical model for analysis of perforation of projectile into ceramic composite targets. *International Journal of Composite Materials, 3*(6B), 17-22

Liu, P., Zhua, D., Yao, Y., Wang, J., & Bui, T. Q. (2016). Numerical simulation of ballistic impact behavior of bio-inspired scale-like protection system. *Materials and Design, 99*, 201–210

Liu, W., Chen, Z., Chen, Z., Cheng, Z., Wang, Y., Chen, X., et al. (2015). Influence of different back laminate layers on ballistic performance of ceramic composite armor. *Materials and Design, 87*, 421–427

Lopez-Puente, J., Arias, A., Zaera, R., & Navarro, C. (2005). The effect of the thickness of the adhesive layer on the ballistic limit of ceramic/metal armours. An experimental and numerical study. *International Journal of Impact Engineering, 32*, 321–336

Ls-dyna keyword user's manual volume II material models R10.0, (2017) Retrieved October 1, 2017, from http://www.dynasupport.com/manuals/ls-dyna-manuals/ls-dyna-manual-r10.0-vol-ii/view

M. Grujicic, M., Pandurangan, B., & d'Entremont, B. (2012). The role of adhesive in the ballistic/structural performance of ceramic/polymer–matrix composite hybrid armor. *Materials and Design, 41*, 380–393

McIntosh, G. (1998). *The Johnson-Holmquist Ceramic Model as used in LS-DYNA2D*. Retrieved October 1, 2017, from http://www.dtic.mil/dtic/tr/fulltext/u2/a357607.pdf

Mishra, P. (2011). *Development and Characterization of Low Cost Composite from Sugarcane Bagasse Waste*. PhD Thesis, National Institute of Technology Rourkela, India

Mobasseri, A. A., Reza Ansari, A. R., Zarei, H. R., Sedighi, M., & Mobasseri, F. (2013). Optimization of Combined Layers Produced by the Ceramic/Composite and ceramic/Aluminum Plates. *Australian Journal of Basic and Applied Sciences, 7*(6), 199-210

Mustafa Übeyli, M., Yıldırım, R. O., & Ögel, B. (2008). Investigation on the ballistic behavior of Al2O3/Al2024 laminated composites. *Journal of Materials Processing Technology, 196*, 356–364

National Institute of Justice (2008) *Ballistic Resistance of Body Armor: NIJ Standard 0101.06*, Washington D.C., U.S. Department of Justice

Ni, C., Jin, F., & Lua, T. (2014). Penetration of sandwich plates with hybrid-cores under oblique ballistic impact. *Theoretical & Applied Mechanics Letters, 4*, 021001

Plate armor, (n.d.). Retrieved October 1, 2017, from https://www.britannica.com

Randjbaran, E., Zahari, R., Jalil, N. A. A., & AbdulMajid D. L. A. (2014). Hybrid composite laminates reinforced with Kevlar/Carbon/Glass woven fabrics for ballistic impact testing. *The Scientific World Journal, 10.1155*, 413753

Reed, J. (1995). *Principles of Ceramic Processing*. New York: Wiley

Richerson, D. (1992). *Modern Ceramic Engineering*. New York: Newcastle Library

Richerson, D. W. (2006). *Modern Ceramic Engineering*. New York: CRC Press

Roeder, B. A., & Sun, C. T. (2001). Dynamic penetration of alumina/aluminum laminates: experiments and modeling. *International Journal of Impact Engineering, 25*, 169-185

Sánchez-Gálvez V., & Díaz-Rubio F. G. (1998). Ballistic impact on ceramic/composite armours. *Transactions on the Built Environment*, Retrieved October 1, 2017, from https://www.witpress.com/Secure/elibrary/papers/SU98/SU98059FU.pdf

Sevkat, E. (2012). Experimental and numerical approaches for estimating ballistic limit velocities of woven composite beams. *International Journal of Impact Engineering, 45*, 16-27

Shokrieh, M. M., & Javadpour, G. H. (2008). Penetration analysis of a projectile in ceramic composite armor. *Composite Structures, 82*, 269–276

Tasdemirci, A. Tunusoğlu, G., & Güden, M. (2012). The effect of the interlayer on the ballistic performance of ceramic/composite armors: Experimental and numerical study. *International Journal of Impact Engineering, 44*, 1-9

Tawadrous, R. I., Attia, W. A., & Laissy M. Y. (2016). Using ceramic plates as shielding for concrete blocks against projectile penetration. *Housing and Building National Research Center Journal*, *12*(3), 263-271

Tunusoğlu, G. (2011). The effects of light-weight interface material on the stress wave propagation in the multilayered composite armor system. M.sc Thesis, İzmir Institute of Technology, Turkey

Wang, R., Zheng, S., & Zheng, Y. (2011). *Polymer Matrix Composites and Technology*. Beijing: Woodhead Publishing

Woodward, R. L. (1990). A simple one-dimensional approach to modeling ceramic composite armor defeat. *International Journal of Impact Engineering, 9*(4), 455-474

Zaera, R., Sanchez-Saez, S., Perez-Castellanos, J. L., & Navarro, C. (2000). Modelling of the adhesive layer in mixed ceramic/metal armours subjected to impact. *Composites: Part A, 31*, 823–833

Zor, M. (2017). *Lecture Notes of Composite Materials*, Izmir, Dokuz Eylül University

APPENDICES

APPENDİX A

Case 1: 6 mm Alumina Ceramic Front Faced Targets

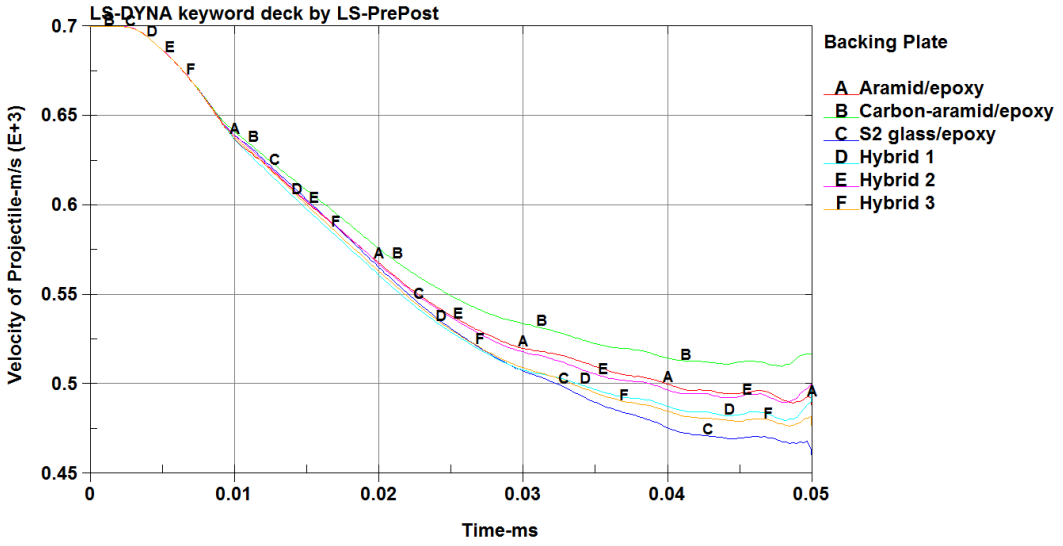


Figure 1 Comparison of Velocity versus Time curve of 16 mm thickness target model with all used backing plates at 700 m/s strike velocity

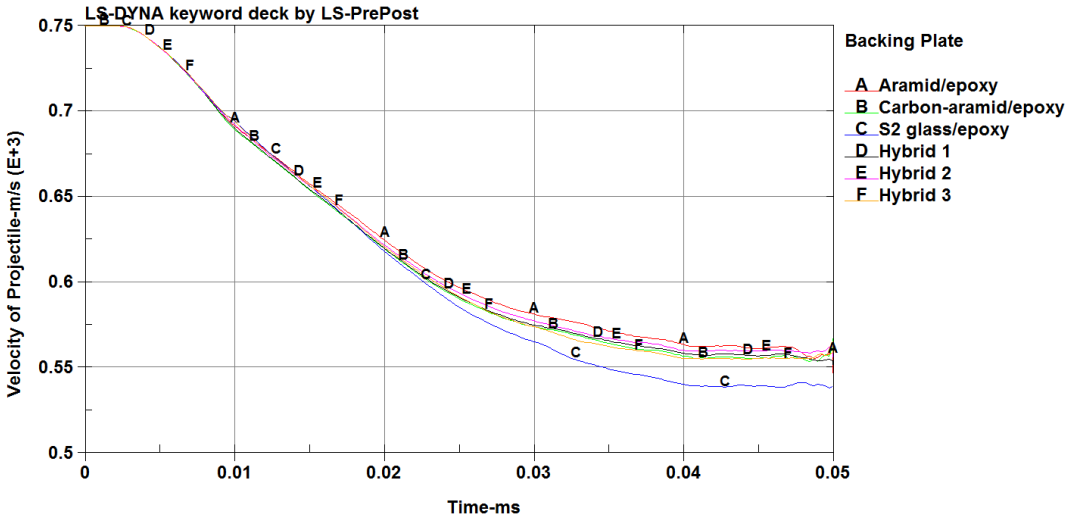


Figure 2 Comparison of Velocity versus Time curve of 16 mm thickness target model with all used backing plates at 750 m/s strike velocity

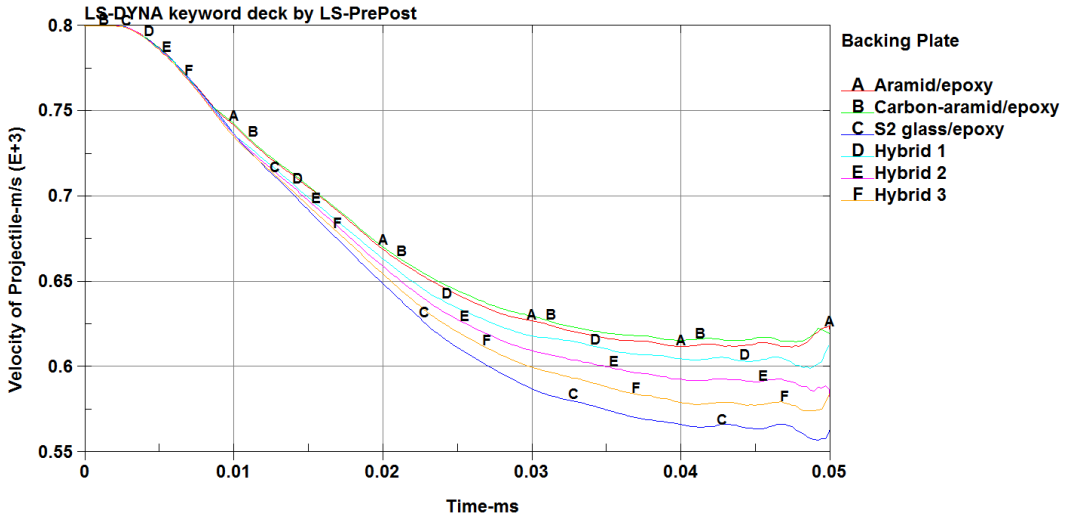


Figure 3 Comparison of Velocity versus Time curve of 16 mm thickness target model with all used backing plates at 800 m/s strike velocity

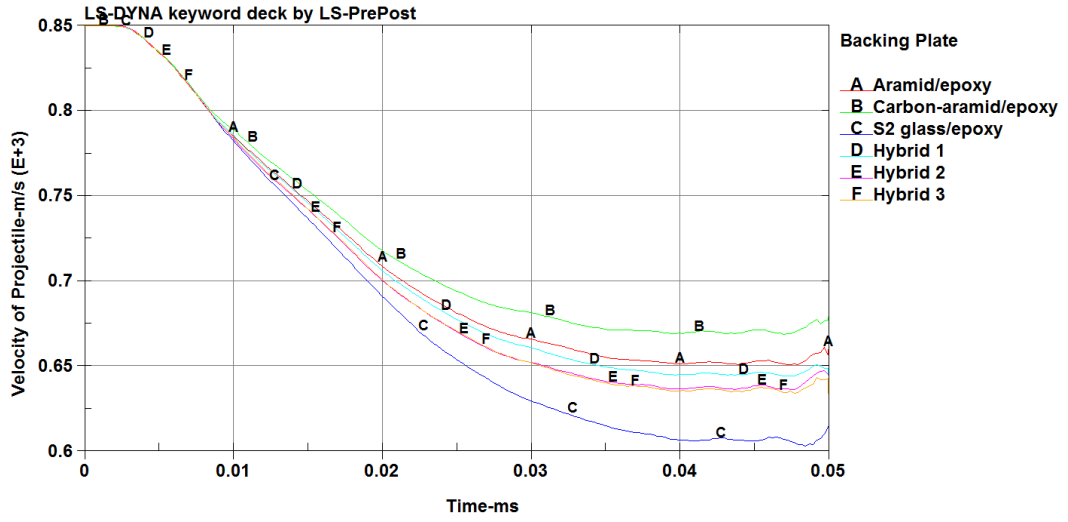


Figure 4 Comparison of Velocity versus Time curve of 16 mm thickness target model with all used backing plates at 850 m/s strike velocity

APPENDİX B

Case 2: 8 mm Alumina Ceramic Front Faced Targets

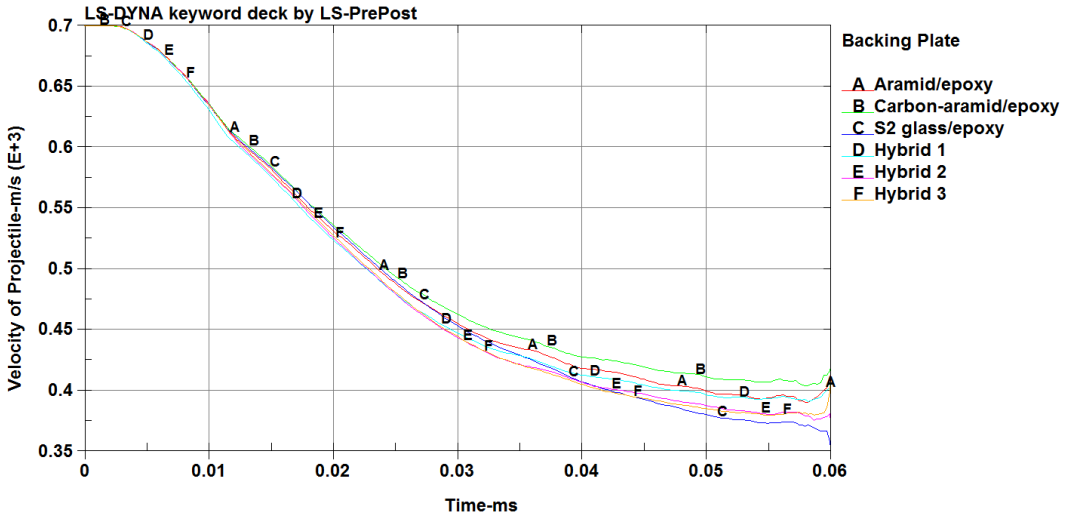


Figure 5 Comparison of Velocity versus Time curve of 18 mm thickness target model with all used backing plates at 700 m/s strike velocity

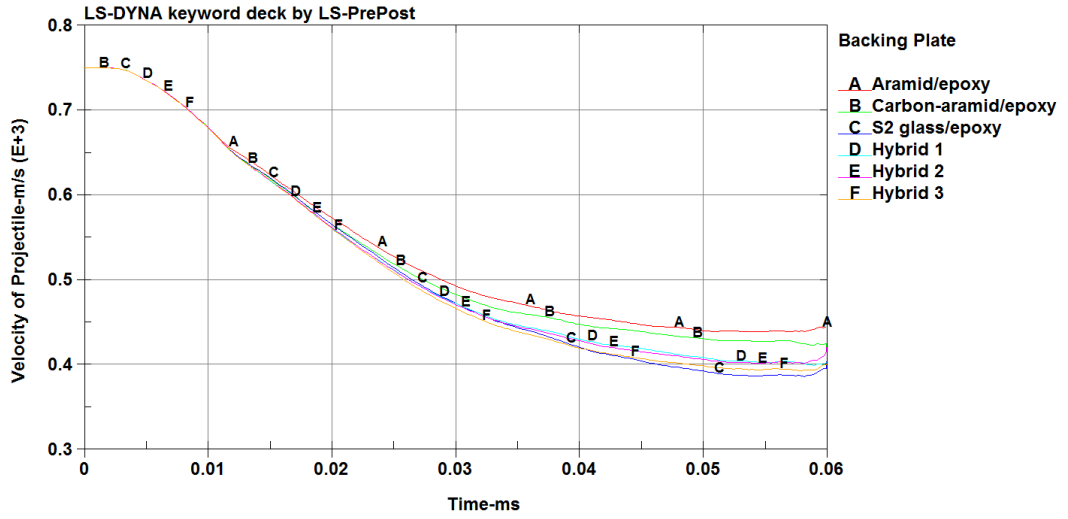


Figure 6 Comparison of Velocity versus Time curve of 18 mm thickness target model with all used backing plates at 750 m/s strike velocity

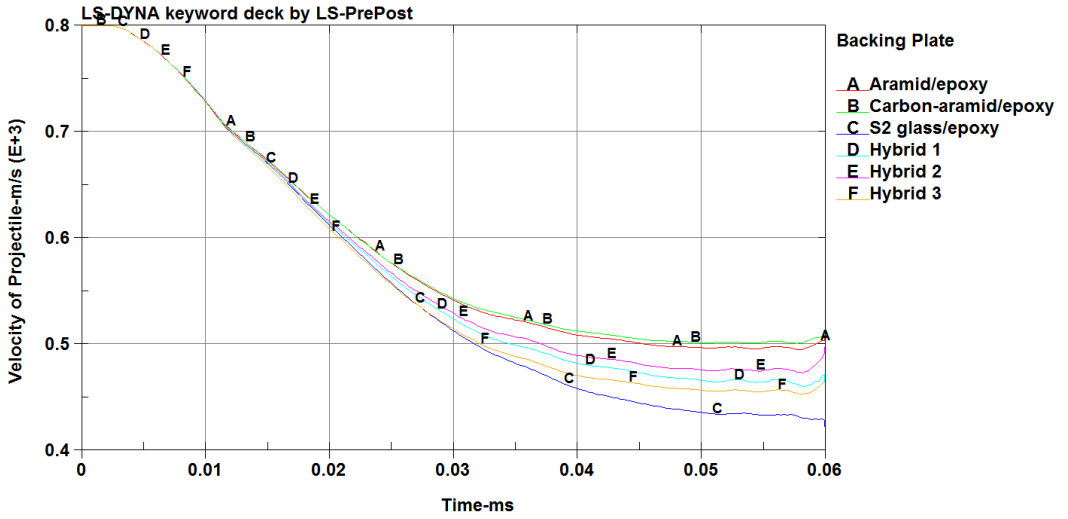


Figure 7 Comparison of Velocity versus Time curve of 18 mm thickness target model with all used backing plates at 800 m/s strike velocity

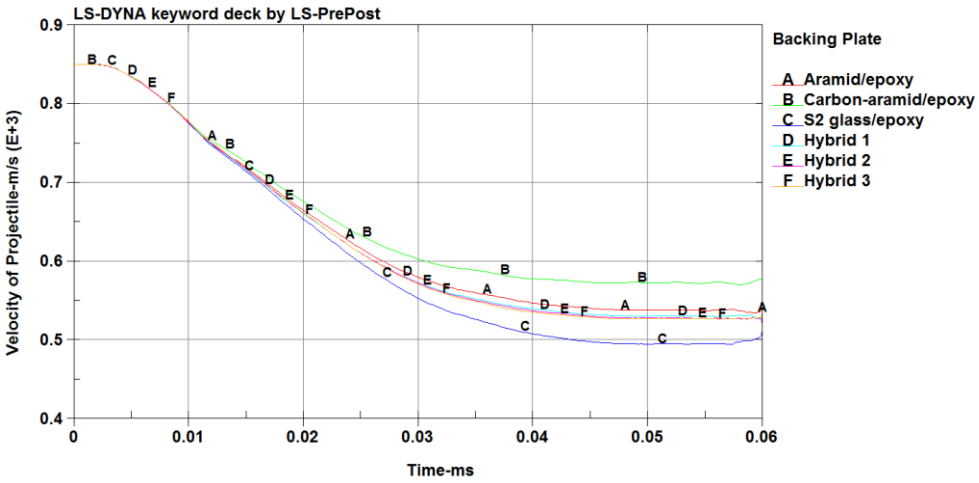


Figure 8 Comparison of Velocity versus Time curve of 18 mm thickness target model with all used backing plates at 850 m/s strike velocity

APPENDİX C

Case 3: 10 mm Alumina Ceramic Front Faced Targets

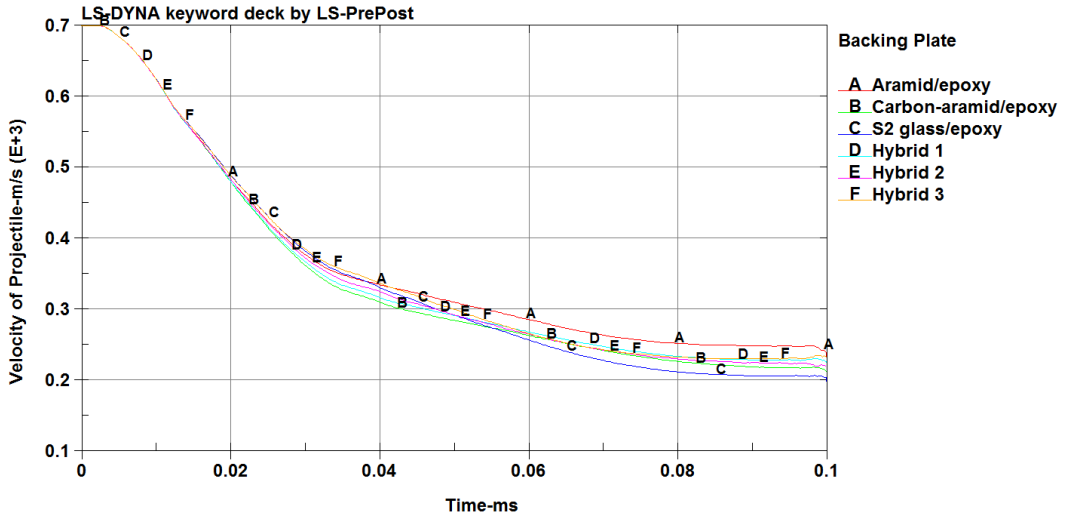


Figure 9 Comparison of Velocity versus Time curve of 20 mm thickness target model with all used backing plates at 700 m/s strike velocity

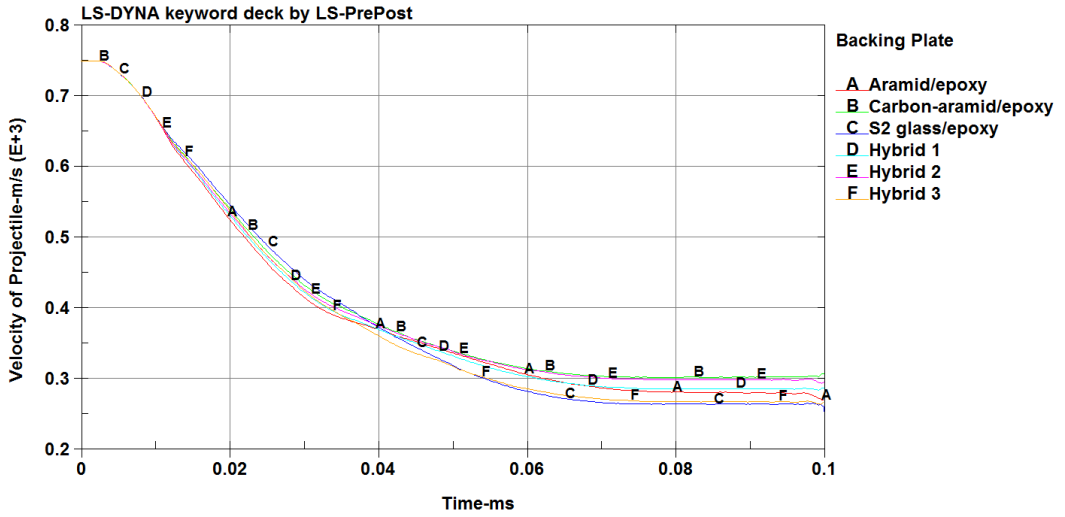


Figure 10 Comparison of Velocity versus Time curve of 20 mm thickness target model with all used backing plates at 750 m/s strike velocity

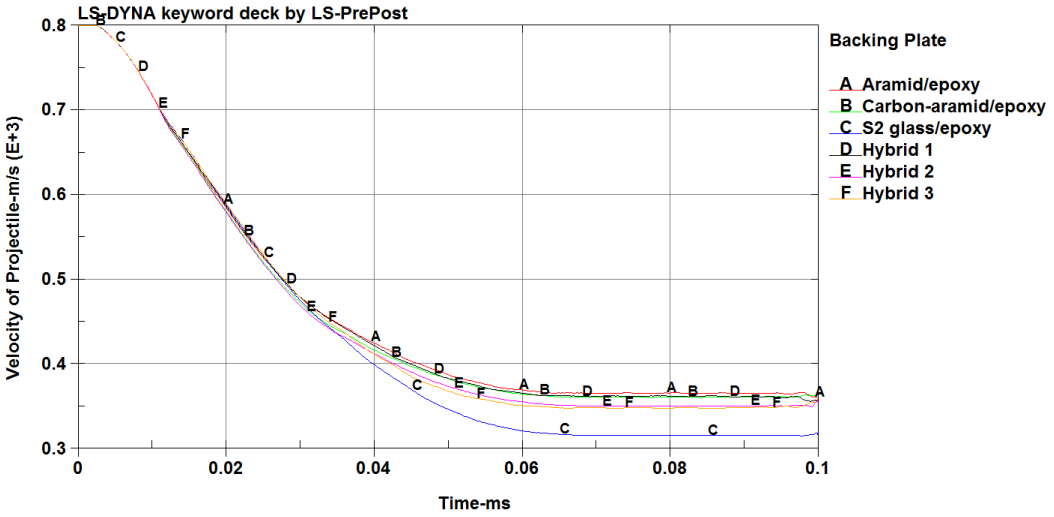


Figure 11 Comparison of Velocity versus Time curve of 20 mm thickness target model with all used backing plates at 800 m/s strike velocity

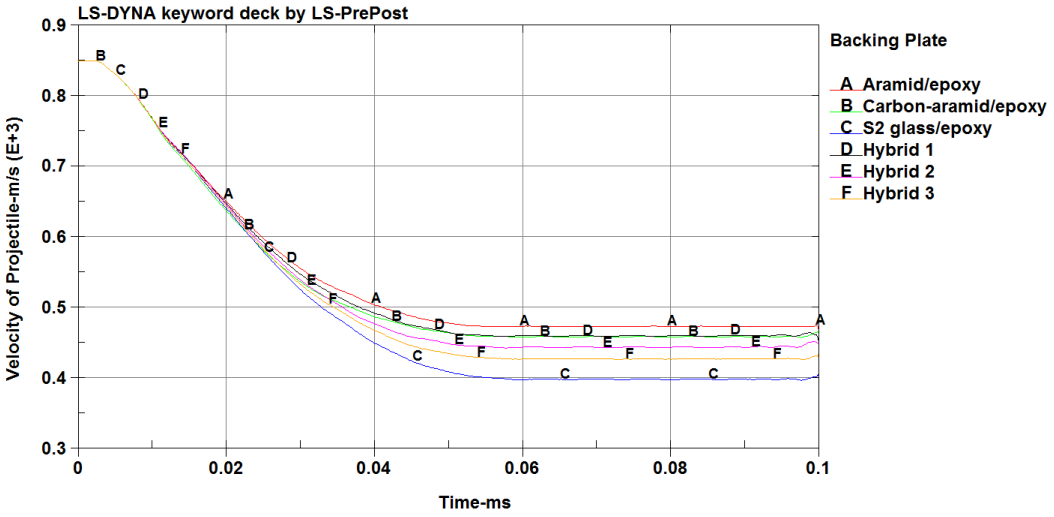


Figure 12 Comparison of Velocity versus Time curve of 20 mm thickness target model with all used backing plates at 850 m/s strike velocity